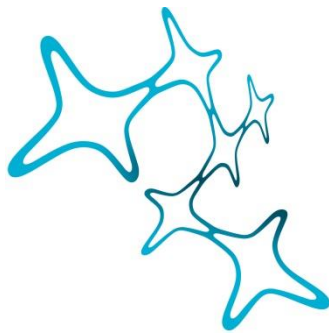

VALIDATION OF GENETICALLY ENCODED SENSORS TO MEASURE INTRACELLULAR POTASSIUM AND METABOLISM IN NEURONS

Bernhard Groschup



Graduate School of
Systemic Neurosciences

LMU Munich



Dissertation der
Graduate School of Systemic Neurosciences der
Ludwig-Maximilians-Universität München

4th of December, 2023

Supervisor and first reviewer:

Prof. Dr. med. Nikolaus Plesnila (Institute for Stroke and Dementia Research)

Second reviewer:

PD Dr. Lars Kunz (Faculty of Biology; Ludwig-Maximilians-Universität München)

Date of Submission: 04.12.2023

Date of Defense: 21.05.2024

Table of Contents

Abstract.....	5
1 Introduction	7
1.1 Neurons	7
1.1.1 Neuronal signal transduction	7
1.1.2 Measuring dynamic processes in neurons.....	8
1.2 Fluorescent proteins as a tool for life sciences	9
1.2.1 Principles of fluorescence	9
1.2.2 Förster resonance energy transfer (FRET).....	10
1.2.3 Green fluorescent protein and engineering of fluorescent proteins	12
1.3 Genetically encoded sensors	13
1.3.1 Intrinsic sensing properties of fluorescent proteins	14
1.3.2 Single fluorophore sensors based on circularly permuted fluorescent proteins	15
1.3.3 FRET-based sensors	17
1.3.4 Considerations for live imaging with genetically encoded sensors.....	19
1.3.4.1 Affinity	20
1.3.4.2 Specificity	20
1.3.4.3 Temperature dependence.....	21
1.3.4.4 pH sensitivity	21
2 Aims.....	23
3 Articles	24
3.1 Study I: Probing Intracellular Potassium Dynamics in Neurons: <i>In vitro</i> and <i>In vivo</i> Assessment of a Genetically Encoded Sensor.....	24
3.2 Study II: Assessing the pH sensitivity of genetically encoded sensors with Dead Cell Imaging.....	56
4 Discussion.....	84
4.1 Readouts of genetically encoded sensors need to be carefully interpreted	84
4.2 Study I: Probing Intracellular Potassium Dynamics in Neurons: <i>In vitro</i> and <i>In vivo</i> Assessment of a Genetically Encoded Sensor.....	84
4.2.1 Main findings of the study.....	84
4.2.2 Limitations of the study.....	85
4.2.3 Comparison of Ic-LysM GEPII 1.0 with other K ⁺ sensors	86
4.3 Study II: Assessing the pH sensitivity of genetically encoded sensors with Dead Cell Imaging.....	88
4.3.1 Detecting pH artifacts of genetically encoded sensors can be challenging	88
4.3.2 Advantages of Dead Cell Imaging	89
4.3.3 Limitations of Dead Cell Imaging.....	90
4.3.4 Implications for the interpretation of results obtained with Dead Cell Imaging ...	91

4.3.5	Comparison of Dead Cell Imaging with other methods to assess pH sensitivity of genetically encoded sensors	92
4.4	Experimental considerations for live cell imaging	93
4.4.1	Optimization of the live cell imaging microscope	94
4.4.2	Environmental control	95
5	Future directions	97
6	References.....	98
7	Acknowledgements	106
8	Curriculum Vitae.....	108
9	List of Publications	109
10	Affidavit	110
11	Declaration of Author Contributions	111

Abstract

Biological processes are highly dynamic throughout all levels of organization, ranging from the molecular level up to the full organism. To understand these dynamic processes, they can be observed with an array of different analytical methods, each with particular advantages and limitations. Since their emergence, genetically encoded sensors quickly became the method of choice for many researchers due to their excellent spatial and temporal resolution and the minimally invasive nature of these sensors. In addition, the ever-growing palette of available sensors allows measurements of a wide range of different analytes. However, genetically encoded sensors also have some key limitations, such as sub-optimal affinity, off-target recognition and environmental sensitivity. Therefore, careful interpretation of results obtained with genetically encoded sensors is warranted and potential confounding factors need to be considered in order to avoid artifactual results. Both studies discussed in this thesis address shortcomings of genetically encoded sensors and how to mitigate them.

In study I we characterized Ic-LysM-GEPII 1.0, a genetically encoded sensor for potassium ions (K^+), with respect to its capacity to resolve neuronal K^+ changes upon neuronal activity. Ic-LysM-GEPII 1.0 was unable to resolve small K^+ dynamics during spontaneous neuronal activity, likely because it might be saturated at physiological K^+ concentrations, but reliably detected more pronounced K^+ decreases during strong, tetanic activity evoked by application of Bicuculline. We confirmed these results *in vivo* by fluorescence lifetime imaging of Ic-LysM-GEPII 1.0 in the cortex of living mice. We could not observe lifetime changes at baseline, but peri-infarct depolarizations induced by occlusion of the middle cerebral artery led to strong increases in the fluorescence lifetime of Ic-LysM-GEPII 1.0. We conclude that Ic-LysM-GEPII 1.0 is able to resolve K^+ dynamics upon strong neuronal activity but needs to be improved with respect to affinity and dynamic range to measure responses elicited by milder stimulation. To aid this development, we developed an optogenetic stimulation approach that allowed us to titrate the sensitivity of Ic-LysM-GEPII 1.0 and will help to compare the performance of different sensor variants.

In study II we developed a novel method to assess the pH sensitivity of genetically encoded sensors without the need for prior purification of the sensor protein. Study II initially aimed to investigate neuronal energy metabolism within the context of GABAergic inhibition. Upon application of GABA to primary cultured neurons, we observed an increase of the FRET ratio of the lactate sensor Laconic, which was mediated by efflux of bicarbonate ions through GABA_A receptors, leading to an acidification of the cytosol. While pH changes can lead to artifactual signal changes of genetically encoded sensors, pH can also act as a second messenger eliciting physiological alterations of the levels of the analyte of interest. Therefore, a signal of a genetically encoded sensor can be an artifact, a real change of analyte levels, or a

combination of both. We developed a cost-effective and easy-to-use method to separate the pH sensitivity of genetically encoded sensors from the pH-induced physiological analyte response by PFA fixation. This approach, which we call Dead Cell Imaging, preserves sensor fluorescence while stopping all physiological processes. Using this method, we confirmed that the signal change of Laconic upon GABA application is a pH artifact. Furthermore, Dead Cell Imaging provides temporal information about the pH sensitivity of a genetically encoded sensor, which can help to identify complex pH artifacts and is not resolved by canonical methods of addressing the pH sensitivity of a sensor.

1 Introduction

1.1 Neurons

1.1.1 Neuronal signal transduction

Neurons are electrically excitable and highly polarized cells, typically consisting of dendrites that meet in the cell body, called soma, from which a single axon projects towards other neurons¹. They form a dense network within the central nervous system and are the main cell type in the brain involved in signal processing. In most cases, the axon of a neuron projects towards the dendrites of other neurons and forms connections, called synapses². While also electrical synapses exist³, the main way of signal transduction at a synapse is chemically via release of neurotransmitters from the presynaptic terminal at the axon⁴. These neurotransmitters then bind to specific receptors at the postsynaptic terminals at the dendrites that mediate downstream effects². Within the neuron, signal transduction is achieved exclusively electrically via so-called action potentials and relies on changes of the neuronal membrane potential⁵.

At rest, neurons have a membrane potential of about -60 to -70 mV⁶ that builds up mainly by activity of the Na⁺/K⁺-ATPase, a transmembrane ATP-driven ion pump, and selective ion channels. The Na⁺/K⁺-ATPase actively pumps 3 Na⁺ ions out of the cell in exchange for 2 K⁺ ions⁷, thereby extruding one positive charge per pump cycle. Ion channels such as potassium leak channels contribute to the formation of the membrane potential by allowing potassium efflux along its concentration gradient, further polarizing the neuron. Binding of excitatory neurotransmitters, e.g., glutamate, to postsynaptic membrane receptors, leads to Na⁺ influx in the cytosol along its concentration gradient, thus depolarizing the membrane. Consequently, voltage-gated Na⁺ channels respond to this depolarization with opening, allowing further influx of Na⁺. This process amplifies the initial depolarization, which in turn activates further voltage-gated Na⁺ channels downstream, thereby enabling propagation of the depolarization along the neuronal membrane. If the initial depolarization is strong enough and surpasses a certain threshold, it sustains itself and evokes an action potential⁵. Action potentials are all-or-nothing events that, once triggered, travel along the axon towards the presynaptic terminal⁶, where they elicit the release of neurotransmitters. After full depolarization, voltage-gated Na⁺ channels close and cannot re-open during a refractory period, thus ensuring that the action potential cannot reverse and propagates unidirectional. Upon strong depolarization, voltage-gated K⁺ channels open, mediating K⁺ efflux along its concentration gradient and therefore leading to a repolarization of the neuronal membrane. During repolarization the membrane potential usually undershoots below resting levels before voltage-gated K⁺ channels close. Activity of the Na⁺/K⁺-ATPase restores the initial ion distribution and therefore the resting

membrane potential⁵. Therefore, due to their role in repolarizing the neuronal membrane during an action potential, potassium ions are crucial for proper neuronal function.

The concentration of potassium ions in neurons ($[K^+]_i$) is around 140 mM⁸, while the extracellular K^+ concentration ($[K^+]_e$) is as low as 3 mM⁹. Thus, an action potential does not only decrease $[K^+]_i$, but also increases $[K^+]_e$. Consequently, small absolute increases in $[K^+]_e$ can lead to large relative changes and may thus have profound effects on the membrane potential¹⁰. In fact, extracellular K^+ strongly influences neuronal excitability¹¹ and the shape of action potentials¹². Due to that, the brain relies on effective mechanisms to clear excessive K^+ from the extracellular space. Astrocytes are the main contributor to this, which efficiently remove K^+ from the extracellular space through specific pumps, cotransporters, and channels, e.g., Na^+/K^+ -ATPase, NKCCs and Kir4.1¹³. It has also been proposed that astrocytes redistribute K^+ via gap junctions from active brain areas with high $[K^+]_e$ to areas with low $[K^+]_e$. This process, called “spatial potassium buffering”, helps to keep local $[K^+]_e$ low and allows proper neuronal signaling during strong or prolonged activity¹⁴. Disruptions in brain K^+ homeostasis lead to severe pathological conditions, thus highlighting the importance of dynamic brain K^+ regulation. For instance, excessive $[K^+]_e$ elevations that overwhelm the clearing mechanisms can lead to epileptic seizures¹⁵ or cortical spreading depolarizations¹⁶. Therefore, precise measurements of brain K^+ dynamics and its regulation are key to better understand the underlying mechanisms of these pathological processes as a basis for the development of novel therapies for affected patients.

1.1.2 Measuring dynamic processes in neurons

Measuring activity and functional changes in neurons can be technically challenging because it requires techniques applicable to the cellular level with high spatial and temporal resolution. For decades the gold standard to measure neuronal activity is electrophysiology¹⁷, which involves placement of electrodes into neuronal cell bodies to record their electrical activity. While this method has excellent sensitivity and temporal resolution, it is invasive and time-consuming as it allows measurements of only one or few neurons at a time.

An alternative to assess neuronal activity is measurement of neuronal Ca^{2+} dynamics using imaging approaches. While Ca^{2+} imaging does not achieve a temporal resolution comparable to electrophysiology, it allows simultaneous recordings from multiple cells or whole tissues. The membrane depolarization during an action potential leads to opening of voltage-gated Ca^{2+} channels and allows Ca^{2+} influx, leading to increase of the neuronal Ca^{2+} levels of up to 100-fold¹⁸. Therefore, Ca^{2+} transients are a reliable indicator for neuronal activity with excellent signal-to-noise ratio. Traditionally, Ca^{2+} imaging utilized fluorescent chemical dyes such as Fura-2 or Fluo-4 that display fluorescence changes upon Ca^{2+} binding. However, these dyes

require acute loading into the cells before the experiment and show limited cellular and subcellular specificity¹⁹. The development of genetically encoded fluorescent sensors for Ca^{2+} managed to overcome these limitations as it allowed expression of Ca^{2+} sensors in a wide range of cell types or subcellular compartments¹⁹. In recent years, live imaging with genetically encoded fluorescent Ca^{2+} sensors became a key technique in the neurosciences, demonstrated by their widespread use and continuous improvement²⁰. However, as previously discussed, Na^+ and K^+ are the main ions involved in action potential propagation and their concentrations have profound effects on neuronal activity. To date, there is no genetically encoded fluorescent sensor for Na^+ ; however, genetically encoded fluorescent sensors for K^+ have recently been developed²¹⁻²⁴. However, there is no comprehensive validation of any of these fluorescent sensors in neurons and it is unclear whether they can resolve K^+ dynamics in response to neuronal activity. Potentially, these sensors might display an inappropriate affinity to resolve $[\text{K}^+]_i$ changes at physiological concentrations or might have a small dynamic range that leads to a low signal-to-noise ratio. Another potential shortcoming is slow kinetics, which would hamper measurement of fast K^+ transients. While these parameters are often described for the purified sensor protein in the original publication, they can vary substantially when expressed in different cell types²³. Therefore, characterization of a fluorescent sensor in the cell type of interest is vital to ensure its performance.

1.2 Fluorescent proteins as a tool for life sciences

1.2.1 Principles of fluorescence

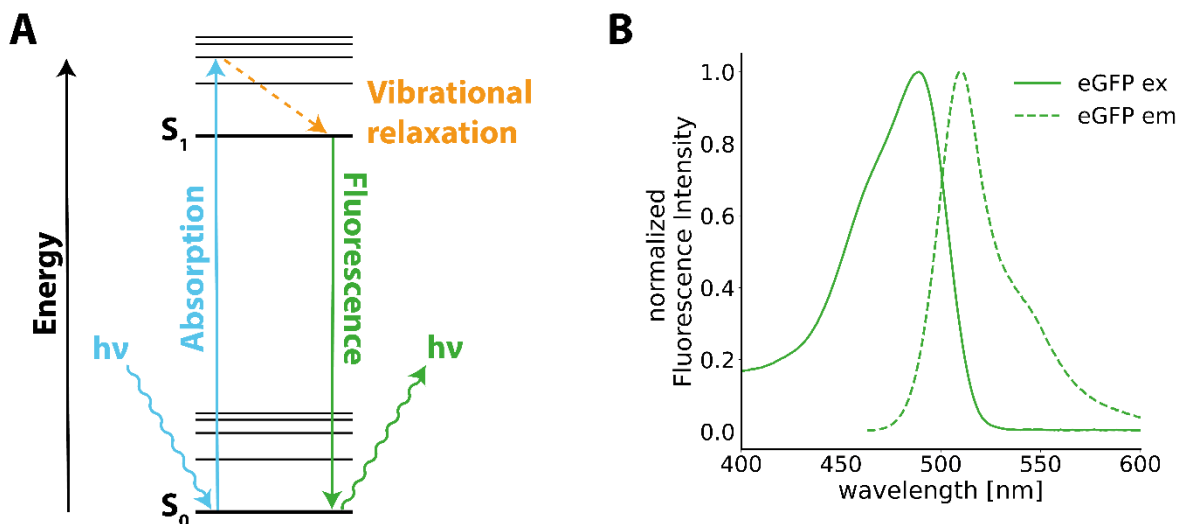


Figure 1: (A) Simplified Jablonski-diagram showing the photophysical principles of fluorescence (modified from Hochreiter et al.²⁵) and (B) excitation and emission spectra of enhanced green fluorescent protein (eGFP²⁶ – created with data from fpbase.org²⁷).

Fluorescence is a form of luminescence and can be generally described as the light emitted by a molecule that has been excited via absorption of one or more photons²⁸. The processes

occurring during fluorescence are usually described using the Jablonski diagram (**Figure 1A**). Absorption of light of a specific wavelength leads to the excitation of the molecule from the ground state S_0 to one of many vibrational states of an excited state S_n . If the molecule got excited to the state S_2 or higher, it relaxes to the first excited state S_1 via a process called internal conversion. The molecule then falls to the lowest vibrational level of S_1 via vibrational relaxation. From there, radiative transition to S_0 can occur by spontaneous emission of a photon, a process called fluorescence. Unless thermal excitation of the fluorescent molecule occurs, the emitted photon is always of lower energy than the absorbed photon, as some energy gets lost due to vibrational relaxation and solvent interaction. Because of that, fluorescence is spectrally red-shifted compared to the excitation light, a process first described by George Gabriel Stokes and therefore termed “Stokes shift” (**Figure 1B**)²⁹. Other general pathways through which the excited molecule can return to the ground state S_0 , namely non-radiative decay via internal conversion or phosphorescence via intersystem crossing to the triplet state T_1 , are described elsewhere³⁰.

1.2.2 Förster resonance energy transfer (FRET)

As discussed, an excited fluorescent molecule can relax to its ground state S_0 via three main pathways: fluorescence, non-radiative decay, and phosphorescence. In the presence of a suitable fluorescent acceptor molecule, however, it can also dissipate its energy via a process called Förster resonance energy transfer (FRET). This process describes the transfer of energy from an excited donor (D) to a suitable acceptor (A) via dipole-dipole coupling between the two molecules. FRET is a non-radiative energy transfer, as it does not involve photon emission from the donor to excite the acceptor molecule. The excited acceptor molecule can subsequently return to its ground state via the emission of a photon (**Figure 2A**).

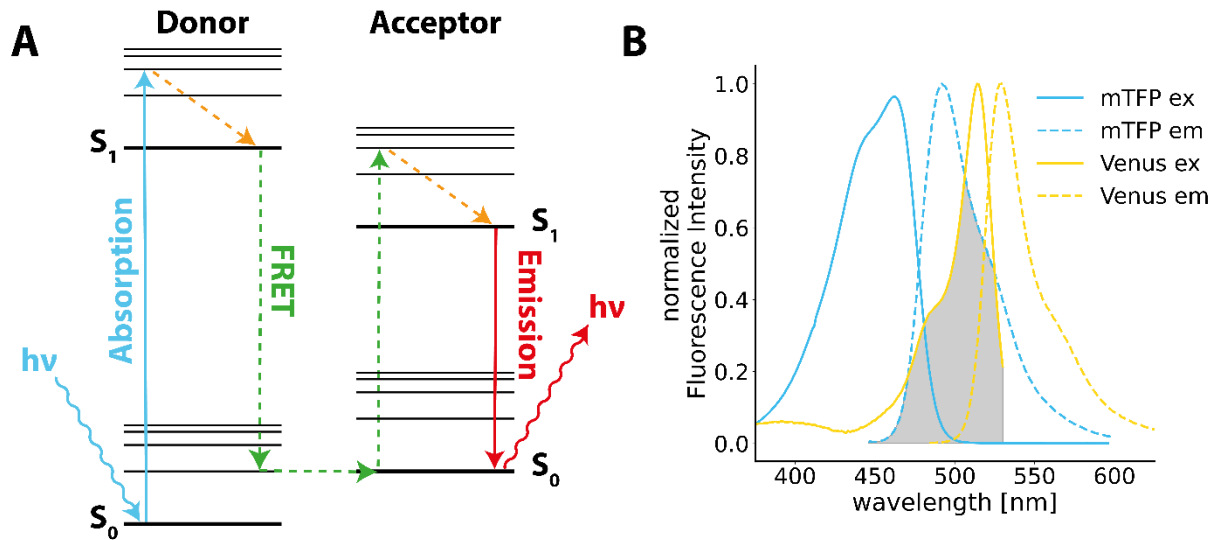


Figure 2: (A) Simplified Jablonski-diagram showing the photophysical principles of FRET (modified from Hochreiter et al.²⁵) and (B) Excitation and emission spectra of the CFP-YFP-based FRET pair mTFP1³¹ and Venus³². Spectra created with data from fbase.org²⁷.

The name Förster resonance energy transfer refers to Theodor Förster, who first described the theoretical underpinnings of this phenomenon³³. He described the rate of energy transfer (k_{FRET}) with the following expression:

$$k_{FRET} = \left(\frac{R_0}{r}\right)^6 \cdot \frac{1}{\tau_{D,0}} \quad (1)$$

$\tau_{D,0}$ is the excited-state lifetime in absence of the acceptor.

r is the distance between donor and acceptor in Å

R_0 is the Förster radius and is defined as:

$$R_0 = 8.785 \times 10^{-5} \cdot \frac{\varphi_{D,0} \cdot \kappa^2 \cdot J}{n^4} \quad (2)$$

$\varphi_{D,0}$ is the quantum yield of the donor in absence of the acceptor

κ is the orientation factor that depends on the angle between the dipoles of donor and acceptor. When the transition dipole moments are perpendicular to each other, κ^2 is 0.

J is the spectral overlap integral between the emission spectrum of the donor and the absorption spectrum of the acceptor

n is the refractive index of the surrounding medium

From these equations it becomes apparent that three basic conditions need to be met for FRET to occur³⁴:

- (1) The emission spectrum of the donor and the excitation spectrum of the acceptor molecule need to overlap (**Figure 2B**), otherwise the spectral overlap integral (and therefore the FRET rate) is zero.

-
- (2) Since the energy transfer relies on dipole-dipole interactions, donor and acceptor need to be sufficiently aligned. If both dipole moments are perpendicular to each other, no dipole-dipole interaction is possible, and FRET cannot occur.
 - (3) The FRET rate depends heavily on the distance between donor and acceptor r . If r is bigger than R_0 (which is typically between 1 and 10 nm), the resulting ratio is smaller than 1, which is amplified by the power of 6. Therefore, donor and acceptor molecules must be in close proximity to allow resonance energy transfer to occur.

As FRET only occurs in close proximity, it is an ideal tool to investigate inter- and intramolecular interaction and can be a powerful tool in the context of biosensing.

1.2.3 Green fluorescent protein and engineering of fluorescent proteins

Fluorescence measurements are common practice in most life science laboratories and have revolutionized many fields of research. An important step for many contemporary applications using fluorescence was the discovery of green fluorescent protein (GFP). GFP was first described as a side-finding in a paper by Shimomura and colleagues in 1962, who reported the isolation of the blue bioluminescent protein Aequorin³⁵. A footnote in the paper states: "A protein giving solutions that look slightly greenish in sunlight though only yellowish under tungsten lights, and exhibiting a very bright, greenish fluorescence in the ultraviolet of a Mineralite, has also been isolated from squeezates." Wild-type GFP is a fluorescent protein that has two excitation peaks at 400 and 480 nm and an emission peak at 508 nm³⁶. GFP was first cloned in 1992³⁷ and shortly after the crystal structure was solved by two independent groups^{38,39}. It consists of 11 β -sheets arranged in a barrel-like structure, containing a single α -helix on which the fluorophore is located. This structure, termed β -can, protects the fluorophore from interactions with the surrounding solvents (**Figure 3**).

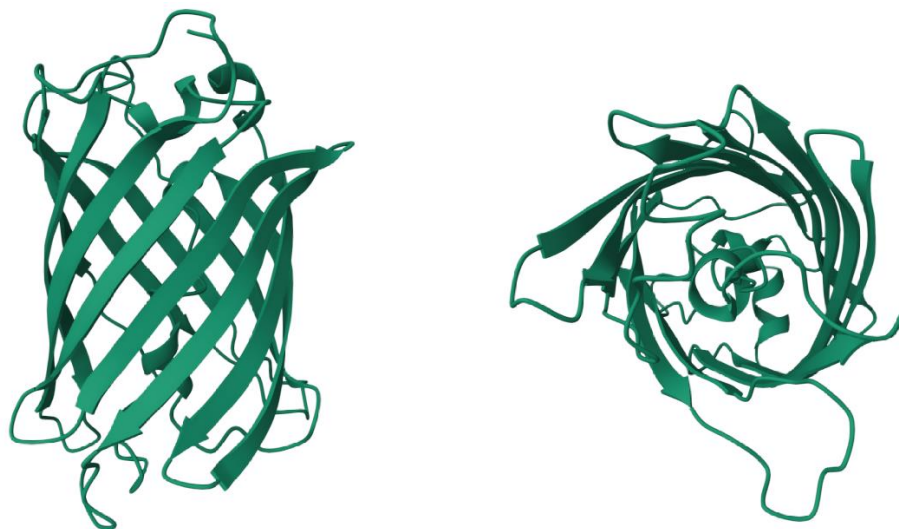


Figure 3: Crystal structure of GFP (created with rscb.org using the PDB ID 1ema)

Chalfie et al. achieved the first heterologous expression of GFP in the prokaryotic and eukaryotic organisms *Escherichia Coli* and *Caenorhabditis elegans*. This demonstrated that GFP is functional and fluorescent without additional substrates or co-factors⁴⁰ other than atmospheric oxygen which is required for the maturation of the fluorophore⁴¹. This crucial property of GFP in combination with the fact that it is genetically encoded and therefore can be easily introduced and targeted in biological systems allowed a wide range of applications in different fields. GFP was soon employed as a reporter gene to study the regulation of gene expression⁴², as cell-type or population specific marker⁴³ and as fusion tag for proteins. At the same time, GFP was engineered towards improved stability, folding efficiency²⁶, brightness^{44,45} and, most crucially, altered spectral properties. Mutations of GFP led to the development of cyan and yellow fluorescent proteins and ultimately the full visible spectrum was covered. The development and optimization of fluorescent proteins based on GFP as well as other subsequently discovered fluorescent proteins continues and is reviewed elsewhere^{46,47}.

1.3 Genetically encoded sensors

Next to labelling specific cell organelles and individual cell populations, one other important application of fluorescent proteins is their use as genetically encoded biosensors. Fluorescent genetically encoded biosensors are proteins that actively change their fluorescent properties upon binding of a biological molecule. Most genetically encoded sensors report via changes of fluorescence intensities or lifetime. Some sensors, however, also employ other photophysical phenomena in addition to intensity changes such as photoactivation to allow precise selection of the measurement population^{48,49} or photo conversion^{50,51}.

Genetically encoded sensors are powerful tools that can resolve biological processes in their native environment with exceptionally high spatial and temporal resolution. Due to their nature as proteins, genetically encoded sensors provide powerful advantages over conventional probes such as amperometric electrodes or chemical fluorescent dyes. They are generally considered non-toxic, are measured with optical methods non-invasively, and allow thus robust and reliable measurements under physiological conditions. As genetically encoded sensors can be expressed under a cell-type specific promoter or targeted to a specific organelle, they exhibit exceptional cellular as well as subcellular specificity. Genetically encoded sensors can be expressed both in 2D cell cultures or whole organisms, allowing scientists to choose their application based on maximizing experimental control or physiologic relevance, respectively. Due to these advantages, genetically encoded sensors have rapidly been utilized to answer question from different fields of life science including plant biology⁵², metabolism⁵³ and neuroscience⁵⁴.

To date, genetically encoded sensors for a wide range of analytes and conditions have been developed and are continuously improved. These include, but are not limited to, sensors for ions (e.g., Ca^{2+20} , K^{+21} , Mg^{2+55} , Zn^{2+56}), nucleotides (e.g., ATP⁵⁷, cAMP⁵⁸, NADH-NAD⁺⁵⁹), metabolites (e.g., glucose⁶⁰, lactate⁶¹, pyruvate⁶²), neurotransmitters (e.g. glutamate⁶³, GABA⁶⁴, dopamine⁶⁵) and other biologically relevant molecules and parameters (e.g., pH⁶⁶, H_2O_2 ⁶⁷, temperature⁶⁸, membrane potential⁶⁹, molecular crowding⁷⁰). The sensor field is rapidly evolving, and the current toolbox of available genetically encoded sensors is summarized in recent reviews⁴⁶.

In general, genetically encoded sensors consist of a sensing domain that binds the analyte of interest and a reporting domain, commonly one or more fluorescent proteins. Binding of the analyte to the binding domain induces a conformational change that results in a change of the fluorescent properties of the reporter⁷¹. The performance of a particular genetically encoded sensor depends heavily on its design. While each sensor is unique and should be carefully assessed for its performance before application, genetically encoded sensors can be classified in general categories based on their design, each with specific advantages and limitations.

1.3.1 Intrinsic sensing properties of fluorescent proteins

Some groups, especially during the early days of the development of fluorescent proteins and genetically encoded sensors, employed and optimized existing sensitivities of fluorescent proteins and used them directly as a sensor. In this case, the fluorescent protein not only acts as a reporter but is also the domain responsible for sensing. For instance, early reports indicated that GFP displays pH sensitivity⁷² while YFP also is sensitive to the chloride concentration⁷³. Introduction of several point mutations led to the development of the pH sensor pHluorin⁷⁴ as well as an YFP mutant with improved chloride sensitivity⁷⁵. Similar approaches have been used for the development of sensors for Ca^{2+76} and redox potential⁷⁷.

This strategy of sensor design is relatively simple as it mainly relies on inducing point mutations in the primary sequence of the fluorescent protein. However, the introduced mutations often increase the flexibility of the tertiary structure and decrease the protection of the chromophore. Therefore, these sensors are often also sensitive to environmental conditions other than the analyte of interest, thus limiting their specificity. However, the main drawback is that most analytes of interest do not affect the fluorescence of GFP-like proteins. Especially larger molecules are shielded from interaction with the chromophore by the β -barrel, making it nearly impossible to use this approach for the design of genetically encoded sensors for those molecules.

1.3.2 Single fluorophore sensors based on circular permuted fluorescent proteins

In order to overcome the limitation of intrinsic environmental sensitivities of fluorescent proteins and to develop sensors for a broader range of analytes, a fluorescent protein needs to be fused with an appropriate sensing domain. As mentioned above, the β -barrel structure of GFP-based fluorescent proteins protects the chromophore in its center and is very rigid. While this provides great stability, it creates challenges for its use as a reporter domain in a genetically encoded sensor, as conformational changes of a sensing domain upon analyte binding are barely relayed to changes of fluorescence⁷⁸. For example, two voltage sensors created by fusion of GFP into voltage-gated ion channels exhibited a fluorescence change of only around 5% and 0.5%^{79,80}. A crucial step in overcoming this limitation was the development of circular permuted fluorescent proteins (cpFPs)^{81,82}. A circular permutation is a rearrangement of the protein sequence which leads to a fusion of the original C- and N-termini with a short linker and creates new termini⁸³. In the case of GFP-based proteins, cpFPs are usually created by relocating the sequence for the amino acids 145-238 to the beginning of the protein, making the amino acids 145 and 144 the new N- and C termini, respectively (**Figure 4A**). cpFPs were shown to robustly assemble in a very similar structure than wild type FPs. They retain their fluorescent spectra and show slightly elevated pK_a values⁸¹, reflecting increased flexibility of the FPs⁷⁸. As the new termini are located closer to the chromophore, fusion of a sensing domain allows better coupling of conformational changes to reporter fluorescence⁸⁴. The new structure of cpFPs usually decreases the rigidity of the β -barrel⁷⁸ and the newly introduced termini create irregularities in the highly organized β -barrel. Therefore, these proteins generally exhibit lower brightness than their non-mutated counterparts due to quenching of the chromophore by interaction with the solvent⁸⁵. Conformational changes induced by analyte binding to the sensing domain can lead to a stabilization of the β -barrel and protection of the chromophore from the solvent, leading to a profound increase of fluorescence (**Figure 4B**).

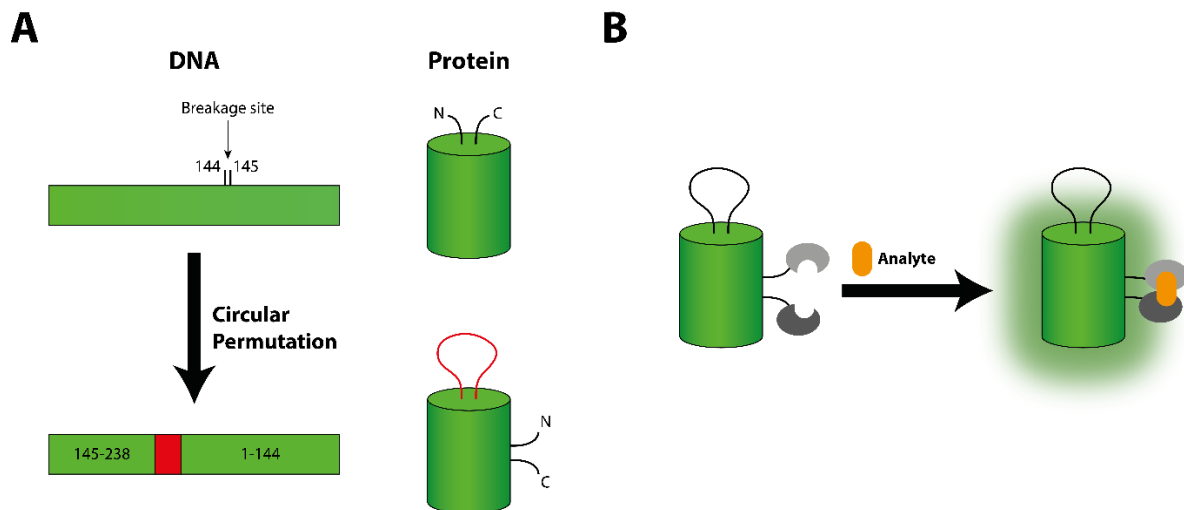


Figure 4: (A) Principle of circular permutation to create novel C- and N-termini. **(B)** Genetically encoded sensor based on a cpFP design. (Adapted from Wang et al.⁸⁶)

This design strategy can yield sensors with exceptionally high dynamic range and signal-to-noise ratio. Already the first Ca^{2+} sensor designed according to this principle exhibited an at this time unprecedented 7-fold increase in fluorescence upon binding of Ca^{2+} ⁸¹, and newly developed sensors are several orders of magnitude better²⁰. A positive side-effect of the high responsiveness of cpFP-based sensors is that also sensing domains that only display small conformational changes can be used to generate sensors with sufficient signal-to-noise range. This allows development of sensors for a higher variety of analytes. Another advantage is that these sensors only contain one fluorescent protein and therefore occupy a smaller bandwidth on the spectrum of fluorescence. This allows simultaneous dynamic measurement of two or more independent analytes^{22,87}. Single fluorophore sensors require also less sophisticated measurement setups and can be applied easier and cheaper, thus increasing their practical applicability.

Despite these advantages, cpFP-based single emission sensors exhibit some general drawbacks. As discussed above, cpFPs are more exposed to the solvent, leading usually to decreased fluorescence. While this allows the generation of sensors with that large dynamic range, it also increases the vulnerability of the sensor to environmental influences. Therefore, cpFP-based sensors are usually more sensitive to pH or small ions than sensors designed using other strategies⁷⁸. Furthermore, these sensors are usually imaged intensimetric using a single excitation, single emission paradigm. This renders these sensors more vulnerable to artifacts based on other factors that influence fluorescence intensity, such as sensor leakage, photobleaching, or changes in the concentration of the sensor, e.g., by changes of the cell volume. The two previous drawbacks can be generally addressed by co-expressing the sensor of interest with a pH sensor⁸⁷ or another fluorescent protein of a different color to perform

ratiometric imaging⁵⁹, respectively. However, this will negate the advantage of using only a single color for imaging and reduce the possibility of multiplexing different sensors. Finally, the development of a new cpFP-based sensors is rather labor intensive because they are usually constructed via rational design⁵².

1.3.3 FRET-based sensors

Next to the use of cpFPs, the other major strategy of developing genetically encoded sensors is based on FRET. In general, most FRET-based sensors consist of a sensing domain that is connected via a flexible linker to two fluorescent proteins forming a FRET pair. Analyte binding to the sensing domain induces a conformational change that alters the distance between the two fluorescent proteins and therefore FRET efficiency (**Figure 5**).

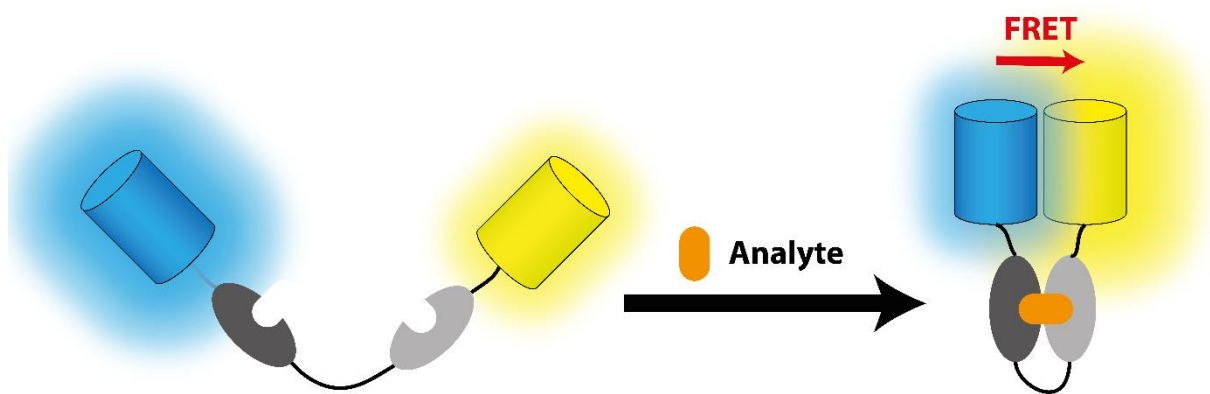


Figure 5: Principle of a FRET-based sensor

As discussed above, there are three main conditions affecting the FRET efficiency of a given fluorescent system, namely the distance between the fluorophores, the spectral overlap between donor emission and acceptor excitation and the orientation of the fluorophore dipole moments relative to each other. Therefore, these three factors need to be considered when designing a FRET-based sensor.

The distance change between the fluorophores depends on the sensing domain. A good sensing domain needs to be able to bind the analyte of interest with high specificity and respond to binding with a profound conformational change that alters the distance between the fluorophores. A class of proteins commonly exploited for the selection of a sensing domain are the bacterial periplasmic proteins (PBPs)⁸⁸. These proteins, which are located between the inner and outer membranes of gram-negative bacteria, bind molecules such as ions, amino acids, and sugars with high specificity, thereby supporting the uptake of these molecules⁸⁹. They are also often dubbed “Venus flytrap proteins”⁹⁰ as they consist of two domains linked with a hinge-region and undergo strong conformational changes upon analyte binding⁹¹. These properties make them ideal for the design of FRET based sensors via attachment of the

fluorescent proteins, as the conformational change reliably changes the distance between donor and acceptor. PBPs often bind the analyte with high affinity which means they can be saturated at concentrations below physiological levels. Therefore, the introduction of additional mutations can be necessary to lower the affinity to physiological levels while preserving specificity⁸⁹.

The spectral overlap between donor emission and acceptor excitation depends on the fluorescent proteins chosen for the FRET pair. The most common combination of fluorescent proteins for the formation of a FRET pair has been based on CFP and YFP⁹². FRET pairs using early versions of these fluorescent proteins suffered from certain drawbacks such as a comparably low quantum yield of CFP⁸⁴ and pH sensitivity of YFP⁹³. While those problems have been partially addressed with newer mutants^{32,94}, imaging of this FRET pair involves excitation of CFP with violet light prone to induce phototoxicity⁹⁵. Also, a certain spectral overlap between the emission spectra of donor and acceptor can be a confounder (**Figure 2B**). More recently, the use of FRET pairs consisting of green and red fluorescent proteins has emerged as an alternative to overcome these limitations. Excitation of the donor GFP is less phototoxic and spectral overlap between both emission spectra is reduced. However, brightness of red fluorescent proteins is usually low which hampers intensity-based FRET measurements. In addition, red fluorescent proteins often tend to dimerize, which interferes with FRET⁹². The development of monomeric red fluorescent proteins with higher brightness have improved the utility of this FRET pair⁹⁶.

Another interesting approach is the use of a bioluminescent proteins called luciferases as a donor for the FRET pair with a YFP based acceptor. Luciferases convert a consumable substrate (luciferin) to luminescence⁹⁷, therefore emit light without the need for excitation by light. The main advantage of this approach, also termed bioluminescence resonance energy transfer (BRET), is that the absence of sample illumination essentially eliminates excitation-induced artifacts⁹⁸.

Improving FRET efficiency by optimizing the relative orientation of the dipole moments of donor and acceptor helps to increase the dynamic range of a given sensor and therefore its ability to detect small signals over background noise. The orientation depends mainly on the length and flexibility of the linker domains connecting the fluorescent proteins with the sensing domain as well as on the orientation of the fluorescent protein. As the dipole orientation is usually difficult to predict, this is the main step of optimization and screening when designing a FRET-based genetically encoded sensor²⁵. For long, flexible linkers the orientation factor is usually considered to be $\kappa^2 = 2/3$, equal to the factor for free rotating molecules. As the theoretical values for the orientation factor κ^2 range from 0 to 4, this is far from ideal dipole-dipole

alignment. Shorter and more rigid linkers can maintain a fluorophore in a more favorable configuration, thereby increasing the orientation factor. An important way for aligning fluorescent proteins is the use of previously discussed cpFPs. As circular permutation introduces new C- and N-termini at different locations of the β -barrel, the orientation of a fluorescent protein can be influenced, and FRET efficiency and dynamic range can be dramatically improved⁹⁹. However, long linkers can increase the distance between the fluorophores and therefore the FRET gain upon binding by decreasing baseline FRET efficiency¹⁰⁰. Therefore, no general design principle for the linker peptides can be postulated and linker sequences need to be optimized individually based on a given sensor.

Compared to cpFP-based sensors, FRET-based genetically encoded sensors are, thanks to their modular design, comparably straight-forward to develop given an appropriate sensing protein is available. However, the sensitivity and dynamic range can often be improved by laborious introduction of point mutations in the sensing domain or variation of the linker length¹⁰¹. Another advantage of genetically encoded sensors is that they can be imaged ratiometric and therefore are not affected by potential confounders such as bleaching or changes in sensor concentration.

However, the dynamic range of FRET sensors is typically smaller than that of cpFP-based sensors, making the detection of smaller signals more challenging. Also, measuring FRET requires either recording of two different colors at the same time or fluorescent lifetime measurements (FLIM). Both imaging modalities are more challenging than imaging of a single fluorophore sensor and require additional equipment. As a FRET sensor consists of two different fluorescent proteins, they occupy a considerable bandwidth of the visible spectrum which is an obstacle for simultaneous imaging of two different sensors. While multiplexing FRET sensors can be achieved, it generally requires spectral unmixing and is therefore technically more challenging¹⁰².

1.3.4 Considerations for live imaging with genetically encoded sensors

Live imaging experiments using genetically encoded sensors are a powerful tool that can help to understand biological processes by following them with exceptional temporal and spatial resolution and precision. However, interpretation of the obtained data is not always straightforward. As discussed above, genetically encoded sensors can have different advantages and drawbacks depending on their design strategy, but there are also general, design-independent caveats and limitations that can lead to false-positive or false-negative results. Therefore, it is important to understand the general limitations of genetically encoded

sensors and to consider them during the design of live cell imaging experiments as well as the interpretation of the obtained data.

1.3.4.1 Affinity

One important aspect to consider for the application of genetically encoded sensors is their affinity for the analyte of interest in relation to its expected concentration. Concentrations of molecules can differ significantly between different organisms, cell types or subcellular compartments. For instance, while the neuronal cytosolic Ca^{2+} concentration is kept low and ranges from around 50-100 nM¹⁸, the neuronal endoplasmic reticulum, which acts as a Ca^{2+} storage, contains around 150 μM of Ca^{2+} ^{103,104}. Furthermore, the extracellular concentration in the mammalian brain even reaches millimolar concentrations^{105,106}. It is no surprise that a Ca^{2+} sensor optimized towards high affinity for cytosolic measurements (e.g., K_D of 46 nM for GCaMP8s²⁰) will be easily saturated when expressed in the endoplasmic reticulum. Such a sensor would remain saturated even during bigger changes of the Ca^{2+} concentration in the endoplasmic reticulum. For such a purpose, a sensor with lowered affinity (e.g., K_D of 150 μM ¹⁰³) needs to be employed. However, such a sensor would not be able to resolve comparably small Ca^{2+} dynamics in the cytosol. These considerations demonstrate that the choice of a sensor with inappropriate affinity can lead to false-negative results. Therefore, the expected analyte concentration should be considered when planning live cell imaging with genetically encoded sensors.

1.3.4.2 Specificity

Another important sensor interference to consider is the specificity of a given sensor for the analyte. Ideally, the sensor signal only responds to the analyte of interest and other molecules do not influence sensor output. However, off-targets exist and can be generally classified in direct and indirect off-targets¹⁰⁷. Direct off-targets influence the sensor signal by acting as an additional ligand. For instance, the genetically encoded sensor for sucrose FLIPSuc90 $\mu\Delta$ 1Venus¹⁰⁸ was shown to respond to trehalose with similar affinity as for sucrose and was used for trehalose monitoring¹⁰⁹.

It is common practice to screen for off-targets while developing new sensors by measuring the sensor response to structurally similar target molecules (e.g., other sugars for a glucose sensor). However, a much higher number of molecules and conditions than can reasonably be screened for are present in a biological system and off-target effects cannot be ruled out with full confidence. Therefore, it is particularly important to be aware of potential off-target effects and analyze the results obtained with imaging of genetically encoded sensors with a critical mind. If available, using two or more different sensors, ideally with different sensing domains, can help to improve the robustness of an experiment.

1.3.4.3 Temperature dependence

Due to their nature as proteins, the function of genetically encoded sensors is temperature dependent. As the GFP expressing organism *Aequoria victoria* is native to the Pacific Ocean, it is not surprising that the temperature optimum of GFP differs from the mammalian one of 37°C. Increasing the temperature from 20°C to 37°C or above usually quenches the fluorescence intensity of GFP and its derivatives^{110,111} and also affects fluorescence anisotropy¹¹² and lifetime¹¹³. Therefore, temperature shifts during an imaging experiment can also affect the signal of genetically encoded sensors. Consequently, unless required by the experimental conditions, temperature needs to be maintained absolutely constant throughout the experiment to avoid artifactual signal changes¹¹⁴. This is particularly important during *in vivo* experiments, where anesthesia or the surgical preparation of the organ of interest lowers the temperature of the imaging field¹¹⁵ thereby producing temperature artifacts. However, temperature can also affect the affinity of a sensor. For instance, the genetically encoded ATP sensor ATeam1.03 shows a higher affinity at 25°C compared to 35°C⁵⁷. Depending on the physiological ATP levels of the cell to be measured, imaging at room temperature can lead to saturation of ATeam1.03 and an absence of a response to a stimulus does not necessarily mean that the ATP levels did not change. Therefore, the temperature-sensitivity of a genetically encoded sensor should be considered when constructing the respective imaging set-up and designing an experiment.

1.3.4.4 pH sensitivity

Another important environmental influence on genetically encoded sensors is their pH sensitivity. As previously described, sensors based on cpFPs usually display a strong pH sensitivity, but also FRET based sensors may react to changes in pH. Within the physiological pH-range, fluorescent proteins generally get quenched by more acidic conditions^{116,117}. Therefore, most single fluorophore sensors show a signal decrease upon acidification. For FRET sensors, pH responses can be more complex, as both fluorescent proteins involved can display different pH sensitivities and the final signal depends on the evolving ratio. Additionally, pH changes can also induce conformational changes in the binding domain that affect the sensor signal or the affinity of analyte binding, further complicating the pH response of a given sensor.

While temperature changes can easily be avoided by appropriate technical approaches, e.g. superfusing cells or exposed organs with pre-heated solutions or heating imaging stages, limiting pH changes during an experiment is considerably more difficult since intracellular pH is affected by a plethora of physiological and pathological processes and its regulation involves a complex network of processes¹¹⁸. For instance, neuronal activity as well as neuronal inhibition leads to acidification of the cytosol^{119 120}. In such a scenario, a response of a

genetically encoded sensor can also stem from a pH-mediated artifact rather than an actual change in analyte levels²⁴. One approach to address this problem is co-expression and simultaneous imaging of a pH sensor with the sensor of interest, which allows mathematical correlation of pH induced changes in both sensors, and therefore correction¹²¹. While this is a powerful approach that can often control for pH artifacts, it ignores that pH changes can also act as a second messenger to regulate biochemical pathways¹²² and therefore can potentially elicit real changes in the analyte level. Therefore, methods that uncouple pH-dependent analyte changes from pH-induced sensor artifacts would be helpful to increase the robustness of live cell imaging experiments with genetically encoded sensors.

2 Aims

Genetically encoded fluorescent sensors are powerful tools that enable dynamic measurements of a wide range of analytes with high temporal and spatial resolution. However, as discussed above, they do suffer from certain drawbacks and their results can be compromised due to factors such as inappropriate affinity, recognition of off-targets or sensitivity to temperature and pH fluctuations. This thesis aims to address some of the difficulties that affect genetically encoded sensors. To that end, the current project had two different objectives.

1. Neuronal $[K^+]$ is directly affected by neuronal activity. However, precise measurements of neuronal K^+ dynamics have been hampered by technological limitations. While the recent development of several genetically encoded sensors for K^+ holds great promise to overcome these limitations, none of these sensors has been systematically tested in neurons. However, as a recent study pointed out, the “physiological characterization of potassium indicators needs to be performed carefully and may need to occur in the exact cell type and physiological context of interest”²³. Therefore, **the first aim of this thesis** was to characterize the genetically encoded K^+ sensor I_c-LysM GEPII 1.0 towards its capacity to resolve K^+ dynamics in response to neuronal activity, both *in vitro* and *in vivo*.
2. As previously discussed, genetically encoded sensors are usually sensitive to pH changes, leading to false positive responses to stimuli that are accompanied by pH changes. However, pH can also act as a second messenger and can therefore affect biochemical pathways and lead to changes in analyte levels. We encountered such a scenario when we observed an increase in the FRET signal of the genetically encoded lactate sensor Laconic in neurons in response to GABA. As pH is known to impact cellular metabolism, this increase could stem from a real lactate increase or a pH artifact. We wanted to disentangle these two potential effects on the FRET signal of Laconic and help other scientists that encounter similar problems. Therefore, **the second aim of this thesis** was to develop a method that isolates the pH sensitivity of genetically encoded sensors from the physiologic response of the analyte. We aimed for a simple, cost-effective method that can be easily applied when encountering such a scenario without large additional investment.

3 Articles

3.1 Study I: Probing Intracellular Potassium Dynamics in Neurons: *In vitro* and *In vivo* Assessment of a Genetically Encoded Sensor

Bernhard Groschup^{1,2}, Gian Marco Calandra^{1,2}, Constanze Raitmayr¹, Joshua Shrouder¹, Gemma Llovera¹, Asal Ghaffari Zaki^{3,4}, Sandra Burgstaller^{5,6}, Helmut Bischof^{6,7}, Emrah Eroglu^{3,4}, Arthur Liesz^{1,2,8}, Roland Malli^{6,9}, Severin Filser^{1,10,11} & Nikolaus Plesnila^{1,2,7,11*}

¹Institute for Stroke and Dementia Research (ISD), LMU University Hospital, LMU Munich, Munich, Germany. ²Graduate School of Systemic Neurosciences, LMU Munich, Planegg-Martinsried, Germany. ³Regenerative and Restorative Medicine Research Center (REMER), Research Institute for Health Sciences and Technologies (SABITA), Istanbul Medipol University, Istanbul, Turkey. ⁴Molecular Biology, Genetics and Bioengineering Program, Faculty of Engineering and Natural Sciences, Sabanci University, Istanbul, Türkiye. ⁵Institut für Klinische Anatomie und Zellanalytik (Österbergstraße 3), Eberhard Karls Universität Tübingen, Germany. ⁶Gottfried Schatz Research Center, Molecular Biology and Biochemistry, Medical University of Graz, Neue Stiftingtalstraße 6/4, 8010 Graz, Austria. ⁷Department of Pharmacology, Toxicology and Clinical Pharmacy, Institute of Pharmacy, University of Tübingen, Auf der Morgenstelle 8, 72076 Tuebingen, Germany. ⁸Munich Cluster for Systems Neurology (SyNergy), Munich, Germany. ⁹BioTechMed-Graz, Mozartgasse 12/II, 8010 Graz, Austria. ¹⁰Deutsches Zentrum für Neurodegenerative Erkrankungen (DZNE), Light Microscope Facility (LMF), Bonn, Germany. ¹¹These authors contributed equally: Severin Filser and Nikolaus Plesnila *email: nikolaus.plesnila@med.uni-muenchen.de

Abstract

Neuronal activity is accompanied by a net outflow of potassium ions (K^+) from the intra- to the extracellular space. While extracellular $[K^+]$ changes during neuronal activity are well characterized, intracellular dynamics have been less well investigated due to lack of respective probes. In the current study we characterized the FRET-based K^+ biosensor lc-LysM GEPII 1.0 for its capacity to measure intracellular $[K^+]$ changes in primary cultured neurons and in mouse cortical neurons *in vivo*. We found that lc-LysM GEPII 1.0 can resolve neuronal $[K^+]$ decreases *in vitro* during seizure-like and intense optogenetically evoked activity. $[K^+]$ changes during single action potentials could not be recorded. We confirmed these findings *in vivo* by expressing lc-LysM GEPII 1.0 in mouse cortical neurons and performing 2-photon fluorescence lifetime imaging. We observed an increase in the fluorescence lifetime of lc-LysM GEPII 1.0 during periinfarct depolarizations, which indicates a decrease in intracellular neuronal $[K^+]$. Our findings suggest that lc-LysM GEPII 1.0 can be used to measure large changes in $[K^+]$ in neurons *in vitro* and *in vivo* but requires optimization to resolve smaller changes as observed during single action potentials.

Introduction

Potassium ions (K^+) are the most abundant intracellular cations in most cell types and are involved in an array of vital processes both on the cellular and supracellular level¹. These processes notably include the diffusion or transport of K^+ across membranes to form an electrochemical gradient. Together with the electrochemical gradients of other ions, it makes up the membrane potential and can be utilized both as energy storage and for intracellular signaling².

Dynamic shifts of intracellular K^+ concentrations are fundamental during signal transduction by neurons, which transmit information via action potentials. After the initial depolarization phase of an action potential, the neuronal membrane is repolarized by the outflow of K^+ through voltage-gated K^+ channels or K^+ leak channels to allow a new action potential to occur^{3,4}. Therefore, the dynamics and the regulation of K^+ ions play a crucial role in neurotransmission, and changes in brain K^+ homeostasis are known to influence neuronal excitability^{5,6} as well as action potential shape^{7,8}. In addition, restoration of the ion gradients after activity, mainly achieved via the Na^+/K^+ -ATPase, is one of the primary energy-consuming processes in neurons, making ion homeostasis a key player in brain energetics and its regulation^{9,10}. Perturbed K^+ dynamics or mutations of K^+ channels are directly responsible for many pathological conditions, such as epilepsy^{11,12} and migraine^{13,14}. In contrast, other disorders, such as ischemic stroke, are often exacerbated or accompanied by perturbed K^+ homeostasis¹⁵.

So far, technical limitations in measuring K^+ fluxes in neurons have hampered our understanding of neuronal K^+ dynamics. While electrode-based K^+ measurements are fast and accurate, they are invasive, can measure K^+ only very locally, and are primarily used to assess extracellular K^+ dynamics^{16,17}. Imaging methods such as MRI^{18,19} or live cell imaging with K^+ sensitive dyes²⁰ can potentially overcome these limitations; however, they lack (sub-)cellular resolution or specificity.

The development of genetically encoded fluorescent sensors for K^+ ions holds great potential for overcoming those limitations, as they can be expressed in a cell-type-specific manner or with subcellular localization. In addition, they allow observation of K^+ dynamics in single neurons and whole tissues non-invasively and can be measured with high temporal resolution. We and others²¹, recently developed novel FRET-based genetically encoded K^+ ion indicators (GEPiIs) with high specificity. While these biosensors may help to understand K^+ dynamics in the brain, they have been mainly tested in non-neuronal cells and have not been characterized neither *in vitro* nor *in vivo* for their feasibility to measure K^+ dynamics in neurons.

Therefore, the aim of the current is to characterize the capacity of GEPs to observe K^+ changes during neurotransmission, both *in vitro* and *in vivo*. To achieve this goal, we expressed the K^+ sensor lc-LysM GEP 1.0 in primary cultured neurons or in the cortex of living mice. We then recorded K^+ signals of individual neurons during either spontaneous or evoked neuronal activity to assess the degree to which lc-LysM GEP 1.0 can resolve K^+ dynamics during neuronal activity.

Methods

Plasmids and cloning

We used plasmids carrying the genetically encoded K^+ sensor I_c-LysM GEPII 1.0 with different subcellular targeting sequences as previously described²¹. The sensor was targeted either to the cytosol (cyto), the plasma membrane (SubPM), or the mitochondria (mito). To achieve AAV-mediated expression, we subcloned the ORFs encoding the different variants of I_c-LysM GEPII 1.0 in AAV backbones under the control of a CAG promoter for ubiquitous expression (pAAV-CAG-GFP, Addgene #37825), a hSyn promoter for neuronal expression (pAAV-hSyn-eGFP, Addgene #50465) or a GFAP promoter for astrocytic expression (pAAV.GFAP.iGABASnFr, Addgene #112172). All three backbones were linearized by cutting out the existing transgenes using BamHI and HindIII restriction sites. These restriction sites were added to cyto-I_c-LysM GEPII 1.0 and SubPM-I_c-LysM GEPII 1.0 via overhang PCR to insert them directly via subcloning. Since mito-I_c-LysM GEPII 1.0 contains a BamHI restriction site, this transgene was inserted using the Gibson Assembly method. After cloning, DNA was transformed into competent DH5 α E. coli bacteria, colonies were screened via colony PCR and candidate clones were confirmed by sequencing before amplification and AAV production.

pAAV.Syn.NES-jRCaMP1b.WPRE.SV40 was a gift from Douglas Kim & GENIE Project (Addgene plasmid # 100851; <http://n2t.net/addgene:100851>; RRID: Addgene_100851). For bacterial expression of jRCaMP1b, the construct was subcloned into EKAR2G_design1_mTFP_wt_Venus_wt vector (Addgene plasmid # 39813) using the restriction sites BamHI and XhoI.

For imaging the concentration of cytosolic calcium ions *in vitro*, we used pGP-AAV-syn-jGCaMP8m-WPRE, a gift from the GENIE Project (Addgene plasmid #162375)²². For optogenetic stimulation, we used pAAV-Syn-ChrimsonR-tdT, a gift from Edward Boyden (Addgene plasmid #59171)²³.

Protein purification:

Bacterial expression plasmids containing I_c-LysM GEPII 1.0 and jRCaMP1b were transformed into Rosetta (DE3) competent cells. For the selection of I_c-LysM GEPII 1.0 and jRCaMP1b positive cells, kanamycin and ampicillin were used, respectively. For purification of the biosensors, positive clones were inoculated in 5 mL LB with appropriate antibiotic, and after 8 hours, the cultures were transferred into 250 mL LB plus antibiotic and incubated at 37°C. At an OD value between 0.4 and 0.6 protein expression was induced using IPTG with a final concentration of 0.5 mM and further incubated for 16 hours at 18 °C. Purification of the 6x histidine-tagged biosensors was performed using gravity-based Ni-NTA affinity chromatography method as described elsewhere²⁴. Purified proteins were concentrated using

Ultracel® Regenerated Cellulose (30kDa MWCO) Amicon tubes and kept at -80°C for further usage. The functionality of the purified biosensors was tested using a SpectraMax i3 Multi-Mode Microplate Reader. Samples were loaded on a 96-well plate with a solid black bottom. The intensimetric calcium biosensors jRCaMP1b were excited at 535/25 nm and emission was collected at 595/35 nm. The FRET-based biosensors Ic-LysM GEPII 1.0 were excited with 430/9 nm and emission was collected at 485/9-535/15 nm, respectively.

AAV Production

Adeno-associated viral particles were produced in HEK293T cells grown in DMEM supplemented with 10% FBS and 100 U/mL Penicillin-Streptomycin in a humidified incubator at 37°C/5% CO₂. Cells were grown to 70-80% confluency and triple transfected with pHelper, pAAV-DJ (both from Cell Biolabs, Cat: VPK-400-DJ) and a pAAV-ITR-vector carrying the transgene. Triple transfection was achieved using polyethylenimine (PEI) titrated to pH 7.0. Two to three days after transfection, cells were detached using 1/80 of the culture volume of 0.5 M EDTA in PBS pH 7.4 and AAV particles were extracted using the AAVpro® Purification Kit (All serotypes) from Takara Bio Inc. (Cat: #6666). Cells were centrifuged at 1700 g for 10 min at 4°C and the supernatant was discarded. The resulting cell pellet was lysed by vortexing it with 650 µL of AAV Extraction Solution A plus. Subsequently, cell debris was pelleted at 14 000 g for 10 min at 4°C and the supernatant was collected in a new tube. Finally, 65 µL of AAV Extraction Solution B was added, and the viral solution was aliquoted and stored for further use at -80°C. AAV titration was performed by qPCR using the AAVpro® Titration Kit (for Real-Time PCR) Ver.2 from Takara (Cat: #6233) according to the manufacturer's instructions. Titration was performed using primers that annealed in the ITR repeats of the viral backbone (ITR F: GGAACCCCTAGTGATGGAGTT and ITR R: CGGCCTCAGTGAGCGA).

Preparation of cryo-stocks of mixed cortical cultures

Cryopreserved mixed cortical cell culture stocks were prepared from E17 embryos of Sprague Dawley rats. Brains were removed and immediately placed in ice-cold HBSS supplemented with 7 mM HEPES pH 7.4. Cortices were dissected, meninges were removed, and the tissue was cut into small pieces with a scalpel. Then the tissues from all embryos of one litter were digested in HBSS supplemented with 0.5% Trypsin and 10 µg/mL DNase I for 15 min at 37°C. Digestion was stopped by the addition of MEM supplemented with 10% FBS, the tissue was washed twice with HBSS and subsequently triturated using a glass Pasteur pipette coated with 4% BSA in HBSS. After counting the concentration of cells in the suspension, the cell suspension was diluted with MEM supplemented with 10% FBS to 2 million cells per mL. Finally, DMSO was added to a volume fraction of 10% and the solution was aliquoted. Aliquots were cryopreserved by placing them in a freezing container filled with isopropanol at -80°C

over night. The next morning, the aliquots were transferred into a liquid nitrogen tank for long-term storage.

Mixed cortical cell cultures from cryo-stocks

All cell culture reagents were purchased from Gibco. Mixed cortical cultures were plated on 15 mm round glass cover slips coated with Poly-D-Lysine at a density of 100,000 cells per cover slip. A cryopreserved aliquot was thawed at 37°C and diluted in an appropriate amount of culture medium (Neurobasal-A medium, no D-glucose, no sodium pyruvate supplemented with 1x B27, 10 mM glucose, 2 mM GlutaMAX™, 1 mM sodium pyruvate and 100 U/mL Penicillin-Streptomycin). The cell suspension was plated on the cover-slips placed in 12-well plates and maintained in a humidified incubator at 37°C/5% CO₂. Half of the culture medium was replaced twice a week and cells were used after 22-24 days. For transgene expression, cells were transduced 3-4 days before the experiment with the appropriate AAV at a MOI of 1000.

Immunostainings

For immunocytochemistry, mixed cortical cultures were washed with PBS and subsequently incubated with 4% paraformaldehyde (PFA)/4% sucrose in PBS for 15 min at room temperature (RT). Fixed cells were washed three times with PBS, incubated with 50 µM NH₄Cl in PBS for 10 min at RT, followed by another three washes with PBS. Fixed cells were then permeabilized using 0.1% TritonX in PBS for 3 min at RT and blocked with blocking buffer (0.2% BSA, 0.2% FCS, 0.02% fish-skin gelatin in PBS) for 1 h at RT. Subsequently, cultures were incubated with primary antibodies against gp-NeuN (Synaptic Systems, 266 004) and mouse-GFAP (Cell Signaling, #3670) diluted in blocking buffer for 2 h at RT. Subsequently, primary antibodies were removed, cells were washed 3 times with PBS for 5 min and then incubated with anti-guinea pig- AlexaFluor® 647 (Jackson, 706-606-148) and anti-mouse AlexaFluor® 594 (Jackson, 715-586-150) diluted in blocking buffer for 1 h at RT. During the last 5 minutes of this step, DAPI (5 µg/mL) was added to stain the nuclei. Finally, coverslips were washed three times with PBS for 5 min each and mounted on microscopy slides. Cells were imaged at a confocal microscope.

For immunohistochemistry, animals virally transduced with AAV-hSyn-Ic-LysM GEPII 1.0 were anesthetized with MMF and transcardially perfused with PBS followed by 4% PFA in PBS until the liver was devoid of blood. Brains were extracted, post-fixed in 4% PFA in PBS overnight and then stored in PBS at 4°C until further use. Brains were mounted in 4% agarose and sectioned using a vibratome to create 100 µm thick brain slices. PFA-fixed brain sections were incubated in a blocking and permeabilizing primary antibody buffer solution (1% BSA, 0.1% fish-skin gelatin, 0.1% Triton X-100, 0.05% Tween 20 in PBS) with rabbit anti-NeuN (Abcam,

ab177487) antibodies at 1:100 dilution on a rotary shaker at 4°C for 2-3 days. Sections were then washed in PBS three times for 30 minutes and incubated with a secondary antibody buffer mix (0.2% BSA, 0.2% FCS, 0.02% fish-skin gelatin in PBS) containing 1:300 anti-rabbit AlexaFluor® 647 (Jackson, 711-606-152) antibody at 4°C on a rotary shaker for two days. Sections were then washed three times in PBS and during the last washing step, DAPI was added at a concentration of 5 µg/mL for 30 minutes to stain the nuclei. Washing using PBS was repeated three times for 30 minutes prior to mounting the sections on glass coverslips. Brain section overviews were imaged with a confocal microscope using a 10x air objective.

Live cell imaging

For live cell imaging of mixed cortical cultures expressing either GCaMP8m or lc-LysM GEPII 1.0, coverslips with the cultures were transferred in an open imaging chamber and placed on an inverted microscope. The microscope was equipped with a 20x air objective (NA 0.8), an LED light source, an emission image splitter, and a CCD camera. Cells were constantly superfused with aCSF (in mM: 125 NaCl, 2.5 KCl, 1.25 NaH₂PO₄, 26 NaHCO₃, 1 MgCl₂, 1.25 CaCl₂, 2 glucose, 0.5 sodium lactate, 0.05 sodium pyruvate) gassed with 5% CO₂/95% air to maintain a stable pH at room temperature. GCaMP8m was excited with 10 Hz at 469 ± 19 nm and emission was collected with a bandpass filter at 525 ± 25 nm. For FRET imaging of lc-LysM GEPII 1.0, cells were excited at 436 ± 10 nm and emitted light was split at 515 nm on the camera for simultaneous recording of mseCFP and cpV using a dichroic mirror (t515lp, Chroma). Emission of the individual channels was collected using bandpass filters (480 ± 15 nm for mseCFP, 535 ± 15 nm for cpV). Depending on the experiment, cells expressing lc-LysM GEPII 1.0 were excited with frequencies ranging from 0.2 to 10 Hz. Exposure time, LED power, and excitation frequencies were adjusted to minimize bleaching and phototoxicity while still obtaining sufficient signal-to-noise ratio. The remaining bleaching was corrected using a custom-written Python script and the data was represented as FRET ratio cpV/mseCFP.

Optogenetic stimulation

For optogenetic stimulation, we co-transduced cultures with AAV-Syn-ChrimsonR-tdT and either AAV-CAG-lc-LysM GEPII 1.0 or AAV-Syn-GCaMP8. Optogenetic stimulation was achieved by placing a red LED (M617L4, Thorlabs) over the cells during imaging using a custom-made 3D-printed holder. To maximize stimulation strength, the emitted light was collected using an aspheric condenser lens. A custom-made microcontroller-gated LED driver allowed programmable and precise light pulses for stimulation. Cells were stimulated with trains of 10 ms light pulses at 1 Hz, allowing enough time in between stimulation trains for complete recovery of the signal.

To avoid imaging artifacts from the stimulation light, a 590 nm long pass filter was placed in front of the LED and additional 550 nm short pass filters were added in the emission light path. The intensity of the excitation light for either GCaMP8m or I_c-LysM GEPII 1.0 was minimized to avoid cross-stimulation of ChrimsonR. If the minimal LED power led to neuronal stimulation, it was further reduced using a neutral density filter OD 1.3.

Animals

Two to three months old male C57BL/6J mice were used. The animals were group-housed under pathogen-free conditions and bred in the animal housing facility of the Center of Stroke and Dementia Research, with food and water provided ad libitum (21 ± 1°C, at 12/12-hour light/dark cycle). All experiments were carried out in compliance with the ARRIVE guidelines and the German National Guidelines for Animal Protection.

Cranial window implantation and stereotactic virus injection

Before use, surgical tools were sterilized in a glass-bead sterilizer (Fine Science Tools). Mice were anesthetized by an i.p. injection of medetomidine (0.5 mg/kg), midazolam (5 mg/kg), and fentanyl (0.05 mg/kg). Subsequently, mice were placed onto a heating blanket (37 °C), and the head was fixed in a stereotactic frame. Eyes were protected from drying by applying eye ointment. The scalp was washed with swabs soaked with 70 % ethanol. A flap of skin covering the cranium was excised using small scissors. The periosteum was scraped away with a scalpel. The prospective craniotomy location over the somato-sensory cortex was marked with a biopsy punch (diameter 4 mm). The exposed skull around the area of interest was covered with a thin layer of dental acrylic (iBond Self Etch, Heraeus Kulzer) and hardened with an LED polymerization lamp (Demi Plus, Kerr). A dental drill (Schick Technikmaster C1, Pluradent) was used to thin the skull around the marked area. After applying a drop of sterile phosphate buffered saline on the craniotomy, the detached circular bone flap was removed with forceps. Subsequently, 0.5 µl of a virus suspension (AAV.PhPeb-Syn.NES- I_c-LysM GEPII 1.0, Vectorbuilder and AAV.9-Syn.NES-jRCAMP1b, Addgene #100851-AAV9 mixed 1:1 to a final concentration of 1x10¹² vg/ml) was injected via a glass capillary and Nanoliter 2020 Injector (World Precision Instruments) at a speed of 50 nl/min into the somatosensory cortex at the following coordinates: -1.5 mm rostrocaudal, -1.5 mm lateral and -0.25 mm dorsoventral. A circular coverslip (4 mm diameter) was placed onto the craniotomy and glued to the skull with histoacryl adhesive (Aesculap). The exposed skull was covered with dental acrylic (Tetric Evoflow A1 Fill, Ivoclar Vivadent), and a head-post was attached parallel to the window for head-fixing mice in subsequent imaging sessions. After surgery, mice received a s.c. dose of the analgesic Carprofen (7.5 mg/kg body weight). Anesthesia was antagonized using Atipamezol (2.5 mg/kg), Naloxone (1.2 mg/kg), and Flumazenil (0.5 mg/kg) i.p. Finally, mice

were allowed to recover in a 35°C warming chamber until full recovery. *In vivo* imaging was commenced three to four weeks after surgery.

Mouse cerebral ischemia model

For remote occlusion of the middle cerebral artery (MCAo) in mice²⁵ the left common carotid artery was exposed and the superior thyroid artery branching was cauterized. The common carotid artery was ligated and the external carotid artery (ECA) was fully occluded. A filament with a diameter of 0.21 ± 0.02 mm (6021PK10, Docol Corporation, Sharon, MA, USA) was inserted through a small incision into the ECA and advanced for 5 mm. A custom-made occlusion filament was inserted into the ECA while the Docol filament was simultaneously removed. The filament was then further advanced along the internal carotid artery towards the middle cerebral artery (MCA). After placing the under the 2-photon microscope the MCA could be occluded remotely. MCA occlusion (MCAo) caused a cortical infarct which induced periinfarct depolarizations waves (PIDs) within the surrounding tissue.

***In vivo* two-photon microscopy**

In vivo two-photon imaging was performed three weeks after cranial window implantation using a Leica SP8 DIVE 2-photon microscope equipped with a fs-laser, a 25x water immersion objective and a motorized stage. Ic-LysM GEPII 1.0 and jRCaMP1b were co-excited at 850 nm and 1045 nm, respectively, and the emission was collected at 450-500 nm and 575-625 nm with non-descanned detectors placed directly behind the objective. Laser power below the objective was kept around 50 mW to minimize phototoxicity. Throughout the imaging session, mice were anesthetized with isoflurane (1% in oxygen, 0.5 l/min) and kept on a heating pad to maintain body temperature at 37°C. XY time-lapse series (7.51 Hz) with 1 μ m axial resolution and 128 x 128 pixels per image frame of Ic-LysM GEPII 1.0 and jRCaMP1b expressing neurons were subsequently recorded at a depth of 150-200 μ m underneath the cortical surface. After 5 min of baseline recordings, periinfarct depolarizations were induced via remote MCAo and recordings were continued for further 10 min. Fluorescence lifetime measurements were subsequently analyzed in LAS X (Leica).

Results

After confirming that we were able to successfully express Ic-LysM GEPII 1.0 in a cell type-specific manner and to target different subcellular compartments (see supplementary figure 1), we explored the potential for resolving K^+ changes during neuronal activity by live cell imaging. Ca^{2+} dynamics were measured in parallel experiments using GCaMP8m to monitor neuronal activity. Ic-LysM GEPII 1.0 fluorescence was measured in rat primary mixed cortical cultures containing neurons and astrocytes.

Ic-LysM GEPII 1.0 resolves $[K^+]$ decreases in response to tetanic neuronal stimulation *in vitro*

During neuronal activity, neurons depolarize due to the inflow of sodium (Na^+) and calcium ions (Ca^{2+}) and repolarize due to the outflow of K^+ . Our goal was to investigate if and to what extent we could observe this K^+ outflow during neuronal activity using Ic-LysM GEPII 1.0. Therefore, as a proof-of-principle experiment, we induced neuronal hyperactivity in our mixed cortical cultures by inhibiting inhibitory neurons with Bicuculline, a selective GABA_A receptor antagonist. Ca^{2+} imaging confirmed that Bicuculline induced a strong, epileptic-like neuronal firing pattern. The addition of Bicuculline for 50 seconds led to an immediate increase of the intensimetric signal of GCaMP8m, which peaked within seconds (Fig 1A and C). After Bicuculline was washed out, the Ca^{2+} signal recovered to baseline. When we applied the same stimulus (50 μ M Bicuculline for 50 seconds) to cultures expressing Ic-LysM GEPII 1.0, we observed a pronounced decrease of the FRET ratio signal by $12.7 \pm 3.4\%$, indicating a reduction in the intracellular K^+ concentration (Fig 1B and D). The FRET ratio signal of the K^+ biosensor continued to decrease even after removing Bicuculline and reached a minimum after 3.9 ± 0.4 minutes before it slowly returned to baseline. These data show that Bicuculline massively reduces cytosolic K^+ levels and demonstrates the suitability of the FRET-based biosensor to monitor K^+ changes in response to neuronal hyperactivity.

Measuring Ic-LysM GEPII 1.0 fluorescence during spontaneous neuronal activity in cultured neurons

After confirming that we can resolve cytosolic $[K^+]$ alterations during intensive neuronal activity associated with large changes in intracellular ion concentrations, we aimed to investigate if we could observe K^+ changes during spontaneous neuronal activity characterized by mainly single action potentials. Ca^{2+} imaging using GCaMP8m showed that our cultures displayed spontaneous neuronal activity, which was completely abolished in the presence of tetrodotoxin (TTX), a potent inhibitor of voltage-gated sodium channels (Fig. 1E). When measuring Ic-LysM GEPII 1.0 fluorescence, the obtained recordings did not display any apparent changes of the FRET ratio signal (Fig 1F). When inhibiting neuronal activity using TTX, the FRET ratio traces

were indistinguishable from the ones before TTX application (Fig 1F). To assess whether the Ic-LysM GEPII 1.0 FRET ratio signals were due to neuronal activity or technical noise, we hypothesized that changes in the FRET ratio signal in response to actual K^+ fluctuations should be independent of signal intensity, while FRET changes due to noise should correlate with signal intensity. To test this hypothesis, we plotted the standard deviation (SD) of the full calcium traces against the average intensity of GCaMP8m. Indeed, our analysis showed no correlation between SD and signal intensity in spontaneously firing neurons (Fig. 1G, gray symbols) indicating that neuronal activity induced changes in the Ca^{2+} signal disturb the correlation between SD and intensity, while in neurons silenced with TTX these parameters correlated well (Fig. 1G, orange symbols) suggesting that the recorded signal represented background noise. Performing the same analysis for signals derived under the same conditions from neurons expressing Ic-LysM GEPII 1.0, we observed no changes between the control condition, i.e., when neurons fired spontaneously (Fig. 1H, gray symbols) and the time when spontaneous neuronal activity was inhibited by TTX (Fig. 1H, orange symbols). These data indicate that neuronal activity did not contribute to the FRET ratio signal changes of Ic-LysM GEPII 1.0., i.e., the recorded signal was background noise. These findings suggest that Ic-LysM GEPII 1.0 is not able to measure changes in intracellular $[K^+]$ elicited by single action potentials or, alternatively, that single action potentials may not result in global reductions of cytosolic $[K^+]$.

Ic-LysM GEPII 1.0 signals following optogenetic stimulation of neurons

Having identified that Ic-LysM GEPII 1.0 can resolve K^+ decreases in response to multiple but not to single action potentials, we wanted to investigate the threshold above which Ic-LysM GEPII 1.0 is able to resolve detectable $[K^+]$ changes in neurons. We combined optogenetic neuronal stimulation with FRET ratio imaging of Ic-LysM GEPII 1.0, allowing us to control neuronal activity during live imaging of $[K^+]$ changes. We chose the red-shifted optogenetic tool ChrimsonR to avoid cross-stimulation with the excitation light during imaging and co-expressed it with either GCaMP8m or Ic-LysM GEPII 1.0 (Fig. 2A). We decided to stimulate our mixed cortical cultures using low-frequency stimulation trains with increasing pulses to investigate the minimal activity required for detecting K^+ changes using Ic-LysM GEPII 1.0. We chose 10 ms as the individual pulse length as this was the shortest duration reliably eliciting a Ca^{2+} signal during imaging with GCaMP8m (see supplementary figure 2). We stimulated neurons with up to 120 light pulses and allowed the signal to return to baseline before triggering the next stimulation train. Each stimulation triggered an individual peak of $[Ca^{2+}]_i$ as evidenced by imaging with GCaMP8m (Fig. 2B, green traces); when measuring K^+ using Ic-LysM GEPII 1.0 we could observe a decrease of FRET ratio signals (normalized FRET change: $-0.63 \pm 0.12\%$) only after a stimulation train of 30 pulses (Fig 2B, purple traces and Fig. 2C), again confirming

that multiple action potentials are necessary to decrease global cytosolic $[K^+]_i$ to levels detectable with Ic-LysM GEPII 1.0. Increasing the number of pulses per stimulation train to 60 or 120 further reduced FRET ratio signals of the K^+ biosensor (normalized FRET changes $-1.12 \pm 0.37\%$ and $-2.31 \pm 0.93\%$, respectively) linearly ($R^2=0.997$).

As we expressed Ic-LysM GEPII 1.0 in neurons and astrocytes, we could also examine the effect of neuronal stimulations on cytosolic $[K^+]_i$ in neighboring astrocytes. However, we did not monitor any significant changes in the FRET ratio signal of Ic-LysM GEPII 1.0 in astrocytes, independent of the number of stimulations (Fig. 2D).

Ic-LysM GEPII 1.0 allows measuring $[K^+]_i$ in neurons *in vivo*

After having characterized Ic-LysM GEPII 1.0 in cultured cells, we wanted to investigate if we can also measure neuronal K^+ dynamics in the brain of living mice by expressing hSyn-Ic-LysM GEPII 1.0 and Syn-jRCaMP1b with AAV-based viral vectors in the cerebral cortex (supplementary figure 3). Since we observed changes of cytosolic $[K^+]_i$ only in response to intense neuronal activity *in vitro*, we expected a similar situation *in vivo*. To generate vigorous neuronal activity *in vivo*, we chose a model resulting in massive depolarizations of all neurons within a given spatial and temporal window. For this purpose, we induced focal cerebral ischemia by remote occlusion of the middle cerebral artery (MCAo; Fig. 3A), a condition well known to cause waves of massive neuronal depolarizations in the vicinity of ischemic tissue, so called periinfarct depolarizations (PIDs) while mice were placed under a 2-photon microscope for simultaneous recordings of jRCaMP1b and Ic-LysM GEPII 1.0. Within minutes of MCA occlusion, PIDs were recorded in the mouse cerebral cortex as evidenced by increases in neuronal $[Ca^{2+}]_i$ spreading in cortical tissue with the expected velocity of about 2 mm/min (Fig. 3B). As a PID also elicits an increase in cerebral blood flow that may interfere with intensity-based fluorescent imaging approaches, we decided to measure jRCaMP1b and Ic-LysM GEPII 1.0 using fluorescence lifetime imaging (FLIM), which is independent of intensity changes and therefore provides a robust readout. PIDs elicited a substantial increase in the fluorescence lifetime of jRCaMP1b by $111 \pm 30\%$ (Fig. 3C), crossing the field of view (Fig. 3D). Having now established *in vivo* FLIM microscopy, we used the same experimental protocol to check if we could measure $[K^+]_i$ changes during PIDs using Ic-LysM GEPII 1.0. For this purpose, we measured the fluorescence lifetime of the donor mseCFP as a proxy of the FRET efficiency of the sensor. After induction of PIDs by cerebral ischemia, we recorded an increase in the fluorescence lifetime of the donor fluorescence of Ic-LysM GEPII 1.0 by $5.9 \pm 2.4\%$ (Fig. 3E). When placing regions of interest in different parts of the field of view, we observed the wave-like character of the PID, confirming that the signal increase occurred in response to the PID (Fig. 3F). Since the fluorescence lifetime of Ic-LysM GEPII 1.0 is inversely correlated with the K^+ concentration, an increase in the lifetime corresponds to a decrease of neuronal $[K^+]_i$

(supplementary figure 4), as is expected during strong neuronal depolarization. As lifetime changes are not affected by intensity or potential volume changes during the PID, confounders are unlikely to account for this effect. When we correlated the normalized fluorescence lifetime values of lc-LysM GEPII 1.0 with those of jRCaMP1b, we could not observe any correlation between the two sensors before PID induction ($R = -0.019$, $p = 0.437$ - Fig 3G). This confirms that we cannot resolve intracellular $[K^+]_i$ changes using lc-LysM GEPII 1.0 during spontaneous neuronal activity. However, an analogous correlation between the FLIM values for lc-LysM GEPII 1.0 and jRCaMP1b during the rising phase of the PID revealed a highly significant correlation ($R = 0.359$, $p < 0.001$ – Fig 3H). The range of FLIM values of jRCaMP1b is considerably more extensive during PIDs, indicating that a very intense neuronal activation is required to elicit changes in $[K^+]_i$ big enough to be detected by lc-LysM GEPII 1.0. These data strongly suggest that we managed for the first time to record neuronal $[K^+]_i$ changes in the brain of living mice.

Discussion

In the current study, we characterized the functionality of the FRET-based genetically encoded K⁺ sensor lc-LysM GEPII 1.0 in neuronal cells with a specific focus on measuring changes of [K⁺]_i during neuronal activation. We provide proof-of-principle evidence that lc-LysM GEPII 1.0 can resolve differences in [K⁺]_i during intense neuronal activity in cultured cells and *in vivo*. We could not detect changes of [K⁺]_i during single action potentials, as observed during spontaneous neuronal activity, either *in vitro* or *in vivo*. However, we successfully measured [K⁺]_i changes in the mammalian brain *in vivo* using the FRET-based K⁺ biosensor if massive neuronal activity was induced.

Brain K⁺ homeostasis is crucial for proper neuronal function, including controlling neuronal excitability or neurovascular and -metabolic coupling²⁶ and its disruption, e.g., through mutations in K⁺ channels are involved in severe neurological pathologies such as epilepsy¹² or migraine²⁷. Therefore, precise monitoring of K⁺ dynamics in brain tissue would be desirable to understand better K⁺ fluxes and how they are controlled. However, this understanding has been hampered by technical challenges.

The emergence of genetically encoded sensors for K⁺²⁸⁻³⁰ sparked hope that imaging approaches can help answer questions that could not be tackled with other methods^{5,31,32}. However, applications of genetically encoded K⁺ sensors to record intracellular neuronal K⁺ dynamics are sparse. One possible reason is that available sensors have a very high affinity for K⁺ and are saturated when expressed in neurons, cells which have a very high intracellular K⁺ concentration of around 140 mM⁹. For the current study, we chose lc-LysM GEPII 1.0, which, at the start of the study, had the highest K_d of all available sensors (i.e., 27 mM *in vitro* and 60 mM in cells^{21,28}). In the meantime, a new generation of K⁺ biosensors optimized for intracellular recordings has been published, yet they still need to be investigated in neurons³⁰.

When we induced hyperactivity in our neuronal cultures using Bicuculline or intensely stimulated these cells optogenetically (at least 30 times at 1 Hz), we observed a decrease of the FRET ratio of lc-LysM GEPII 1.0, indicating a reduction in neuronal [K⁺]_i. This is expected, as K⁺ outflow is the main contributor to neuronal repolarization after an action potential and was also corroborated by all so far published studies measuring intracellular K⁺ dynamics in neurons using genetically encoded sensors independent of the stimulation paradigm^{28,29,33}. Before concluding that lc-LysM GEPII 1.0 indeed measures [K⁺]_i, it is important to consider that next to changes in [K⁺]_i strong neuronal activity also leads to an intracellular acidification by up to 0.3 pH units^{34,35}. Since genetically encoded sensors are based on fluorescent proteins prone to pH-induced changes, intracellular pH shifts may result in apparent changes in [K⁺]_i. Wu and colleagues suggested that the decrease of the signal of the K⁺ sensor GINKO2 was, to a large

degree, caused by acidification of the neuronal cytoplasm rather than K^+ changes²⁹. The specific pH stability of the K^+ indicator used in the current study, i.e., Ic-LysM GEPII 1.0, has not been evaluated; however, Ic-LysM GEPII 1.0 is derived by only 3 point mutations from GEPII 1.0, which shows only negligible pH sensitivity in the physiological range²¹. Therefore, it is reasonable to conclude that the decrease of the FRET ratio of Ic-LysM GEPII 1.0 in response to Bicuculline observed in the current study is indeed caused by a reduction in $[K^+]_i$. Hence, we can conclude with a reasonable confidence level that Ic-LysM GEPII 1.0 accurately detects $[K^+]_i$ during neuronal activity.

After ensuring the general functionality of Ic-LysM GEPII 1.0 in neurons, we aimed to investigate whether the biosensor can detect changes of $[K^+]_i$ occurring during single action potentials. Our cultured cortical neurons displayed spontaneous neuronal activity consisting of multiple single action potentials as evidenced by single, sharp increases in $[Ca^{2+}]_i$, which could be silenced with the inhibitor of voltage-gated sodium channels TTX. After characterizing these robust spontaneous $[Ca^{2+}]_i$ fluctuations in our cell culture system, we transduced our cells with Ic-LysM GEPII 1.0. We could not observe any distinguishable changes in the Ic-LysM GEPII 1.0 signals that indicated spontaneous K^+ dynamics. In addition, the signal was not affected by TTX-induced neuronal silencing and correlated with the expression level of the sensor. These findings suggest that Ic-LysM GEPII 1.0 failed to detect $[K^+]_i$ changes induced by single action potentials. This conclusion is further supported by the observation that controlled optogenetic stimulation of neurons with low frequencies also failed to elicit any change in Ic-LysM GEPII 1.0 fluorescence.

These data may be interpreted in three ways: 1) either Ic-LysM GEPII 1.0 is not sensitive enough to resolve small changes of $[K^+]_i$, or 2) up to a certain number of action potentials $[K^+]_i$ does not decrease in the cytoplasm or decreases only in the vicinity of the cell membrane, or 3) both scenarios are valid. To understand which of these scenarios is the most likely, it is essential to know that $[K^+]_i$ in neurons is around 140 mM while in the extracellular space, it is only 3 mM⁶. In addition, the extracellular space only makes up about 20% of the brain volume³⁶. Hence, a change of a few mM of potassium can lead to a significant relative change of $[K^+]_e$, while barely affecting $[K^+]_i$. As the membrane potential is determined by the ratio between intra- and extracellular ions, the contribution of K^+ to the membrane potential is nearly exclusively governed by $[K^+]_e$ ³⁷. Therefore, most studies investigating K^+ alterations in response to neuronal activity measured extracellular rather than intracellular changes. For example, strong, tetanic neuronal stimulation or epileptic seizures reliably lead to increases of $[K^+]_e$ that plateau around 10 to 12 mM^{38,39}, likely because of efficient K^+ clearance via astrocytes^{39,40}. Cortical spreading depolarizations can further increase extracellular K^+ levels to around 65 mM^{38,41,42}. In contrast, strong tetanic stimulation of frog motor neurons led to a decrease of intracellular

[K⁺] by not more than 5 mM⁴³, while Raimondo *et al.* estimated that epileptic seizures lead to a decrease of intracellular potassium concentrations of only 2 mM⁴⁴. The relatively small activity-dependent changes in intracellular potassium are even more relevant when considering spontaneous neuronal activity. A single action potential leads to an increase of extracellular potassium by only 0.2-0.8 mM^{45,46}. Hence, changes in [K⁺]_i are most likely much smaller.

As the EC₅₀ of Ic-LysM GEPII 1.0 (27 mM – 60 mM) is far from the intracellular K⁺ concentration in neurons (~140 mM), the sensor will either be close to saturation or fully saturated when expressed in the intracellular space. Indeed, Ic-LysM GEPII 1.0 is saturated at 150 mM potassium and a drop to 100 mM leads to a change of the dynamic range by only about 10%²¹. Therefore, small changes of intracellular K⁺ are unlikely to elicit a change of the FRET ratio of Ic-LysM GEPII 1.0 strong enough to be resolved. We conclude that to resolve intracellular K⁺ changes in response to spontaneous neuronal activity, Ic-LysM GEPII 1.0 needs to be improved towards lower affinity for K⁺.

Combining live cell imaging with optogenetic stimulation can be used to control [K⁺] changes tightly and therefore allows comparing the performance of potential candidate variants. This might help facilitating the development of improved potassium sensors focusing on resolving K⁺ changes during neuronal activity. The inability to measure [K⁺]_i following single action potentials can be attributed to the anticipated little changes in [K⁺]_i in such scenarios and the very low EC₅₀ of Ic-LysM GEPII 1.0 for neuronal measurements.

Despite these shortcomings of Ic-LysM GEPII 1.0 for the measurement [K⁺]_i in neurons, we were able to express Ic-LysM GEPII 1.0 in cortical neurons at a sufficiently high level to be visualized by *in vivo* imaging and to perform the first measurements of [K⁺]_i in the living mouse brain. Like in cultured cells, we did not detect any changes of [K⁺]_i during spontaneous neuronal activity. However, we observed increased fluorescence lifetime (FLIM) of Ic-LysM GEPII 1.0 during massive neuronal depolarizations triggered by cerebral ischemia. Other groups already used imaging approaches to measure [K⁺] in response to cortical depolarization waves *in vivo*, however, only in the extracellular space. Transient extracellular K⁺ increases were recorded after injection of the K⁺-sensitive dye APG-2 in the cisterna magna⁴⁷ or topical application of GINKO2 on the open cortex in mice²⁹. Wu and colleagues tried to measure [K⁺]_i dynamics in neurons and astrocytes of drosophila in response to induced neuronal activity; however, they reported that their data obtained with the single fluorophore sensor GINKO2, which displays a strong pH dependency, is quite likely confounded by activity-induced acidification artifacts²⁹. Also, cortical depolarization waves cause intracellular acidification in neurons^{48,49}; however, as discussed above, GEPIIs are considerably more pH stable than GINKO2. Therefore, we do

not expect that pH affected our measurements considerably. Future measures with improved GEPs in terms of K_D and pH stability and a pH-sensor such as pHRed⁵⁰ could help disentangle the actual potassium signal from a potential pH artifact⁵¹.

Our data show that intracellular K^+ imaging in neurons is, in principle, possible *in vivo*. However, the low K_D of lc-LysM GEP 1.0 and the high technical requirements of such measurements (in vivo FLIM) currently limit the practical use of this approach. Hence, optimizing lc-LysM GEP 1.0 with respect to affinity, dynamic range, and fluorescence intensity is critical to allowing the measurement of intracellular K^+ to become a standard tool in neuroscience research. We believe such a task is worth pursuing because reliably detecting intracellular K^+ dynamics *in vivo* will help investigating neuronal phenomena and other critical neurobiological processes such as astrocytic K^+ clearance and spatial K^+ buffering^{31,32}.

In conclusion, we provide a first functional characterization of lc-LysM GEP 1.0 in cortical neurons both *in vitro* and *in vivo*. We show that lc-LysM GEP 1.0 can resolve $[K^+]$ changes in response to intense neuronal activity, however, fails to detect K^+ dynamics in response to mild activity or single action potentials. Future optimization of lc-LysM GEP 1.0, especially with respect to an increased K_D , is needed for allowing precise K^+ measurements in physiologic settings.

References

- 1 Zacchia, M., Abategiovanni, M. L., Stratigis, S. & Capasso, G. Potassium: From Physiology to Clinical Implications. *Kidney Dis (Basel)* **2**, 72-79, doi:10.1159/000446268 (2016).
- 2 McDonough, A. A. & Fenton, R. A. Potassium homeostasis: sensors, mediators, and targets. *Pflugers Arch* **474**, 853-867, doi:10.1007/s00424-022-02718-3 (2022).
- 3 Bean, B. P. The action potential in mammalian central neurons. *Nat Rev Neurosci* **8**, 451-465, doi:10.1038/nrn2148 (2007).
- 4 Tanner, G. R. & Tzingounis, A. V. The mammalian nodal action potential: new data bring new perspectives. *Adv Physiol Educ* **46**, 693-702, doi:10.1152/advan.00171.2021 (2022).
- 5 Rasmussen, R., O'Donnell, J., Ding, F. & Nedergaard, M. Interstitial ions: A key regulator of state-dependent neural activity? *Prog Neurobiol* **193**, 101802, doi:10.1016/j.pneurobio.2020.101802 (2020).
- 6 Somjen, G. G. Ion regulation in the brain: implications for pathophysiology. *Neuroscientist* **8**, 254-267, doi:10.1177/1073858402008003011 (2002).
- 7 Mitterdorfer, J. & Bean, B. P. Potassium currents during the action potential of hippocampal CA3 neurons. *J Neurosci* **22**, 10106-10115, doi:10.1523/JNEUROSCI.22-23-10106.2002 (2002).
- 8 Gonzalez Sabater, V., Rigby, M. & Burrone, J. Voltage-Gated Potassium Channels Ensure Action Potential Shape Fidelity in Distal Axons. *J Neurosci* **41**, 5372-5385, doi:10.1523/JNEUROSCI.2765-20.2021 (2021).
- 9 Attwell, D. & Laughlin, S. B. An energy budget for signaling in the grey matter of the brain. *J Cereb Blood Flow Metab* **21**, 1133-1145, doi:10.1097/00004647-200110000-00001 (2001).
- 10 Howarth, C., Gleeson, P. & Attwell, D. Updated energy budgets for neural computation in the neocortex and cerebellum. *J Cereb Blood Flow Metab* **32**, 1222-1232, doi:10.1038/jcbfm.2012.35 (2012).
- 11 de Curtis, M., Uva, L., Gnatkovsky, V. & Librizzi, L. Potassium dynamics and seizures: Why is potassium ictogenic? *Epilepsy Res* **143**, 50-59, doi:10.1016/j.eplepsyres.2018.04.005 (2018).
- 12 Kohling, R. & Wolfart, J. Potassium Channels in Epilepsy. *Cold Spring Harb Perspect Med* **6**, doi:10.1101/cshperspect.a022871 (2016).
- 13 Auffenberg, E. *et al.* Hyperexcitable interneurons trigger cortical spreading depression in an Scn1a migraine model. *J Clin Invest* **131**, doi:10.1172/JCI142202 (2021).
- 14 Al-Karagholi, M. A., Ghanizada, H., Nielsen, C. A. W., Hougaard, A. & Ashina, M. Opening of ATP sensitive potassium channels causes migraine attacks with aura. *Brain* **144**, 2322-2332, doi:10.1093/brain/awab136 (2021).
- 15 Takahashi, S., Shibata, M. & Fukuuchi, Y. Role of sodium ion influx in depolarization-induced neuronal cell death by high KCl or veratridine. *Eur J Pharmacol* **372**, 297-304, doi:10.1016/s0014-2999(99)00208-3 (1999).
- 16 Moon, J. *et al.* Dual Electrochemical Microsensor for Real-Time Simultaneous Monitoring of Nitric Oxide and Potassium Ion Changes in a Rat Brain during Spontaneous Neocortical Epileptic Seizure. *Anal Chem* **88**, 8942-8948, doi:10.1021/acs.analchem.6b02396 (2016).
- 17 Oceau, J. C., Faas, G., Mody, I. & Khakh, B. S. Making, Testing, and Using Potassium Ion Selective Microelectrodes in Tissue Slices of Adult Brain. *J Vis Exp*, doi:10.3791/57511 (2018).
- 18 Elabyad, I. A., Kalayciyan, R., Shanbhag, N. C. & Schad, L. R. First in vivo potassium-39 ((3)(9)K) MRI at 9.4 T using conventional copper radio frequency surface coil cooled to 77 K. *IEEE Trans Biomed Eng* **61**, 334-345, doi:10.1109/TBME.2013.2294277 (2014).

-
- 19 Atkinson, I. C., Claiborne, T. C. & Thulborn, K. R. Feasibility of 39-potassium MR imaging of a human brain at 9.4 Tesla. *Magn Reson Med* **71**, 1819-1825, doi:10.1002/mrm.24821 (2014).
- 20 Rimmele, T. S. & Chatton, J. Y. A novel optical intracellular imaging approach for potassium dynamics in astrocytes. *PLoS One* **9**, e109243, doi:10.1371/journal.pone.0109243 (2014).
- 21 Bischof, H. *et al.* Novel genetically encoded fluorescent probes enable real-time detection of potassium in vitro and in vivo. *Nat Commun* **8**, 1422, doi:10.1038/s41467-017-01615-z (2017).
- 22 Zhang, Y. *et al.* Fast and sensitive GCaMP calcium indicators for imaging neural populations. *Nature* **615**, 884-891, doi:10.1038/s41586-023-05828-9 (2023).
- 23 Klapoetke, N. C. *et al.* Independent optical excitation of distinct neural populations. *Nat Methods* **11**, 338-346, doi:10.1038/nmeth.2836 (2014).
- 24 Bischof, H. *et al.* Purification and Application of Genetically Encoded Potassium Ion Indicators for Quantification of Potassium Ion Concentrations within Biological Samples. *Curr Protoc Chem Biol* **11**, e71, doi:10.1002/cpch.71 (2019).
- 25 Burrows, F. E., Bray, N., Denes, A., Allan, S. M. & Schiessl, I. Delayed reperfusion deficits after experimental stroke account for increased pathophysiology. *J Cereb Blood Flow Metab* **35**, 277-284, doi:10.1038/jcbfm.2014.197 (2015).
- 26 Dunn, K. M. & Nelson, M. T. Potassium channels and neurovascular coupling. *Circ J* **74**, 608-616, doi:10.1253/circj.cj-10-0174 (2010).
- 27 Lafreniere, R. G. *et al.* A dominant-negative mutation in the TRESK potassium channel is linked to familial migraine with aura. *Nat Med* **16**, 1157-1160, doi:10.1038/nm.2216 (2010).
- 28 Shen, Y. *et al.* Genetically encoded fluorescent indicators for imaging intracellular potassium ion concentration. *Commun Biol* **2**, 18, doi:10.1038/s42003-018-0269-2 (2019).
- 29 Wu, S. Y. *et al.* A sensitive and specific genetically-encoded potassium ion biosensor for in vivo applications across the tree of life. *PLoS Biol* **20**, e3001772, doi:10.1371/journal.pbio.3001772 (2022).
- 30 Torres Caban, C. C. *et al.* Tuning the Sensitivity of Genetically Encoded Fluorescent Potassium Indicators through Structure-Guided and Genome Mining Strategies. *ACS Sens* **7**, 1336-1346, doi:10.1021/acssensors.1c02201 (2022).
- 31 Suryavanshi, P., Reinhart, K. M., Shuttleworth, C. W. & Brennan, K. C. Action Potentials Are Critical for the Propagation of Focally Elicited Spreading Depolarizations. *J Neurosci* **42**, 2371-2383, doi:10.1523/JNEUROSCI.2930-20.2021 (2022).
- 32 Monai, H. *et al.* Adrenergic inhibition facilitates normalization of extracellular potassium after cortical spreading depolarization. *Sci Rep* **11**, 8150, doi:10.1038/s41598-021-87609-w (2021).
- 33 Ehinger, R. *et al.* Slack K(+) channels attenuate NMDA-induced excitotoxic brain damage and neuronal cell death. *FASEB J* **35**, e21568, doi:10.1096/fj.202002308RR (2021).
- 34 Raimondo, J. V., Irkle, A., Wefelmeyer, W., Newey, S. E. & Akerman, C. J. Genetically encoded proton sensors reveal activity-dependent pH changes in neurons. *Front Mol Neurosci* **5**, 68, doi:10.3389/fnmol.2012.00068 (2012).
- 35 Xiong, Z. Q., Saggau, P. & Stringer, J. L. Activity-dependent intracellular acidification correlates with the duration of seizure activity. *J Neurosci* **20**, 1290-1296, doi:10.1523/JNEUROSCI.20-04-01290.2000 (2000).
- 36 Nicholson, C. & Hrabetova, S. Brain Extracellular Space: The Final Frontier of Neuroscience. *Biophys J* **113**, 2133-2142, doi:10.1016/j.bpj.2017.06.052 (2017).
- 37 Wright, S. H. Generation of resting membrane potential. *Adv Physiol Educ* **28**, 139-142, doi:10.1152/advan.00029.2004 (2004).
- 38 Futamachi, K. J., Mutani, R. & Prince, D. A. Potassium activity in rabbit cortex. *Brain Res* **75**, 5-25, doi:10.1016/0006-8993(74)90767-7 (1974).

-
- 39 Heinemann, U. & Lux, H. D. Ceiling of stimulus induced rises in extracellular potassium concentration in the cerebral cortex of cat. *Brain Res* **120**, 231-249, doi:10.1016/0006-8993(77)90903-9 (1977).
- 40 Larsen, B. R., Stoica, A. & MacAulay, N. Managing Brain Extracellular K(+) during Neuronal Activity: The Physiological Role of the Na(+)/K(+)-ATPase Subunit Isoforms. *Front Physiol* **7**, 141, doi:10.3389/fphys.2016.00141 (2016).
- 41 Enger, R. *et al.* Dynamics of Ionic Shifts in Cortical Spreading Depression. *Cereb Cortex* **25**, 4469-4476, doi:10.1093/cercor/bhv054 (2015).
- 42 Lehmenkuhler, A. & Richter, F. Cortical Spreading Depolarization (CSD) Recorded from Intact Skin, from Surface of Dura Mater or Cortex: Comparison with Intracortical Recordings in the Neocortex of Adult Rats. *Neurochem Res* **45**, 34-41, doi:10.1007/s11064-019-02737-0 (2020).
- 43 Grafe, P., Rimpel, J., Reddy, M. M. & ten Bruggencate, G. Changes of intracellular sodium and potassium ion concentrations in frog spinal motoneurons induced by repetitive synaptic stimulation. *Neuroscience* **7**, 3213-3220, doi:10.1016/0306-4522(82)90243-3 (1982).
- 44 Raimondo, J. V., Burman, R. J., Katz, A. A. & Akerman, C. J. Ion dynamics during seizures. *Front Cell Neurosci* **9**, 419, doi:10.3389/fncel.2015.00419 (2015).
- 45 Baylor, D. A. & Nicholls, J. G. Changes in extracellular potassium concentration produced by neuronal activity in the central nervous system of the leech. *J Physiol* **203**, 555-569, doi:10.1113/jphysiol.1969.sp008879 (1969).
- 46 Sykova, E., Rothenberg, S. & Krekule, I. Changes of extracellular potassium concentration during spontaneous activity in the mesencephalic reticular formation of the rat. *Brain Res* **79**, 333-337, doi:10.1016/0006-8993(74)90428-4 (1974).
- 47 Bazzigaluppi, P., Dufour, S. & Carlen, P. L. Wide field fluorescent imaging of extracellular spatiotemporal potassium dynamics in vivo. *Neuroimage* **104**, 110-116, doi:10.1016/j.neuroimage.2014.10.012 (2015).
- 48 Zhou, N., Gordon, G. R., Feighan, D. & MacVicar, B. A. Transient swelling, acidification, and mitochondrial depolarization occurs in neurons but not astrocytes during spreading depression. *Cereb Cortex* **20**, 2614-2624, doi:10.1093/cercor/bhq018 (2010).
- 49 Sun, X. *et al.* Simultaneous monitoring of intracellular pH changes and hemodynamic response during cortical spreading depression by fluorescence-corrected multimodal optical imaging. *Neuroimage* **57**, 873-884, doi:10.1016/j.neuroimage.2011.05.040 (2011).
- 50 Tantama, M., Hung, Y. P. & Yellen, G. Imaging intracellular pH in live cells with a genetically encoded red fluorescent protein sensor. *J Am Chem Soc* **133**, 10034-10037, doi:10.1021/ja202902d (2011).
- 51 Tantama, M., Martinez-Francois, J. R., Mongeon, R. & Yellen, G. Imaging energy status in live cells with a fluorescent biosensor of the intracellular ATP-to-ADP ratio. *Nat Commun* **4**, 2550, doi:10.1038/ncomms3550 (2013).

Acknowledgements

The current study was mainly funded by a joint grant provided by the Deutsche Forschungsgemeinschaft (DFG, German Research Foundation) and the Austrian Science Fund (FWF) to NP (PL249/15-1) and RM. Further funding was received by the DFG under Germany's Excellence Strategy within the framework of the Munich Cluster for Systems Neurology (EXC 2145SyNergy – ID 390857198; NP and AL).

Author Contributions

B.G., S.B., H.B., R.M. and N.P. conceived the study and contributed to the study design. B.G., G.M.C., C.R., J.S., G.L., A.G.Z. and S.F. contributed to the acquisition and analysis of the data. B.G., E.E., A.L., R.M., S.F. and N.P. contributed to the interpretation of the data. B.G., S.F. and N.P. drafted the manuscript. All authors read and approved the final manuscript.

Competing Interests

The authors declare no competing interests.

Data availability

The data generated during the study are available from the corresponding author upon request.

Figures

Figure 1

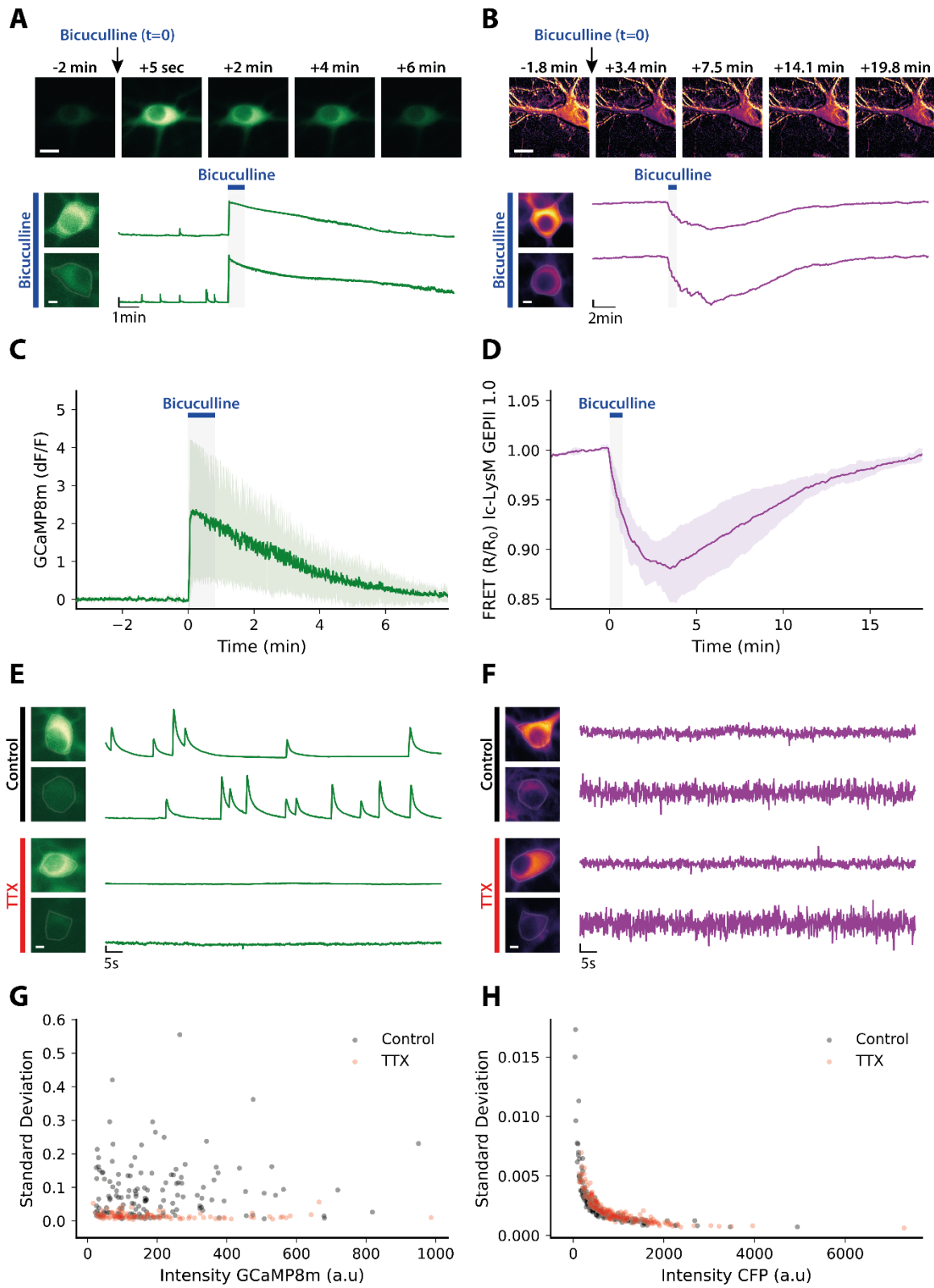


Figure 2

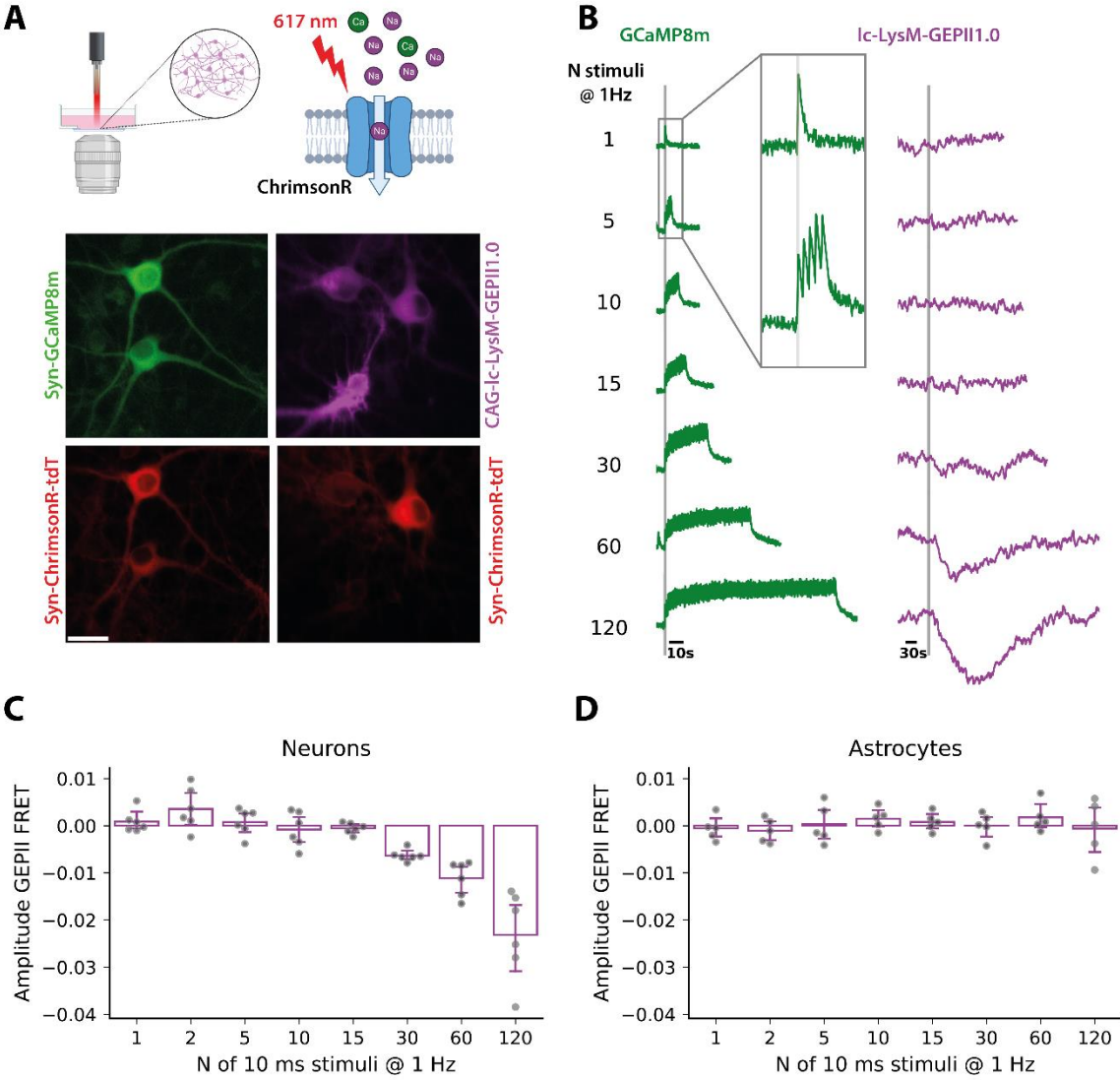


Figure 3

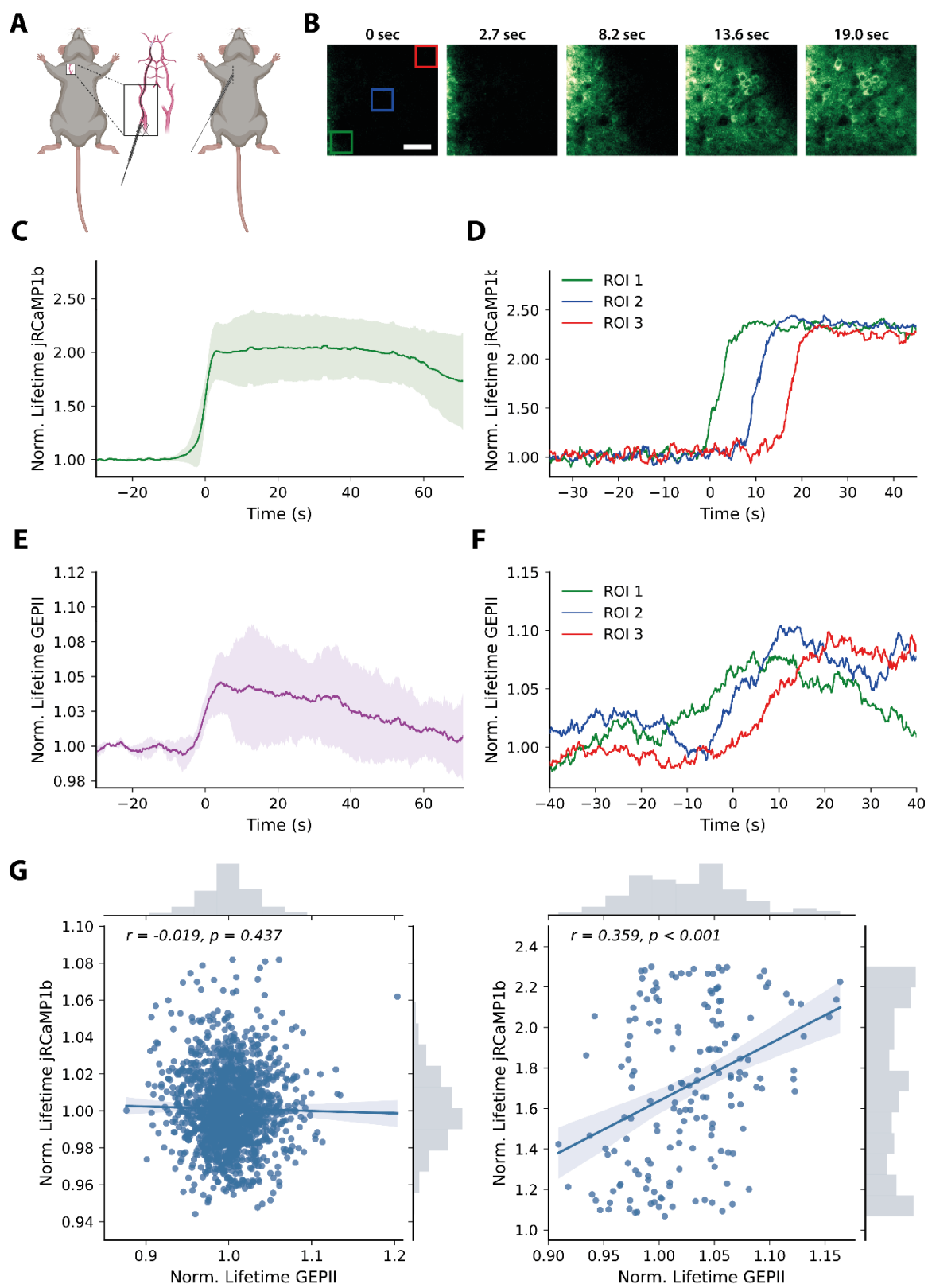


Figure Legends

Figure 1: Ic-LysM GEPII 1.0 resolves neuronal potassium changes only upon strong stimulation (A) Neurons expressing GCaMP8m were treated with 50 μM Bicuculline for 50 seconds. The time series shows a lasting increase of the intensity of GCaMP8m. Scale bar represents 15 μM . Below are example traces of the response to Bicuculline of two individual neurons with different intensities of GCaMP8m. Scale bar represents 5 μM . **(B)** Bicuculline leads to a decrease of the FRET ratio of Ic-LysM GEPII 1.0. Images are pseudocolored according to the FRET ratio. Scale bar represents 5 μM . **(C)** Average trace of the GCaMP8m response to Bicuculline (N = 4 experiments). Traces are represented as mean \pm SD. **(D)** Averaged trace of the Ic-LysM GEPII 1.0 response to Bicuculline (N = 5 experiments). Traces represented as mean \pm SD. **(E)** Calcium traces of individual neurons with either high or low baseline intensity (scale bar: 5 μM). Neurons under control conditions show clear spontaneous activity, which is completely inhibited in the presence of 500 nM TTX. **(F)** Potassium traces of individual neurons with either high or low baseline intensity (scale bar: 5 μM). No obvious signal above noise is observed and no difference between control condition and 500 nM TTX can be detected. Noise is considerably bigger in cells with lower baseline intensity of Ic-LysM GEPII 1.0. **(G)** Standard deviation of the traces recorded from neurons expressing GCaMP8m plotted against baseline intensity under various conditions. No clear correlation can be observed for the control condition (grey, 142 neurons in 8 experiments) or Bicuculline treatment (blue, 104 neurons in 4 experiments). In contrast, neurons silenced with TTX show a clear correlation between SD and intensity (red, 112 neurons in 7 experiments). **(H)** Standard deviation of the traces recorded from neurons expressing Ic-LysM GEPII 1.0 plotted against the baseline intensity of the donor. There is no difference between neurons under control conditions (grey, 152 neurons in 13 experiments) and in the presence of TTX (red, 192 neurons in 13 experiments). Both cases show a clear correlation of standard deviation with intensity. For Bicuculline, standard deviation does not correlate with the intensity of CFP (blue, 45 neurons in 5 experiments).

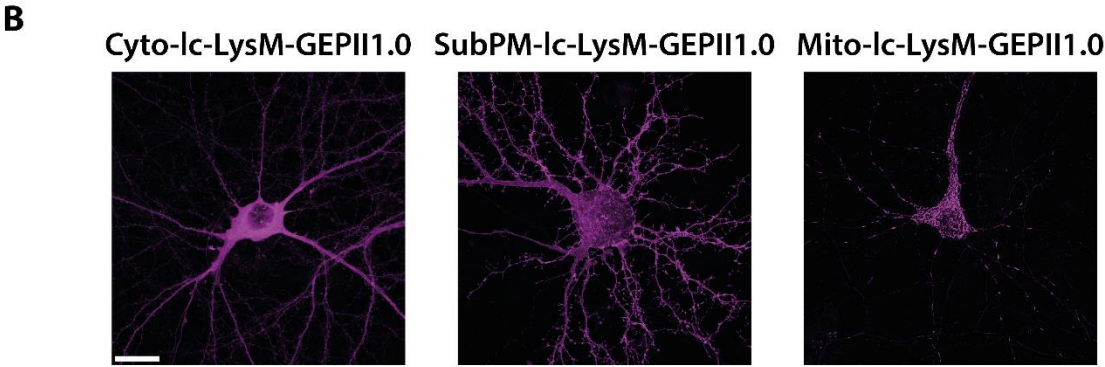
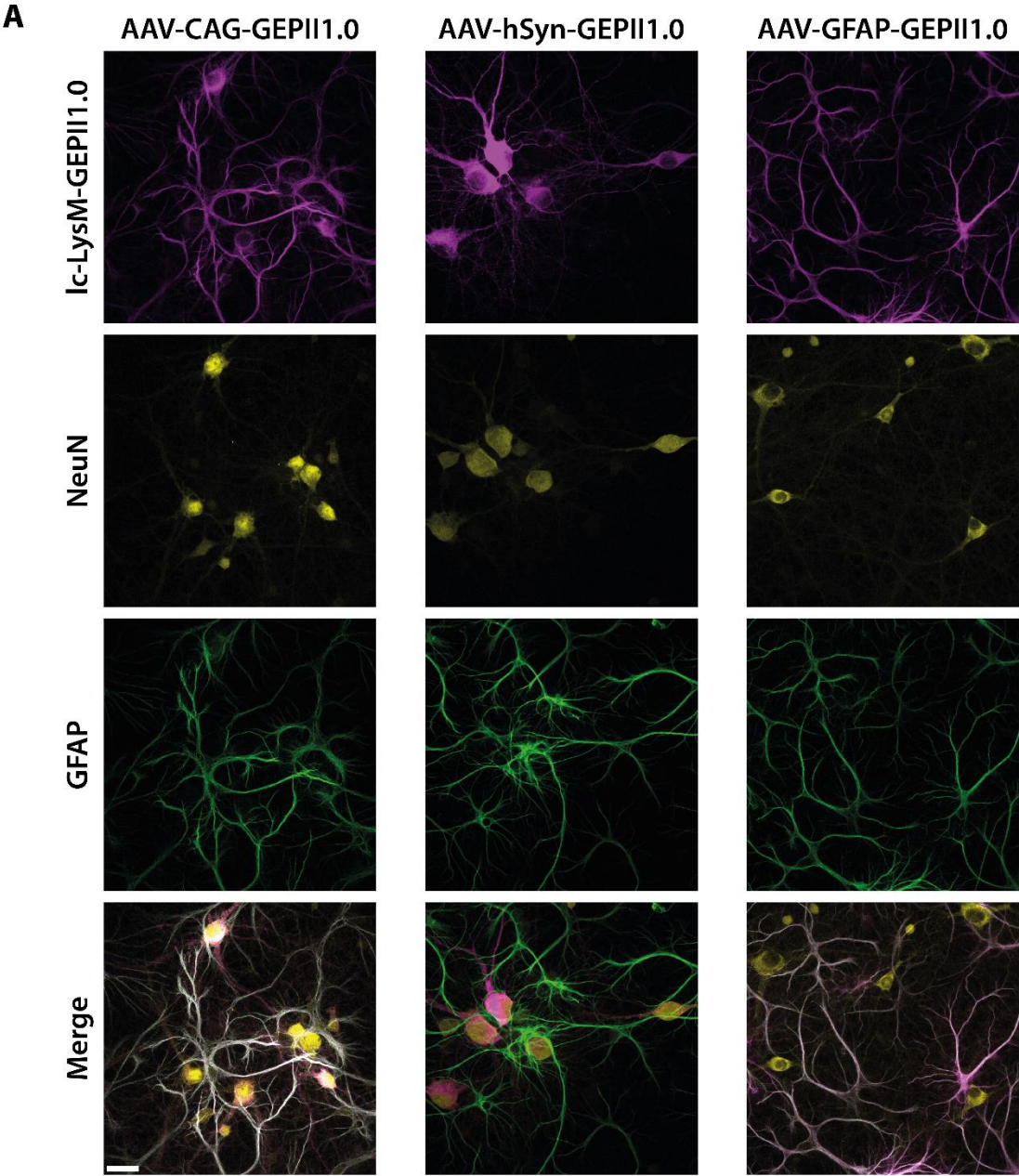
Figure 2: Optogenetic stimulation to fine-tune responsivity of Ic-LysM GEPII 1.0 (A) Schematic illustration of the setup for optogenetic stimulation of ChrimsonR during live cell imaging (created with BioRender.com). Cells are illuminated with a LED with an emission peak at 617 nm. Cells were co-transduced with AAV-Syn-GCaMP8m and AAV-Syn-ChrimsonR-tdT (left) or AAV-CAG-Ic-LysM GEPII 1.0 and AAV-Syn-Chrimson-tdT (right) to allow imaging of calcium in neurons or potassium in neurons and astrocytes during neuronal stimulation respectively. Scale bar represents 25 μM **(B)** Cells were stimulated with 10 ms pulses at a stimulation rate of 1 Hz. Representative traces of GCaMP8m (left) and Ic-LysM GEPII 1.0 (right) in response to different amounts of pulses. Each pulse elicited a calcium spike indicating

successful and robust stimulation. Potassium changes were only visible after a train of 30 or more stimulations. **(C)** Quantification of the amplitudes of the normalized FRET ratio of Ic-LysM GEPII 1.0 expressed in neurons in response to an increasing number of stimuli. A drop of neuronal potassium levels was observed starting at 30 stimulations and increased with the number of additional stimulations. Amplitudes were quantified as the difference of the FRET ratios between the baseline before the stimulation and the mean of the last two frames of each train of stimulation. Data is represented as Mean \pm SD (N = 46 neurons in n = 6 experiments). **(D)** Quantification of the amplitudes of the normalized FRET ratio of Ic-LysM GEPII 1.0 expressed in astrocytes. Stimulation has no effect on the astrocytic FRET ratio of Ic-LysM GEPII 1.0. Data is represented as Mean \pm SD (N = 18 astrocytes in n = 5 experiments).

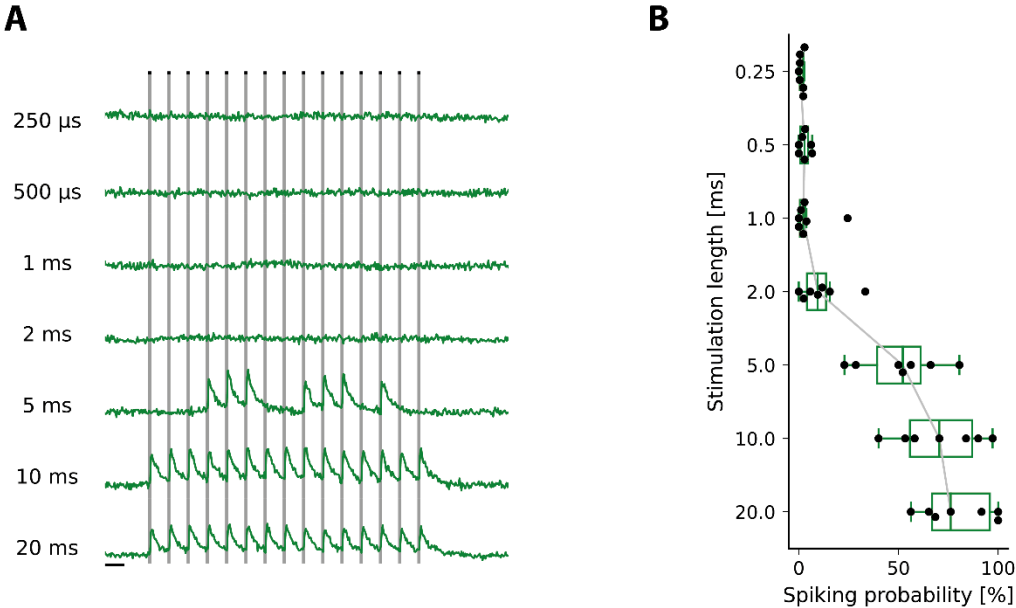
Figure 3: *In vivo* imaging of Ic-LysM GEPII 1.0 during a peri-infarct depolarization in the cortex of living mice **(A)** Schematic illustration of the surgical procedure (created with BioRender.com). Peri-infarct depolarizations (PID) were elicited via insertion of a filament into the external carotid artery and subsequent occlusion of the middle cerebral artery during the imaging session. **(B)** Pseudocolored image strip shows the intensity of jRCaMP1b during a PID over time. Neuronal calcium levels increase in a synchronized wave like manner. **(C)** Average FLIM response of jRCaMP1b during a PID show a robust increase of the fluorescence lifetime. Data is represented as mean \pm SD. To overlap PIDs from individual experiments (N = 3), we set the half-maximal FLIM increase $t=0$. **(D)** FLIM responses of individual regions of interest (indicated in **3B**) placed along the field of view of a single recording show the wave-like character of the PID. **(E)** Average FLIM responses of Ic-LysM GEPII 1.0 during PIDs (N = 3) show an increase of the fluorescence lifetime of Ic-LysM GEPII 1.0, indicating a decrease of the neuronal potassium levels. Data represented as mean \pm SD. **(F)** FLIM of Ic-LysM GEPII 1.0 also shows the wave-like character of the PID. **(G)** Correlation of the normalized lifetimes of jRCaMP1b and Ic-LysM GEPII 1.0 during baseline imaging (left) and during the rising phase of the CSD (right). No significant correlation during baseline imaging could be observed whereas during the CSD, increases of the lifetime of jRCaMP1b correlate significantly with increases of Ic-LysM GEPII 1.0

Supplementary figures

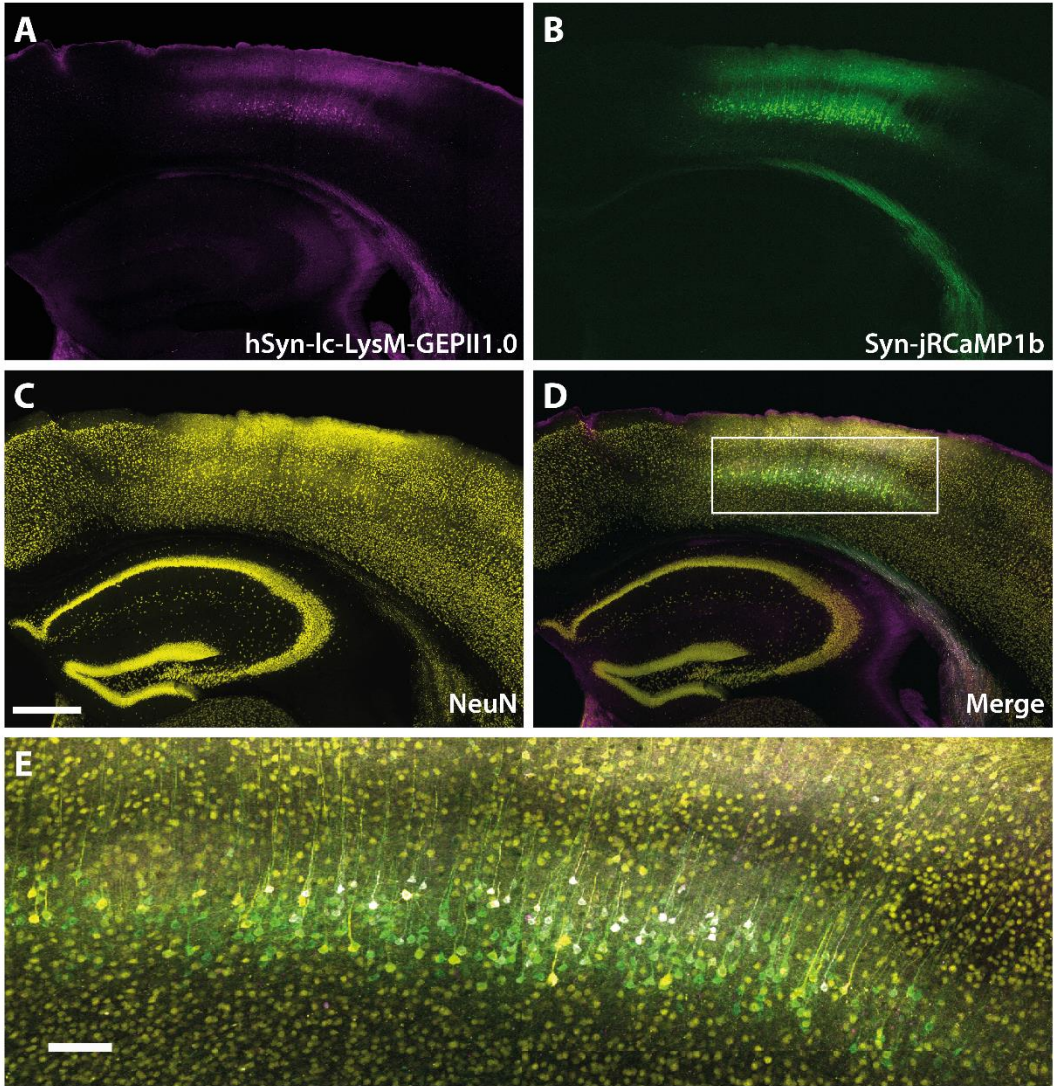
Supplementary figure 1



Supplementary figure 2

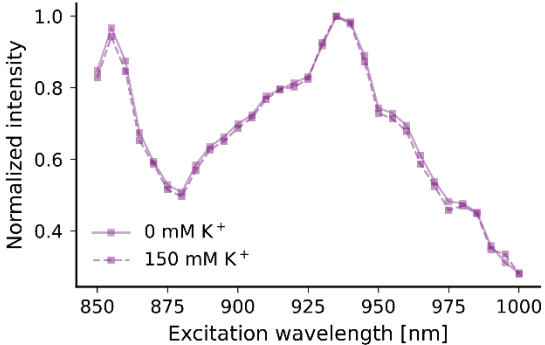


Supplementary figure 3

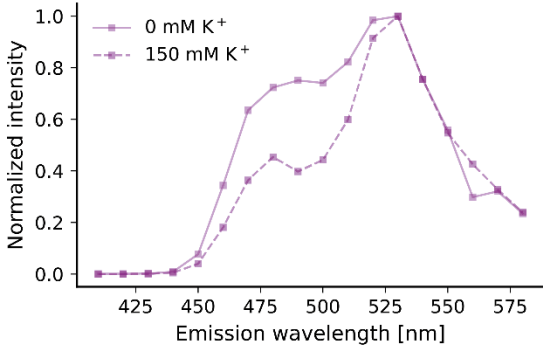


Supplementary figure 4

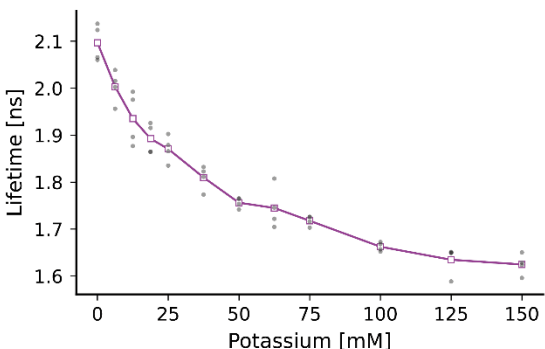
A



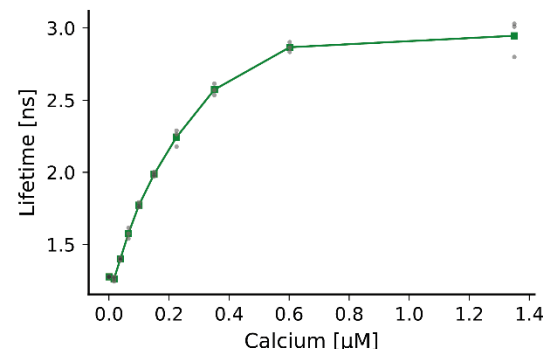
B



C



D



Supplementary Figure Legends

Supplementary Figure 1: Expression of Ic-LysM GEPII 1.0 in different cell types and compartments (A) Mixed cortical cultures containing neurons and astrocytes were transduced with different AAVs to express Ic-LysM GEPII 1.0 either ubiquitously (left), specifically in neurons (middle) or in astrocytes (right). The cultures were fixed and counterstained with NeuN and GFAP to confirm cell-type specific expression. Scale bar represents 25 μ M. **(B)** Expression of Ic-LysM GEPII 1.0 in different subcellular compartments of a neuron. Expression of Ic-LysM GEPII 1.0 was targeted either to the cytosol (left), the plasma membrane (middle) or the mitochondrial matrix (right). Scalebar represents 20 μ M.

Supplementary Figure 2: Minimal pulse length of optogenetic stimulus for reliable stimulation (A) Example trace of an individual neuron expressing GCaMP8m and ChrimsonR-tdT. Stimulation trains containing 15 stimuli at 0.5 Hz were delivered. Individual stimuli between different stimulation trains increased in duration of the individual pulse length from 250 μ s to 20 ms. Scale bar represents 2 seconds. **(B)** Quantification of the spiking probability in response to different pulse lengths. Spiking probability was calculated per cell as number of spikes correlating with the stimulation divided by the amount of stimuli (e.g. 15). Each data point is the mean spiking probability of all cells per experiment. Data is represented as mean \pm SD. N = 7 Experiments.

Supplementary Figure 3: Expression of Ic-LysM GEPII 1.0 and jRCaMP1b in neurons in the cortex of mice. Maximum intensity projections of brain slice overviews of neurons in layer 2/3 after viral labelling with Ic-LysM GEPII 1.0 **(A)** and jRCaMP1b **(B)**. Neuronal cell bodies were counterstained with NeuN **(C)**. Scale bar represents 500 μ M. **(D)** Both sensors overlap with the NeuN signal and confirm expression of the sensors in neurons. **(E)** Magnification of region indicated in (D). Scalebar represents 100 μ M.

Supplementary Figure 4: 2-Photon Excitation and emission spectra of Ic-LysM GEPII 1.0 and FLIM calibrations of Ic-LysM GEPII 1.0 and jRCaMP1b All presented data were acquired using recombinant protein of the respective sensor in a 10 mM HEPES solution containing different concentrations of potassium. To keep the osmolarity of the solution constant, it always contained a total of 150 mM of NaCl and KCl. When KCl was reduced, NaCl was increased accordingly. **(A)** 2-Photon excitation spectrum of Ic-LysM GEPII 1.0 in the presence of 0 or 150 mM K^+ . **(B)** Emission spectrum of Ic-LysM GEPII 1.0 in the presence of 0 or 150 mM K^+ . Excitation was at 850 nm. **(C)** FLIM calibration of Ic-LysM GEPII 1.0 with different concentrations of K^+ . Data is represented as mean. n = 4 Experiments **(D)** FLIM calibration of jRCaMP1b with different concentrations of Ca^{2+} . Data is represented as mean. n = 3 Experiments

3.2 Study II: Assessing the pH sensitivity of genetically encoded sensors with Dead Cell Imaging

Bernhard Groschup^{1,2}, Constanze Raitmayr¹, Nikolaus Plesnila^{1,2,3*}

¹Institute for Stroke and Dementia Research (ISD), LMU University Hospital, LMU Munich, Munich, Germany. ²Graduate School of Systemic Neurosciences, LMU Munich, Planegg-Martinsried, Germany. ³Munich Cluster for Systems Neurology (SyNergy), Munich, Germany.
*email:nikolaus.plesnila@med.uni-muenchen.de

Abstract

Genetically encoded sensors have become a widely used tool to study cellular function as they allow measurement of a wide range of different analytes with exceptional spatial and temporal resolution. However, owing to their nature as proteins, most genetically encoded sensors show a considerable sensitivity to pH changes, which can induce artifacts and lead to false-positive results. Interpretation of signals of genetically encoded sensors is further complicated by the fact that changes in intracellular pH can also elicit physiological responses of the analyte levels, making it hard to disentangle real result from pH artifact. Here we propose an easy and cost-effective method, called Dead Cell Imaging, to isolate the pH sensitivity of genetically encoded sensors from physiological from physiological analyte changes. We show that GABA application to neurons, which also elicits acidification, leads to an increase in the FRET signal of the genetically encoded lactate sensor Laconic. PFA fixation of cells expressing Laconic preserved the fluorescence of the sensor, allowing us to perform imaging experiments without interference of cellular lactate production. The Laconic response to acidification in PFA fixed cells closely resembled the response to GABA in live cells, indicating a pH artifact. Dead Cell Imaging also was able to confirm pH artifacts observed with other sensors, proving its general usefulness in addressing pH sensitivity of genetically encoded sensors. Furthermore, Dead Cell Imaging reproduced complex, bi-phasic responses of the ATP sensor ATeam1.03 by providing important time-resolved information on the pH sensitivity of genetically encoded sensors that is usually not addressed using canonical methods. Therefore, Dead Cell Imaging can be a valuable tool for assessing the pH sensitivity of genetically encoded sensors in an easy and cost-effective way.

Introduction

To understand the changes in the concentration of specific molecules and ions underlying biological processes, researchers have developed various techniques such as electrophysiology or microdialysis to monitor cell physiology. Over the last two decades, developing and improving genetically encoded sensors has added a new valuable method with unique properties to the experimental toolbox¹. Genetically encoded sensors have been developed for many different molecules such as ions^{2,3}, metabolites⁴, neurotransmitters⁵, and membrane potential⁶, among others. These sensors combine high spatial and temporal resolution as they can be expressed with cell-type and subcellular specificity, be measured on the single-cell or tissue level, and give real-time readouts⁷. In addition, live cell imaging of genetically encoded sensors is non-invasive, allowing for more physiologic readouts.

Despite these strengths, genetically encoded sensors have some common drawbacks that include recognition of off-targets, difficulty to calibrate, and, owing to their nature as proteins, susceptibility to their environment, e.g., sensitivity to temperature and pH⁸. While the temperature is usually maintained constant throughout the experiment, the intracellular pH is more dynamic and can change depending on the particular stimulation protocol, leading potentially to artifactual sensor responses. Co-imaging the sensor of interest with a pH sensor and subsequent pH calibration can allow correcting for pH artifacts⁹. However, this approach is challenging, time-consuming, and not always feasible with available imaging setups. An easier way to determine the pH dependency of a specific sensor is via *in vitro* experiments using purified sensor protein^{10,11}. However, this approach provides only end-point measurements and lacks temporal information. Notably, it can be problematic in the case of FRET sensors, where both fluorophores may have different kinetics in their pH response. Another problem is that pH changes can be a second messenger, eliciting physiologic responses¹². Therefore, simply changing the intracellular pH is insufficient to prove that a response is due to an artifact, making it challenging to disentangle valid signals from sensor artifacts in response to certain stimuli in a living system.

In this study, we developed an experimental approach to isolate the pH sensitivity of genetically encoded sensors from the actual cellular response to acidification. First, we investigated the effect of GABA, which causes intracellular acidification, on the concentration of intracellular lactate in primary cultured neurons and observed that two different lactate sensors^{13,14}, which are different regarding their pH sensitivity, yielded different results. In the second step, we eliminated the physiologic lactate response while maintaining the fluorescence and pH sensitivity of the sensor fluorophores. To that end, we fixed the cells expressing Laconic with paraformaldehyde (PFA). Performing imaging on these fixed cells while changing the extracellular pH reproduced the Laconic response to GABA observed in living cells. This result

demonstrated that the increase in the Laconic signal was primarily due to a pH artifact rather than an actual lactate increase in response to the GABA stimulation. This method, called "Dead Cell Imaging," potentially provides a cheap and easy way to assess the pH sensitivity of any genetically encoded sensor in scenarios where pH changes can also affect the steady-state levels of the analyte of interest.

Methods

Plasmids and cloning

We obtained the following plasmids encoding the individual sensors from Addgene: Laconic/pcDNA3.1(-) (Addgene plasmid #44238); pAAV-CAG-LiLac (Addgene plasmid #184570); ATeam1.03-nD/nA/pcDNA3 (Addgene plasmid #51958); pcDNA3.1 FLII12Pglu-700uDelta6 (Addgene plasmid #17866) and pC1-SypHer3s (Addgene plasmid #108118). For the AAV production, all sensors not already present in an AAV backbone were subcloned in the backbone of pAAV-CAG-GFP (Addgene plasmid #37825) between the restriction sites BamHI and HindIII.

AAV Production

Adeno-associated viral (AAV) particles were generated in HEK293T cells cultivated in DMEM supplemented with 10% FBS and 100 U/mL of Penicillin-Streptomycin. The cells were maintained in a humidified atmosphere at 37°C with 5% CO₂ until they reached a confluency of 70-80%. For viral production, cells were transfected with three plasmids: pHelper, pAAV-DJ (both Cell Biolabs, Cat: VPK-400-DJ), and a pAAV-ITR vector which housed the transgene. Transfection was performed using polyethylenimine (PEI) that was adjusted to a pH of 7.0. Post-transfection (approximately 2-3 days), the cells were detached using an EDTA solution (0.5 M in PBS, pH 7.4) at a ratio of 1/80 of the culture's volume. The AAV particles were purified using the AAVpro® Purification Kit (All serotypes) from Takara Bio Inc. (Cat: #6666). The cells were centrifuged at 1700 g for 10 minutes at 4°C. The supernatant was discarded and the cell pellet was resuspended in 650 µL of AAV Extraction Solution A plus to lyse the cells. The cell debris were pelleted by centrifugation at 14,000 g for 10 minutes at 4°C, and the resultant supernatant containing the released AAV particles was transferred a fresh tube. To this solution, 65 µL of AAV Extraction Solution B was added and the solution was aliquoted and stored at -80°C for subsequent experiments.

AAV titration was performed by qPCR using the AAVpro® Titration Kit (for Real Time PCR) Ver.2 from Takara (Cat: #6233) according to the manufacturer's instructions. For titration, primers targeting the ITR repeats of the viral backbone were used (ITR F: GGAACCCCTAGTGATGGAGTT and ITR R: CGGCCTCAGTGAGCGA).

Preparation of cryo-stocks of mixed cortical cultures

Mixed cortical cell cultures were obtained from E17 embryos of Sprague Dawley rats and subsequently cryopreserved. After extraction, brains were immediately immersed in ice cold HBSS supplemented with 7 mM HEPES (pH 7.4). After the cortices were isolated and the meningeal layers were removed, the tissue was minced using a scalpel. Tissue harvested from the entire litter were collectively subjected to enzymatic digestion in HBSS containing 0.5%

Trypsin and 10 µg/mL DNase I at 37°C for 15 minutes. To stop the enzymatic reaction, MEM supplemented with 10% FBS was added. After washing the tissue twice with HBSS, it was gently triturated using a glass Pasteur pipette coated with 4% BSA in HBSS.

After determining the cellular density, the suspension was diluted with MEM supplemented with 10% FBS to a concentration of 2 million cells per mL. An appropriate amount of DMSO was added to obtain a volume fraction of 10% before the solution was aliquoted. For the cryopreservation process, aliquots were placed within a container filled with isopropanol and stored at -80°C overnight. The following day, these aliquots were relocated to a liquid nitrogen storage tank for long-term storage.

Mixed cortical cell cultures from cryostocks

All reagents used for cell culture were purchased from Gibco. Mixed cortical cultures were seeded onto 15 mm round glass cover slips that had been coated with Poly-D-Lysine. Each cover slip was seeded with a density of 100,000 cells. The culture medium (Neurobasal-A medium, no D-glucose, no sodium pyruvate (Cat: A2477501) supplemented with 1x B27 (Cat: 17504-044), 10 mM glucose (Cat: A2494001), 2 mM GlutaMAX™ (Cat: 35050061), 1 mM sodium pyruvate (Cat: 11360039) and 100 U/mL Penicillin-Streptomycin (Cat: 15140-122)) was pre-warmed to 37°C. A frozen aliquot was quickly thawed, diluted to the appropriate concentration with culture medium and subsequently plated onto coverslips placed in 12-well plates. The cultures were maintained in a humidified incubator at 37°C with 5% CO₂ and half of the culture medium was replaced every 3-4 days. The cultures were used for experiments after 22 days in vitro and 3-4 days before the experiment, cells were transduced with AAVs at a MOI of 1000 to express the sensor of interest.

Live cell imaging

To perform live cell imaging on mixed cortical cultures expressing the sensor of interest, the cultures on coverslips were transferred to an open imaging chamber, which was then placed on an inverted microscope (Axio Observer Z1, Zeiss). The microscope was equipped with a 20x air objective - NA 0.8, a LED light source (Colibri 7, Zeiss), an emission image splitter (Optosplit II, Cairn Research), and a CCD camera (Orca Flash 4.0, Hamamatsu Photonics). During the experiment, the cells were continuously superfused with room temperature ACSF (in mM: 125 NaCl, 2.5 KCl, 1.25 NaH₂PO₄, 26 NaHCO₃, 1 MgCl₂, 1.25 CaCl₂, 2 glucose, 0.5 sodium lactate, 0.05 sodium pyruvate) that was gassed with 5% CO₂/95% air. For stimulation, drugs or reagents were diluted in aCSF and superfused over the cells.

FRET sensors with the FRET pair CFP/YFP (Laconic, ATeam1.03nD/nA and FLII12Pglu-700uDelta6) were excited at 0.2 Hz at 436 ± 10 nm. To record FRET, emitted light was split at 515 nm to separate the CFP and YFP channels, which were filtered through additional

bandpass filters (480 ± 15 nm and 535 ± 15 nm respectively). LiLac was excited at 0.2 Hz at 436 ± 10 nm and emitted light was filtered through a bandpass filter (480 ± 20 nm). SypHer3s was sequentially excited at 0.1 Hz at 405 ± 10 nm and 500 ± 10 nm and for both excitation wavelengths, emission was recorded at 535 ± 15 nm. The pH signal was expressed as ratio xx/xx nm. At the end of each experiment with SypHer3s, a pH calibration was performed to obtain absolute pH values. To that end, cells were superfused with HEPES buffered aCSF (in mM: 125 NaCl, 2.5 KCl, 1.25 NaH_2PO_4 , 10 HEPES, 1 MgCl_2 , 1.25 CaCl_2 , 2 glucose, 0.5 sodium lactate, 0.05 sodium pyruvate) adjusted to pH 7.4, containing 10 μM Nigericin to clamp intracellular pH to the extracellular value. aCSF adjusted to different pH values (6.4, 6.8, 7.2, 7.6, 8.0) was used and SypHer3s values at each pH were fitted to a sigmoidal curve, which was subsequently used to calculate the absolute pH values of each frame of the experiment. Exposure time, LED power, and excitation frequencies were adjusted to minimize bleaching and phototoxicity while still obtaining sufficient signal-to-noise ratio. Remaining bleaching was corrected using a custom-written Python script.

Dead Cell Imaging

For Dead Cell Imaging (DeCeIm), cells expressing the sensor of interest were PFA fixed before imaging. Culture medium was removed and cells were washed with 1x PBS before incubation with 4% PFA/4% sucrose in PBS for 15 minutes at room temperature. Subsequently, cells were washed 3 times with PBS and incubated with 50 μM NH_4Cl for 10 minutes at room temperature followed by 3 final washes with PBS. Cells were stored at 4°C until further use. Before dead cell imaging, cells were permeabilized with 0.1% TritonX in PBS for 3 minutes. Imaging of the individual sensors was performed in 1x PBS equilibrated to the desired pH values using the same imaging modalities described above.

Results

GABA application to neurons leads to an increase in the FRET signal of the genetically encoded lactate sensor Laconic

We hypothesized that not only excitatory, but also inhibitory neurotransmission should affect postsynaptic neuronal metabolism. Since lactate is a crucial energy metabolite and lactate levels are influenced by glycolysis and oxidative phosphorylation (OXPHOS), we measured lactate using the genetically encoded lactate sensor Laconic. We expressed Laconic in primary cortical cultures from E17 Sprague-Dawley rats containing neurons and astrocytes and performed live cell imaging (Fig. 1A). When we exposed neurons to 200 μ M GABA, we observed a pronounced increase in the FRET ratio of Laconic (Fig. 1B+D). The peak of the Laconic signal even surpassed the response to the calibration stimulus of 10 mM lactate. When looking at the fluorescence intensity values for the individual donor and acceptor channels, we found opposite dynamics of mTFP and Venus, indicating an actual FRET response (Fig. 1C). To quantify this increase in the FRET ratio of Laconic, we performed linear fits of the data during baseline and the initial phase (first 20 s) of the GABA stimulus (Fig. 1D). The slope during GABA was significantly higher than during baseline (BL: -0.000014 ± 0.000046 vs. GABA: 0.00058 ± 0.00022 , $p < 0.001$), confirming that GABA robustly elicits an increase in the neuron FRET signal of Laconic. As this increase indicated a potential metabolic effect of GABAergic inhibition on neuronal metabolism, we aimed to identify which pathway GABA elicits this effect. We were able to reproduce this increase in the neuronal FRET ratio of Laconic by exposing our cultures to 50 μ M of Muscimol, a specific GABA_A receptor agonist (Fig. 1E, Slope BL: -0.000013 ± 0.000044 vs. Muscimol: 0.000642 ± 0.000324 , $p = 0.0033$). Inhibition of GABA_A receptors by 25 μ M Bicuculline weakened the response to Laconic to GABA (Supplementary Fig. 1, Slope GABA: 0.000606 ± 0.000146 vs. GABA + Bicuculline: 0.000231 ± 0.000062 , $p = 0.0044$). In contrast, the application of the specific GABA_B receptor agonist Baclofen was unable to elicit this effect (Supplementary Fig. 1, Slope BL: -0.000010 ± 0.000034 vs. Baclofen: 0.000010 ± 0.000067 , $p = 0.99$).

Potential pH artifact due to GABA-mediated neuronal acidification via bicarbonate efflux through GABAA receptors

These data strongly suggested that the increase in the FRET ratio of Laconic is mediated via GABA_A receptor activation. GABA_A receptors are permeable to chloride as well as to bicarbonate. The effect was still present when we substituted all chloride with gluconate (see Supplementary Fig. 2). However, in bicarbonate-free HEPES buffered ACSF, it was entirely abolished (Fig. 1F – Slope BL: 0.00000070 ± 0.0000061 vs. Baclofen: 0.000040 ± 0.000049 , $p = 0.074$), implying that the effect is mediated via bicarbonate. As bicarbonate is a critical component of the physiologic pH buffering system, we measured pH dynamics in response to

GABA application using SypHer3s. We observed significant cytosolic acidification of neurons ($p < 0.001$) in response to GABA, with the pH dropping from 7.24 ± 0.07 at baseline to 7.00 ± 0.09 (Fig. 1G). This pronounced acidification opens the possibility that the increase in the FRET signal of Laconic may be due to a pH artifact rather than an actual lactate accumulation.

To address this, we repeated the experiments with LiLac, a recently published genetically encoded lactate sensor with a reduced sensitivity to pH¹³. Upon application of GABA, we observed an initial decrease in the signal followed by an increase above baseline levels (Fig. 1H). The signal peaked and started to recover to baseline levels before GABA was removed. As the fluorescence intensity of LiLac is inversely correlated with the lactate concentration, this signal corresponds to an initial increase in cytosolic lactate levels, followed by a decrease. These results contrast the pronounced increase observed when measuring lactate using Laconic, indicating that at least one of these results, if not both, are confounded by pH. To get an idea of how strong the acidification in response to GABA influences the signal of both sensors, we correlated the normalized signals of each sensor with the pH value measured at the same time relative to the start of the application of GABA. We found that the signal of Laconic shows a near-perfect linear correlation with the pH values (Fig. 1I, slope = -0.131, $R^2 = 0.984$). In contrast, the intensity changes of LiLac exhibit a much weaker correlation with the pH values (slope = -0.033, $R^2 = 0.466$).

PFA fixation maintains sensor fluorescence and decouples lactate sensitivity from pH sensitivity

The previous data indicate that the acidification in response to GABA application confounds the lactate measurements, especially when using Laconic. However, since pH is also known to affect energy metabolism, the signal could also stem from an actual increase in lactate in the cytosol of our cultured neurons. Since in living cells, artificially decreasing neuronal pH, e.g., via acidification of the extracellular space, would consistently reproduce a potential metabolic regulation by pH, we wanted to isolate the pH sensitivity from the metabolic response to acidification. We decided to fix the cells with paraformaldehyde (PFA) to remove their metabolic response before imaging these cells (Fig. 2A). PFA fixation has been shown to leave the fluorescence lifetime of GFP-based fluorophores unchanged, which implies that fixation does not affect the fluorophore and potentially leaves their pH sensitivity intact¹⁵.

After PFA fixation we could still observe fluorescence both for cells expressing Laconic and LiLac (Fig. 2B). When we performed dead cell imaging on these cells and exposed them to lactate or pyruvate, we did not observe a prominent response of the sensor (Fig. 2C), indicating that the sensing domain of the sensor is not functional after fixation or that the fixation interferes with the conformational changes required to alter the FRET signal.

We then assessed if the pH sensitivity of Laconic after PFA fixation was maintained by changing the pH of the PBS we used for imaging from 7.24 to 7.00, i.e., the same acidification elicited by GABA in neurons. We observed an increase in the FRET signal of Laconic (Fig. 2D+E) resembling the increase in the FRET signal after GABA application in live cells both regarding directionality and amplitude (Supplementary Fig. 3A). Surprisingly, the fluorescence intensity values of the two fluorophores displayed opposite dynamics with an increase in the mTFP signal and a decrease in the Venus signal (Fig. 2F), implying that the signal change of Laconic stems from a real FRET change usually evoked by lactate binding. When we performed dead cell imaging on PFA-fixed cells that expressed LiLac and used the same pH drop as before, we observed a decrease in the fluorescence intensity (Fig. 2G+H). This decrease partially resembles the initial dip in the LiLac signal during GABA application in a live cell imaging setting. During live cell imaging, however, this dip is brief and followed by a transient increase in the signal, while during dead cell imaging, it is persistent. The decrease in the signal during Dead Cell Imaging exceeds the response of the live cells in amplitude (Supplementary Fig. 3B). This implies that the LiLac response to GABA during live cell imaging might arise from a combination of two separate, antagonizing effects, namely a pH-dependent, artifactual decrease in the signal and a transient, non-pH dependent increase in the LiLac signal that might be attributed to a change of intracellular lactate.

Laconic exhibits a stronger pH dependency than LiLac

Next, we wanted to titrate the pH dependency of both Laconic and LiLac to compare their degree of pH sensitivity and determine from which level of acidification an artifactual response confounds the results of the specific sensor. We performed dead cell imaging and subjected the cells to acidification ranging from 0.02 to 0.5 pH units. As expected, we observed an increase in the FRET signal of Laconic that increased with stronger acidifications (Fig. 3A). Likewise, the signal intensity of LiLac decreased with stronger acidifications (Fig. 3B). We then plotted the normalized amplitudes of the signal changes for both sensors against the corresponding acidification (Fig. 3C). For better comparability between the pH responses of both sensors, we used the absolute values of the signal change, ignoring the directionality of the response. We observed a linear correlation between signal change and the pH drop for Laconic (slope = 0.167, $R^2 = 0.97$) and LiLac (slope = 0.112, $R^2 = 0.95$). While LiLac was proposed to exhibit a significantly higher pH stability than Laconic, these data show that the raw signal changes of Laconic are only roughly 1.5 times bigger than LiLac's.

However, when we consider that LiLac has a much larger dynamic range than Laconic (Supplementary Fig. 3C+D) and adjust the data by the response of each sensor to an application of 10 mM lactate (Fig. 3D), Laconic appears to be nearly 12 times more pH sensitive compared to LiLac (slope Laconic: 7.72 vs. slope LiLac: 0.66).

Dead cell imaging can resolve the kinetics of an artifactual pH response

After showing that dead cell imaging can assess and compare the pH sensitivity of different genetically encoded sensors for lactate, we wanted to investigate if this method can also be applied to other sensors. We performed dead cell imaging on PFA-fixed cells expressing either the ATP sensor ATeam1.03 or the glucose sensor FLII¹²Pglu-700 μ δ 6. We then acidified the extracellular pH from 7.24 to 7.00. In addition, we performed live cell imaging of cells expressing the same sensors and applied GABA. We observed a matching decrease in the signal of FLII¹²Pglu-700 μ δ 6 for both live cell imaging and dead cell imaging, indicating that the signal change is due to pH and not due to a decrease of the glucose levels (Supplementary Fig. 4).

When we applied GABA to living cells expressing ATeam1.03, we observed a biphasic response of the FRET signal with a transient initial increase in the signal, followed by a sustained decrease that recovered with some delay upon removal of GABA (Fig. 4A+E). Interestingly, this biphasic signal is not reflected in the single FRET channels. However, both channels decrease in response to GABA with different kinetics (Fig. 4C). The fluorescence of the donor, mseCFP, decreases faster than the fluorescence of the acceptor, cp173-Venus, thereby causing the initial FRET ratio increase. Subsequently, the donor channel reaches a minimum and shows a slight signal recovery, while the acceptor channel continues to decrease throughout the application of GABA.

When we performed DeCelm and acidified the extracellular space, we could observe a very similar biphasic response (Fig. 4B+F) of the FRET ratio than in the live cell imaging setting. Like before, this initial peak of the FRET signal in the dead cell imaging setting was mediated by both individual channels decreasing in intensity at different rates (Fig. 4D). After the initial increase, the FRET signal decreases due to the donor channel increasing and the acceptor channel continuing to decrease at a slower rate, implying a pH-dependent FRET effect. As the data recorded using DeCelm recapitulates the same dynamics as the response of live cell imaging to GABA, we can confidently assume that both biphasic response components are merely pH artifacts. These data exemplify that pH-dependent signal changes of genetically encoded sensors, especially ones with two fluorophores, can be complex and display a time-dependent component. DeCelm can be a viable method to help unravel and understand the kinetics of a pH-dependent response during live cell imaging.

Discussion

In the current study, we propose a simple and cost-effective method, Dead Cell Imaging (DeCelm), to assess the pH dependency of genetically encoded biosensors. We showed that genetically encoded biosensors expressed in cells maintain their fluorescence after PFA fixation. In addition, the fluorescence of the fixed sensor proteins displayed a pH sensitivity similar to unfixed conditions. Therefore, we propose DeCelm as a novel and valid method to investigate the pH sensitivity of genetically encoded sensors and isolate pH artifacts from correct measurements of the parameter of interest.

We initially aimed to assess if neuronal inhibition by GABA has an effect on neuronal metabolism and observed a pronounced increase in the FRET signal of Laconic in response to GABA. Using the well-established pharmacology for GABA receptors, we found that the GABA_A receptor agonist Muscimol reproduced the lactate increase, while inhibition of GABA_A receptors with Bicuculline attenuated the lactate increase. In addition, stimulation of GABA_B receptors with Baclofen failed to induce this effect. Therefore, activation of GABA_A receptors was responsible for eliciting the observed increase in the Laconic signal. Following up on this, we found that this effect was mediated by bicarbonate efflux through GABA_A receptors rather than chloride influx. A major source of intracellular bicarbonate ions is conversion of CO₂ produced via mitochondrial respiration to HCO₃⁻¹⁶, therefore a metabolic feedback mechanism influencing the lactate levels appears reasonable. Indeed, bicarbonate ions are known to act as second messenger and are also involved in metabolic regulations^{17,18}.

However, bicarbonate efflux also elicits a pronounced intracellular acidification^{19,20}, which we confirmed by pH measurements using SypHer3s. Laconic is pH sensitive and responds to pH changes with an increase in the FRET signal¹⁴, therefore, we were suspicious of a potential pH artifact. When we employed another lactate sensor with improved pH stability, LiLac¹³, we indeed observed contrasting dynamics in response to GABA. Correlation of the Laconic signals with the pH dynamics confirmed a near-perfect correlation of Laconic with pH, indicating that the Laconic response is largely governed by pH.

We then used PFA fixation to decouple the pH sensitivity of Laconic from a potential pH-mediated regulation of the cellular metabolism. PFA fixation preserved the fluorescence of Laconic. In addition, PFA-fixed Laconic displayed a pH sensitivity similar to that of unfixed Laconic in live cells, indicating that the observed response to GABA is due to a pH artifact rather than a real change in the lactate levels. We then performed Dead Cell Imaging on cells expressing LiLac and observed a decrease in the signal upon acidification. These results contrasted with the short signal decrease followed by an increase that we observed in live cells, indicating that the LiLac response in live cells consists of a pH-dependent and pH-

independent component. These findings underscore the importance of considering the pH sensitivity when interpreting signals from genetically encoded sensors.

Next, expanding the applicability of Dead Cell Imaging, we demonstrated its utility in assessing the pH sensitivity of other sensors, such as ATeam1.03²¹ and FLII12Pglu-700 $\mu\delta$ ²². Dead Cell Imaging recapitulated the biphasic response observed during live cell imaging with ATeam1.03, characterized by an initial increase followed by a sustained decrease. Therefore, Dead Cell Imaging confirmed the pH-dependent artifact of both components, whereas the published end-point pH titration only suggests a decrease upon acidification²¹. The biphasic response stems from pH-dependent bleaching of both sensor fluorophores with different kinetics. These data highlight the complexity of pH artifacts of FRET sensors and the importance of assessing the kinetics of their pH sensitivity.

One caveat is that PFA is a chemical cross-linking agent that can alter protein function²³. In accordance with this, Laconic was unable to respond to lactate after PFA fixation, indicating that the sensor functionality is impaired. However, PFA fixation did not affect the fluorescence of the genetically encoded sensors examined, likely because fluorescence of fluorescent proteins depends on the chromophore, which is protected within the β -barrel structure²⁴. As PFA fixation leaves the tertiary structure of proteins largely unchanged²⁵ and the β -barrel has no obvious clefts or holes that would allow access to the chromophore for larger molecules^{26,27}, PFA fixation is unlikely to affect the fluorescent properties of fluorescent proteins. In accordance with this, PFA fixation of GFP-based proteins does not alter their fluorescence lifetime¹⁵, which is an intrinsic property that depends on the chromophore and its environment²⁸. As the pH-sensitivity of a genetically encoded sensor depends mainly on the fluorophores rather than the sensing domains⁸ and PFA fixation does not alter fluorescence of GFP-based proteins, Dead Cell Imaging can provide valuable information on the pH sensitivity of genetically encoded sensors. However, as Dead Cell Imaging cannot confidently describe the full pH sensitivity of the sensor, data obtained with this method must be interpreted with care. We recommend considering Dead Cell Imaging as a useful tool to confirm suspicions that an observed response is a pH artifact. However, the absence of a response during Dead Cell Imaging is not sufficient to conclusively rule out the presence of a pH artifact.

Our study highlights the complexity of pH-dependent responses and emphasizes the need to interpret live cell imaging data carefully. Dead cell imaging can provide additional kinetic information about the pH sensitivity of genetically encoded sensors that cannot easily be addressed using the conventional method of diluting purified proteins in buffers of different pH^{10,11}. Since it is cost-efficient, easy to use, and accessible to all laboratories capable of

performing live cell imaging, we are convinced that dead cell imaging can be a valuable tool to help improve the rigidity of data obtained during live cell imaging experiments.

References

- 1 Germond, A., Fujita, H., Ichimura, T. & Watanabe, T. M. Design and development of genetically encoded fluorescent sensors to monitor intracellular chemical and physical parameters. *Biophys Rev* **8**, 121-138, doi:10.1007/s12551-016-0195-9 (2016).
- 2 Lodovichi, C., Ratto, G. M., Trevelyan, A. J. & Arosio, D. Genetically encoded sensors for Chloride concentration. *J Neurosci Methods* **368**, 109455, doi:10.1016/j.jneumeth.2021.109455 (2022).
- 3 Zhang, Y. *et al.* Fast and sensitive GCaMP calcium indicators for imaging neural populations. *Nature* **615**, 884-891, doi:10.1038/s41586-023-05828-9 (2023).
- 4 Barros, L. F., Ruminot, I., Sandoval, P. Y. & San Martin, A. Enlightening brain energy metabolism. *Neurobiol Dis* **184**, 106211, doi:10.1016/j.nbd.2023.106211 (2023).
- 5 Sabatini, B. L. & Tian, L. Imaging Neurotransmitter and Neuromodulator Dynamics In Vivo with Genetically Encoded Indicators. *Neuron* **108**, 17-32, doi:10.1016/j.neuron.2020.09.036 (2020).
- 6 Bando, Y., Grimm, C., Cornejo, V. H. & Yuste, R. Genetic voltage indicators. *BMC Biol* **17**, 71, doi:10.1186/s12915-019-0682-0 (2019).
- 7 Barros, L. F. *et al.* Current technical approaches to brain energy metabolism. *Glia* **66**, 1138-1159, doi:10.1002/glia.23248 (2018).
- 8 Koveal, D. Functional principles of genetically encoded fluorescent biosensors for metabolism and their quantitative use. *Journal of Neurochemistry*, doi:10.1111/jnc.15878 (2023).
- 9 Berg, J., Hung, Y. P. & Yellen, G. A genetically encoded fluorescent reporter of ATP:ADP ratio. *Nat Methods* **6**, 161-166, doi:10.1038/nmeth.1288 (2009).
- 10 Bischof, H. *et al.* Novel genetically encoded fluorescent probes enable real-time detection of potassium in vitro and in vivo. *Nature Communications* **8**, 1422 (2017).
- 11 Zhao, Y., Shen, Y., Wen, Y. & Campbell, R. E. High-performance intensimetric direct-and inverse-response genetically encoded biosensors for citrate. *ACS Central Science* **6**, 1441-1450 (2020).
- 12 Dechant, R. *et al.* Cytosolic pH is a second messenger for glucose and regulates the PKA pathway through V-ATPase. *EMBO J* **29**, 2515-2526, doi:10.1038/emboj.2010.138 (2010).
- 13 Koveal, D. *et al.* A high-throughput multiparameter screen for accelerated development and optimization of soluble genetically encoded fluorescent biosensors. *Nat Commun* **13**, 2919, doi:10.1038/s41467-022-30685-x (2022).
- 14 San Martin, A. *et al.* A genetically encoded FRET lactate sensor and its use to detect the Warburg effect in single cancer cells. *PLoS One* **8**, e57712, doi:10.1371/journal.pone.0057712 (2013).
- 15 Joosen, L., Hink, M. A., Gadella, T. W., Jr. & Goedhart, J. Effect of fixation procedures on the fluorescence lifetimes of Aequorea victoria derived fluorescent proteins. *J Microsc* **256**, 166-176, doi:10.1111/jmi.12168 (2014).
- 16 Cordat, E. & Casey, J. R. Bicarbonate transport in cell physiology and disease. *Biochemical Journal* **417**, 423-439 (2009).
- 17 Acin-Perez, R. *et al.* Cyclic AMP produced inside mitochondria regulates oxidative phosphorylation. *Cell metabolism* **9**, 265-276 (2009).
- 18 Ruminot, I. *et al.* NBCe1 mediates the acute stimulation of astrocytic glycolysis by extracellular K⁺. *Journal of Neuroscience* **31**, 14264-14271 (2011).
- 19 Chen, J. C. & Chesler, M. A bicarbonate-dependent increase in extracellular pH mediated by GABAA receptors in turtle cerebellum. *Neurosci Lett* **116**, 130-135, doi:10.1016/0304-3940(90)90398-s (1990).
- 20 Kaila, K., Paalasmaa, P., Taira, T. & Voipio, J. pH transients due to monosynaptic activation of GABAA receptors in rat hippocampal slices. *Neuroreport* **3**, 105-108 (1992).

-
- 21 Imamura, H. *et al.* Visualization of ATP levels inside single living cells with fluorescence resonance energy transfer-based genetically encoded indicators. *Proc Natl Acad Sci U S A* **106**, 15651-15656, doi:10.1073/pnas.0904764106 (2009).
- 22 Takanaga, H., Chaudhuri, B. & Frommer, W. B. GLUT1 and GLUT9 as major contributors to glucose influx in HepG2 cells identified by a high sensitivity intramolecular FRET glucose sensor. *Biochimica et Biophysica Acta (BBA)- Biomembranes* **1778**, 1091-1099 (2008).
- 23 Hoffman, E. A., Frey, B. L., Smith, L. M. & Auble, D. T. Formaldehyde crosslinking: a tool for the study of chromatin complexes. *J Biol Chem* **290**, 26404-26411, doi:10.1074/jbc.R115.651679 (2015).
- 24 Craggs, T. D. Green fluorescent protein: structure, folding and chromophore maturation. *Chemical Society Reviews* **38**, 2865-2875 (2009).
- 25 Toews, J., Rogalski, J. C. & Kast, J. Accessibility governs the relative reactivity of basic residues in formaldehyde-induced protein modifications. *Analytica chimica acta* **676**, 60-67 (2010).
- 26 Yang, F., Moss, L. G. & Phillips, G. N., Jr. The molecular structure of green fluorescent protein. *Nat Biotechnol* **14**, 1246-1251, doi:10.1038/nbt1096-1246 (1996).
- 27 Zimmer, M. Green fluorescent protein (GFP): applications, structure, and related photophysical behavior. *Chem Rev* **102**, 759-781, doi:10.1021/cr010142r (2002).
- 28 Berezin, M. Y. & Achilefu, S. Fluorescence lifetime measurements and biological imaging. *Chem Rev* **110**, 2641-2684, doi:10.1021/cr900343z (2010).

Author Contributions

B.G. and N.P. conceived the study and contributed to the study design. B.G. and C.R. contributed to the acquisition and analysis of the data. B.G. and N.P. contributed to the interpretation of the data. B.G. and N.P. drafted the manuscript. All authors read and approved the final manuscript.

Competing Interests

The authors declare no competing interests.

Data availability

The data generated during the study are available from the corresponding author upon request.

Figures

Figure 1

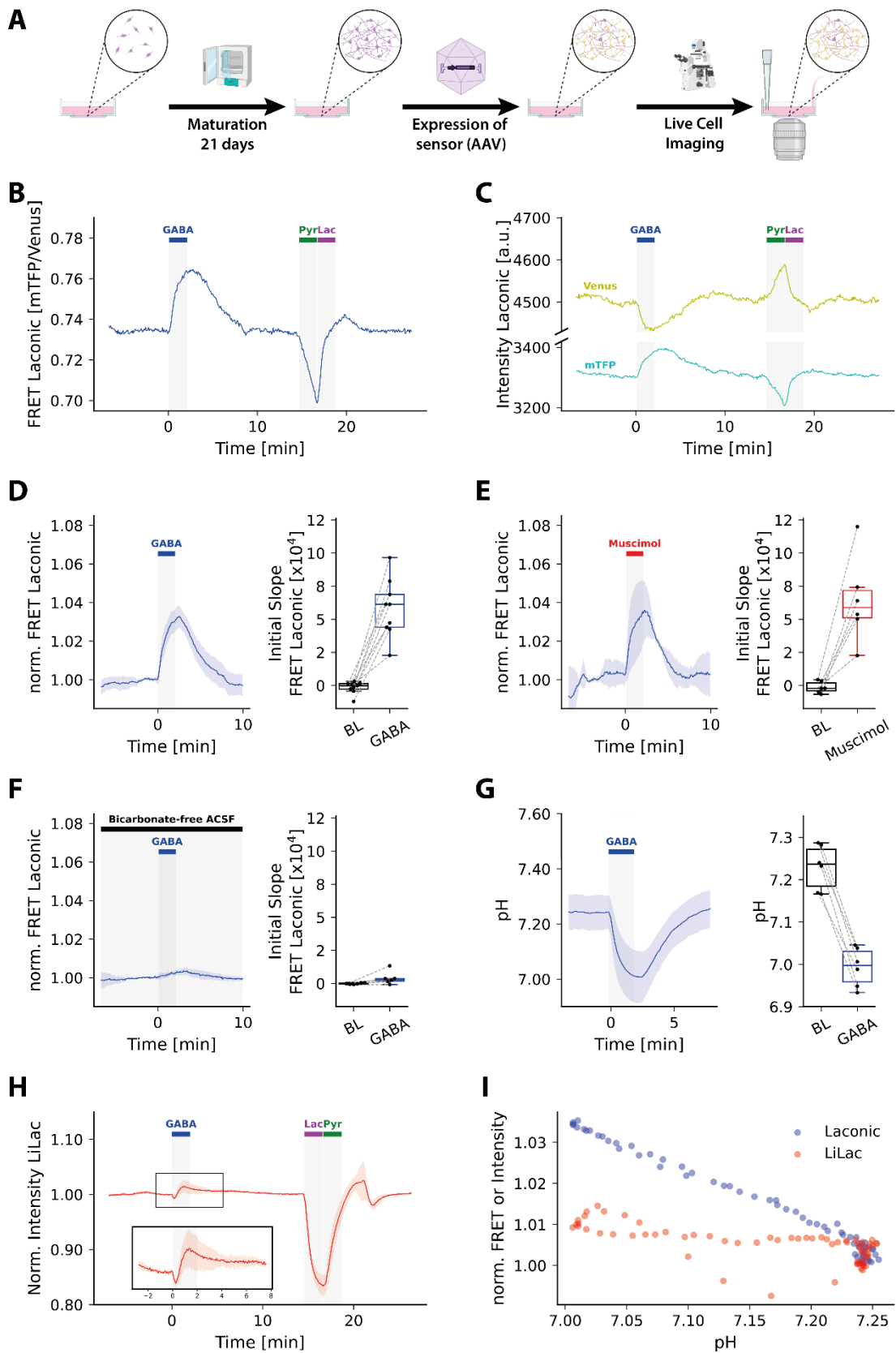


Figure 2

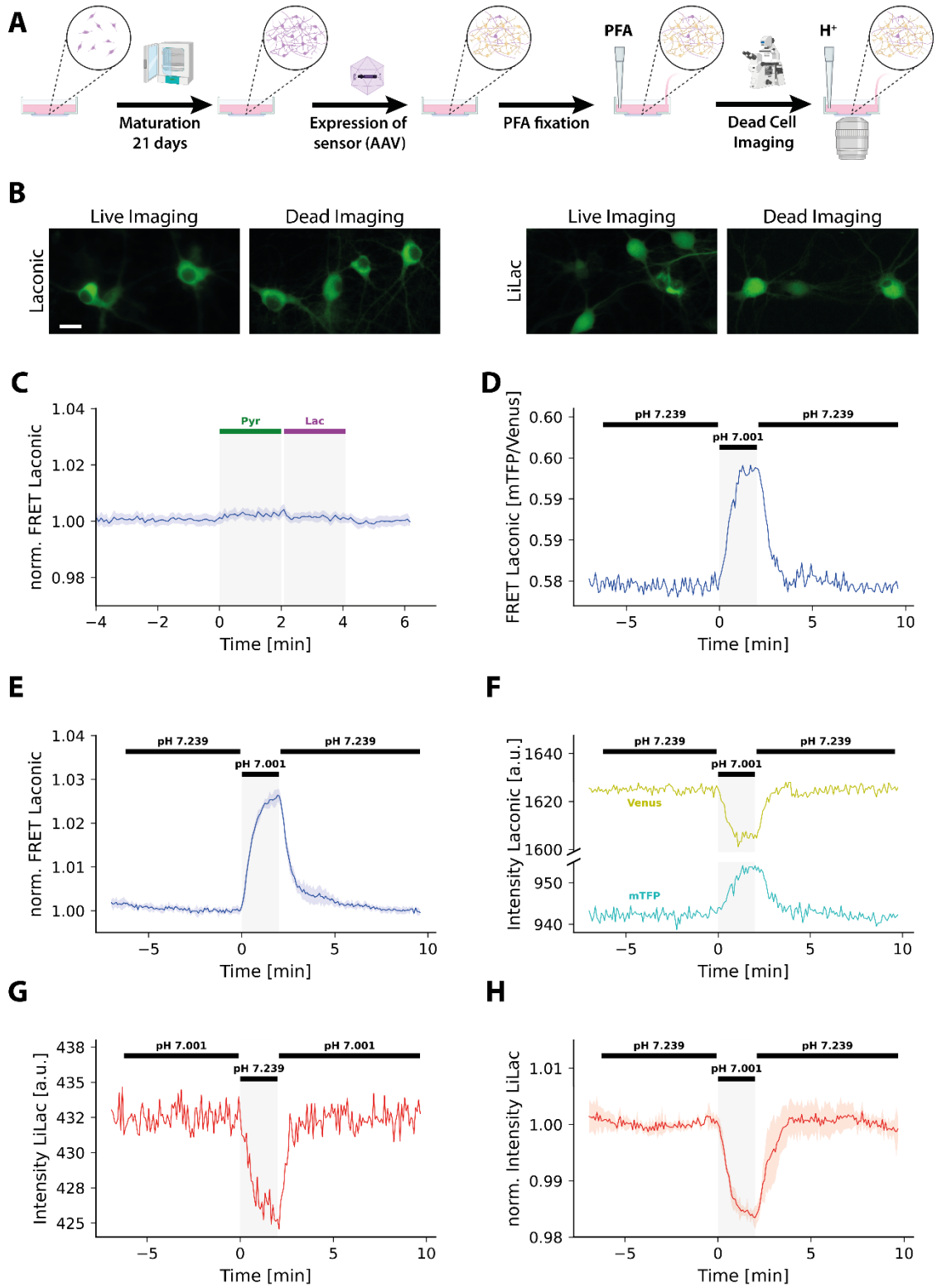


Figure 3

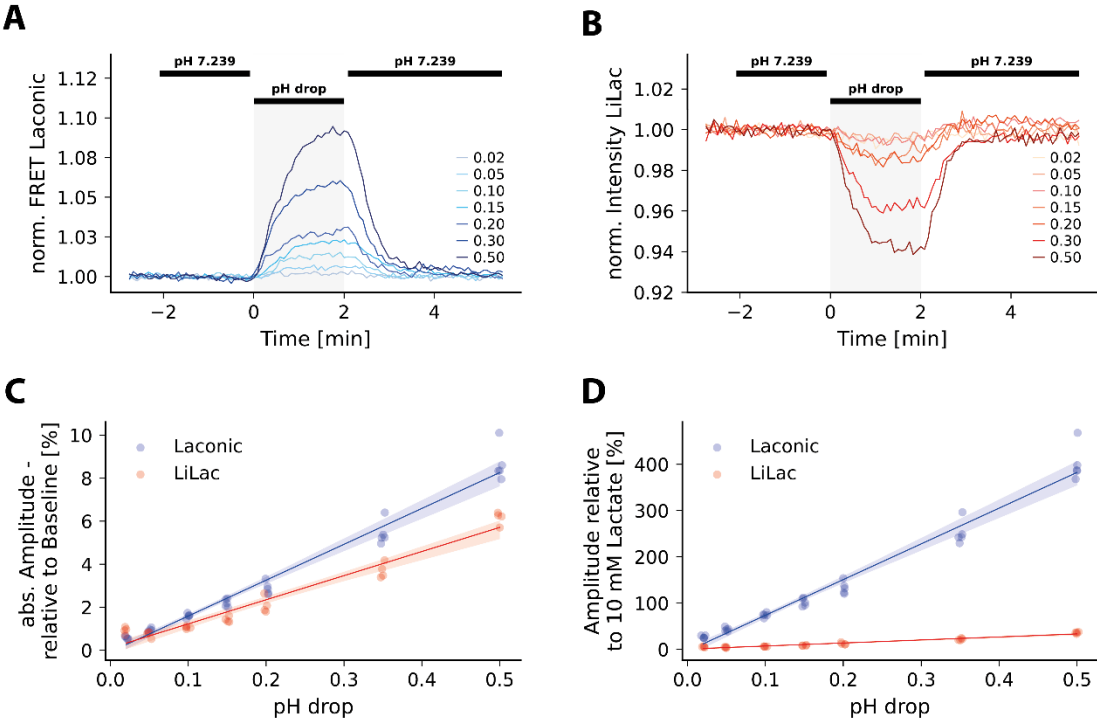


Figure 4

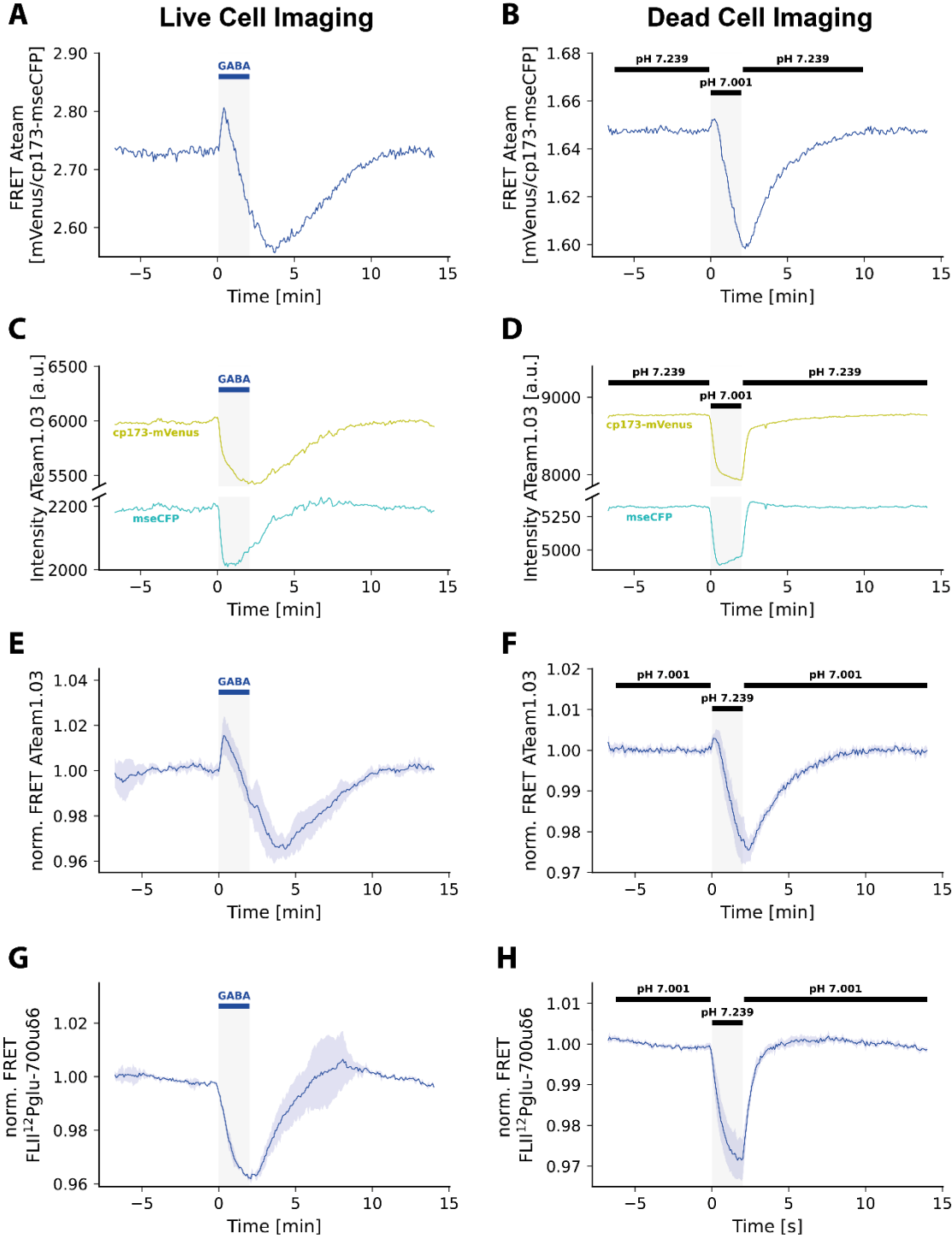


Figure Legends

Figure 1: GABA leads to an artefactual increase in the FRET signal of Laconic expressed in neurons (A) Overview over live cell imaging experiment. Primary mixed cortical cultures from E17 Sprague-Dawley rats were grown to maturity for 21 days and transduced with AAVs to express the sensor of interest. Coverslips containing the cells were transferred to an inverted microscope and live cell imaging was performed with continuous superfusion with ACSF gassed with 5% CO₂/95% air. (B) Example trace of the FRET ratio of Laconic expressed in a single neuron. 200 μ M GABA leads to an increase in the FRET ratio. The subsequent calibration of Laconic with 10 mM pyruvate and 10 mM lactate shows that Laconic does measure lactate. (C) Traces of the individual channels of the Laconic trace shown in (B). Traces show an opposite behavior, indicating that FRET occurs. (D) Averaged trace (left) and quantification of the slope (right) of the response of Laconic to 200 μ M GABA (n = 9 experiments). Traces for all neurons of each experiment were normalized the combined trace is represented as mean \pm SD. Slopes were calculated by a linear fit of the 24 frames before GABA application (BL) and the first 5 frames after GABA application (GABA) for each cell. Each data point represents the mean slope of an individual experiment. (E) Averaged trace (left – mean \pm SD) and quantification of the slope (right) of the response of Laconic to 50 μ M Muscimol (n = 6 experiments). (F) Averaged trace (left – mean \pm SD) and quantification of the slope (right) of the response of Laconic to 200 μ M GABA in bicarbonate-free ACSF (n = 6 experiments). (G) Averaged trace (left – mean \pm SD) and quantification of the amplitude (right) of the response of SypHer3s to 200 μ M GABA. At the end of each experiment, a pH calibration was performed and the absolute pH for each single trace was calculated. Therefore, the trace represents the mean of all individual cells (n = 97 cells in 6 experiments). (H) Averaged trace of the normalized response of LiLac to 200 μ M GABA (n = 5 experiments). The calibration of LiLac with 10 mM lactate and 10 mM pyruvate shows that the LiLac signal intensity inversely correlates with the cytosolic lactate concentration. (I) Correlation of the normalized average signals of Laconic (blue) and LiLac (red) with the average pH value at each time point with respect to the application of GABA (n = 68 data points per sensor).

Figure 2: PFA fixed cells maintain their fluorescence and show a pH sensitivity (A) Overview over dead cell imaging experiment. Primary mixed cortical cultures from E17 Sprague-Dawley rats were grown to maturity for 21 days and transduced with AAVs to express the sensor of interest. Cells were then PFA fixed and afterwards, coverslips containing the fixed cells were transferred to an inverted microscope and dead cell imaging was performed with continuous superfusion with PBS. (B) Representative image of cells expressing Laconic (left) or LiLac (right) during live cell imaging or during imaging after PFA fixation. Scalebar represents 20 μ m. (C) Averaged trace of the FRET ratio of PFA fixed cells expressing Laconic

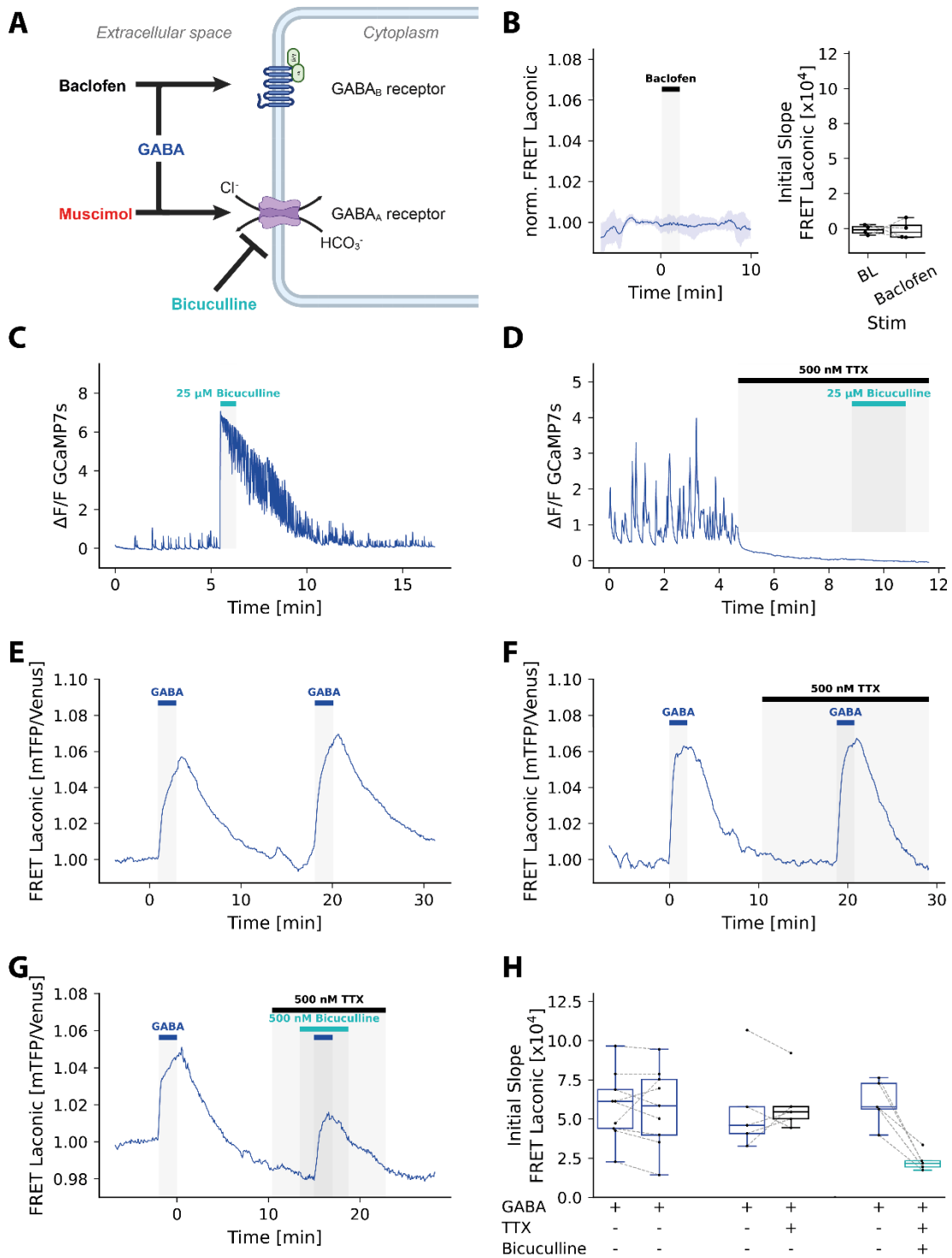
after exposure to 10 mM lactate or 10 mM pyruvate Trace represents mean \pm SD of a single experiment (n = 25 cells). No significant response of Laconic can be observed. **(D)** Example trace of the FRET ratio of Laconic from a single neuron after PFA fixation. Acidification from 7.239 to 7.001 leads to an increase in the FRET ratio. **(E)** Averaged trace of the response of Laconic after PFA fixation to acidification (mean \pm SD, n = 6 experiments) **(F)** Traces of the individual channels of the Laconic trace shown in (D). Traces show an opposite behavior, indicating that FRET occurs. **(G)** Example trace of a single neuron expressing LiLac after PFA fixation. Acidification leads to a decrease in the signal intensity. **(H)** Averaged trace of the response of LiLac after PFA fixation to acidification (mean \pm SD, n = 4 experiments).

Figure 3: pH titration using PFA fixed cells shows that LiLac is less pH sensitive than Laconic **(A)** Normalized FRET ratio changes of a single PFA fixed neuron expressing Laconic after exposure to different acidifications. Baseline pH of 7.239 was acidified by values ranging from 0.02 to 0.5. **(B)** Normalized intensity changes of a single PFA fixed neuron expressing LiLac after exposure to different acidifications. **(C)** Correlation of the amplitudes of the signal changes of Laconic (blue, n = 5 experiments) and LiLac (red, n = 4 experiments) with the corresponding acidifications. Each data point represents the mean amplitude of all neurons of one experiment. Shadow represents 95% confidence interval. Directionality of the amplitude was ignored for better comparability. **(D)** Correlation as in (C), however amplitudes of the signal changes of Laconic (blue, n = 5 experiments) and LiLac (red, n = 4 experiments) were normalized by the amplitude of the response of the respective sensor to 10 mM lactate. The adjusted data shows that amplitude changes of LiLac depend less on pH. Each data point represents the mean amplitude of all neurons of one experiment. Shadow represents 95% confidence interval.

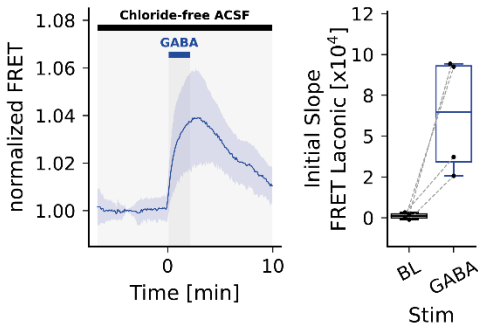
Figure 4: Dead cell imaging can resolve the dynamics of pH induced artefacts **(A)** Example trace of live cell imaging of ATeam1.03 expressed in a single neuron. 200 μ M GABA leads to an initial increase in the FRET ratio followed by a sustained decrease. **(B)** Example trace dead cell imaging of ATeam1.03 from a single, PFA fixed neuron. Acidification leads to a similar response of the PFA fixed ATeam1.03 with an initial increase followed by a sustained decrease. **(C)** Traces of the individual channels of the live cell imaging trace of ATeam1.03 shown in (A). Both cp173-mVenus and mseCFP respond to 200 μ M GABA with a decrease in the signal intensities with different kinetics. **(D)** Traces of the individual channels of the dead cell imaging trace of ATeam1.03 shown in (B). Both cp173-mVenus and mseCFP respond to acidification with a decrease in the signal intensities with different kinetics, similar than in (C). **(E)** Averaged trace of the normalized responses of ATeam1.03 to 200 μ M GABA during live cell imaging (mean \pm SD, n = 3). **(F)** Averaged trace of the normalized responses of ATeam1.03 to acidification during dead cell imaging (mean \pm SD, n = 5).

Supplementary Figures

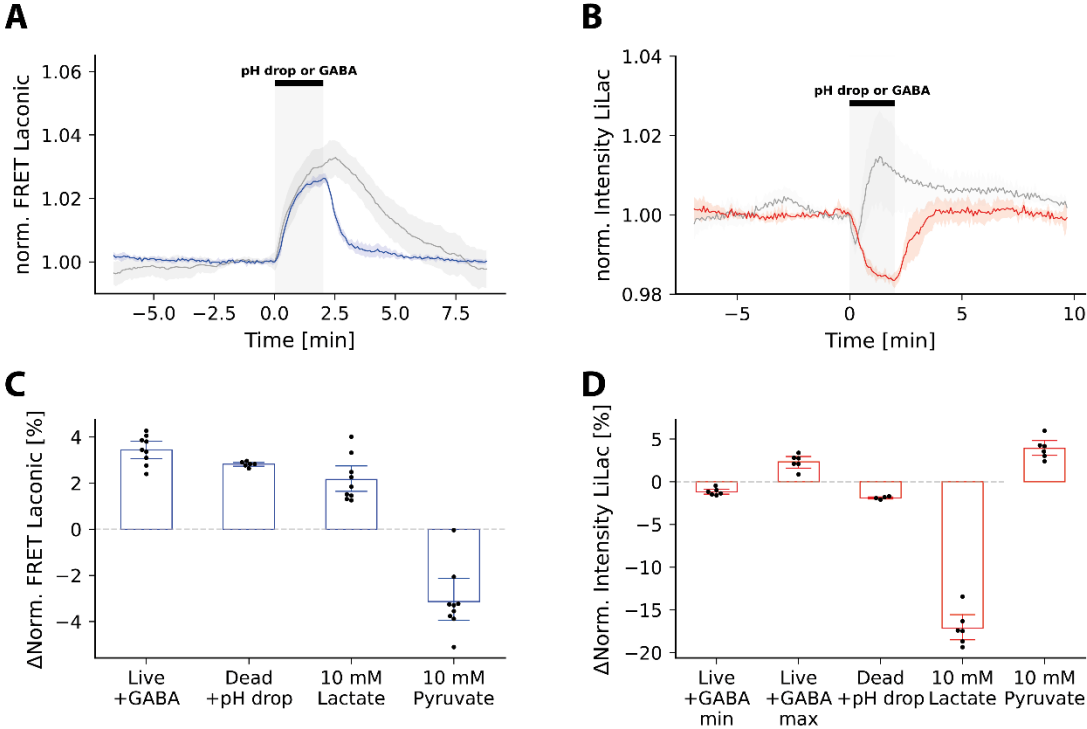
Supplementary Figure 1



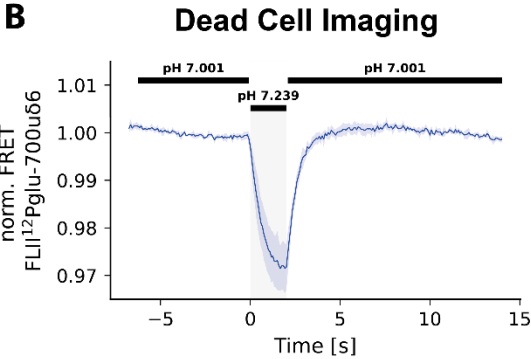
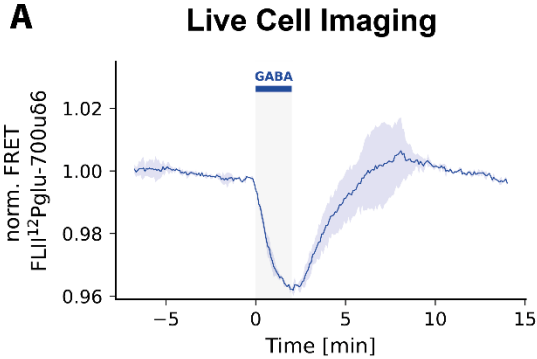
Supplementary Figure 2



Supplementary Figure 3



Supplementary Figure 4



Supplementary Figure Legends

Supplementary Figure 1: The increase in the FRET signal of Laconic in response to GABA is GABA_A receptor mediated (A) Schematic overview over the pharmacology of GABA receptors. Baclofen and Muscimol are specific agonists for GABA_B and GABA_A receptors respectively, while Bicuculline is a specific GABA_A receptor antagonist. GABA_A receptor activation leads to inflow of chloride and simultaneous outflow of bicarbonate ions. **(B)** Averaged trace (left – mean ± SD) and quantification of the slope (right) of the response of Laconic to 30 μM Baclofen (n = 4 experiments). **(C+D)** Representative example traces of single neurons expressing GCaMP7s proving that Bicuculline needs to be applied in the presence of TTX to avoid seizure-like neuronal activity leading to metabolic artefacts. **(C)** Application of 25 μM Bicuculline alone leads to a seizure-like firing behavior. **(D)** 500 nM TTX abolish the seizure-like behavior elicited by Bicuculline. **(E-H)** Representative example traces of the FRET ratio of Laconic show that the increase in the Laconic signal in response to GABA can be diminished by inhibition of GABA_A receptors using Bicuculline. A first application of GABA is used for relative quantification of a second application of GABA with or without TTX or Bicuculline. **(E)** The effect of GABA on Laconic is reproducible and the responses are not changed between first and second application. **(F)** TTX does not affect the GABA response. **(G)** Bicuculline in the presence of TTX (to avoid epileptic-like firing) does reduce the amplitude of the GABA response. **(H)** Quantification of the slopes in response to the first GABA application compared to a second application of GABA (n = 9), GABA in the presence of TTX (n = 5) or GABA in the presence of TTX and Bicuculline (n = 5).

Supplementary Figure 2: The increase of Laconic in response to GABA is not due to GABA_A receptor mediated chloride flux Averaged trace (left – mean ± SD) and quantification of the slope (right) of the response of Laconic to 200 μM GABA in bicarbonate-free ACSF (n = 4 experiments).

Supplementary Figure 3: Comparison of live and dead cell imaging of Laconic and LiLac **(A)** Overlay of the averaged traces of Laconic during dead cell imaging (blue – shown in Figure 2E) and live cell imaging (grey – shown in Figure 1D) for comparison. Traces are similar in direction and amplitude. **(B)** Overlay of the averaged traces of LiLac during dead cell imaging (red – shown in Figure 2H) and live cell imaging (grey – shown in Figure 1H) for comparison. Traces are similar in direction and amplitude. **(C)** Amplitudes of the normalized FRET ratio changes of Laconic in response to 200 μM GABA, 10 mM lactate or 10 mM pyruvate during live cell imaging (n = 9) or to acidification during dead cell imaging (n = 6). The effect of GABA or acidification on Laconic is comparable to the dynamic range as determined by application of lactate and pyruvate. **(D)** Amplitudes of the normalized intensity changes of LiLac in response to 200 μM GABA (both amplitudes of initial decrease and subsequent increase), 10

mM lactate or 10 mM pyruvate during live cell imaging (n = 6) or to acidification during dead cell imaging (n = 4). The effect of GABA or acidification on LiLac is considerably smaller compared to the dynamic range.

Supplementary Figure 4: Dead cell imaging reproduces the effect of GABA on FLII¹²Pglu-700uδ6 (A) Averaged trace of the normalized responses of FLII¹²Pglu-700uδ6 to 200 μM GABA during live cell imaging (mean ± SD, n = 2). **(F)** Averaged trace of the normalized responses of FLII¹²Pglu-700uδ6 to acidification during dead cell imaging (mean ± SD, n = 4).

4 Discussion

4.1 Readouts of genetically encoded sensors need to be carefully interpreted

Genetically encoded sensors are a powerful tool for understanding biological pathways and have frequently become the method of choice thanks to their unique combination of spatial and temporal resolution while allowing minimally invasive measurements. Their usefulness is demonstrated by the fact that over the last decades, sensors for a multitude of analytes have been developed and are continuously improved. Despite the unquestionable advantages of genetically encoded sensors, some key interferences such as recognition of off-targets, insufficient affinity for the analyte or sensitivity to the environment can confound their readout. As those confounders can, in the worst-case, lead to false-negative or false-positive results, data obtained with a genetically encoded sensor need to be carefully interpreted with respect to the properties of the sensor and the biological system that has been studied.

This thesis addresses two projects that involve different scenarios of sensor shortcomings. It characterizes a genetically encoded FRET sensor for K^+ , Ic-LysM GEPII 1.0²¹, for its capacity to resolve neuronal K^+ dynamics in response to neuronal activity. While Ic-LysM GEPII 1.0 can resolve K^+ dynamics in response to strong neuronal activity both *in vitro* and *in vivo*, it fails to detect K^+ changes during spontaneous or mild activity. Furthermore, this thesis addresses the widespread problem of pH sensitivity of genetically encoding sensors and proposes a simple and cost-effective protocol, Dead Cell Imaging, to help identify if the response of a given sensor might be a pH artifact. Both projects will be discussed below, followed by general considerations on how to improve the robustness of results obtained via live cell imaging with genetically encoded sensors.

4.2 Study I: Probing Intracellular Potassium Dynamics in Neurons: *In vitro* and *In vivo* Assessment of a Genetically Encoded Sensor

4.2.1 Main findings of the study

In this study we report a characterization of the genetically encoded K^+ sensor Ic-LysM GEPII 1.0 and its capacity to resolve K^+ dynamics in response to neuronal activity. To provide a comprehensive overview, we performed these experiments both in primary mixed cortical cell cultures containing neurons and astrocytes as well as *in vivo* in cortical neurons of mice.

We found that Ic-LysM GEPII 1.0 responds to intense neuronal activity *in vitro* evoked by application of Bicuculline with a decrease in the FRET ratio, indicating a K^+ decrease. In addition, we observed CSD-evoked increases in the fluorescence lifetime of Ic-LysM GEPII 1.0 *in vivo*, which also corresponds to a K^+ decrease. This is in line with the expectation as neuronal repolarization after activity is mediated by K^+ efflux⁵ and indicates that Ic-LysM GEPII

1.0 is able to measure K⁺ dynamics in neurons. To the best of our knowledge, this represents the first recording of intracellular mammalian K⁺ dynamics *in vivo* using an imaging approach.

Furthermore, we show that the sensitivity of lc-LysM GEPII 1.0 in neurons is restricted to intense activity with large bulk changes of [K⁺]_i. We could not resolve any K⁺ changes upon spontaneous neuronal activity both *in vitro* and *in vivo*. Inducing activity *in vitro* via optogenetic stimulation showed that lc-LysM GEPII 1.0 does not respond to single or few action potentials. This is likely not because the K⁺ levels do not change in response to mild stimulation but rather because the resulting K⁺ decrease was too small for detection with lc-LysM GEPII 1.0. We attributed this lack of sensitivity to the affinity of lc-LysM GEPII 1.0, which is reported to be 27.4 mM²¹ and therefore not optimal for recording intracellular K⁺ dynamics. Therefore, optimization of lc-LysM GEPII 1.0 is required to allow K⁺ measurements in response to spontaneous activity and more physiological stimulation paradigms.

Finally, we established imaging of lc-LysM GEPII 1.0 while simultaneously inducing neuronal activity using optogenetic stimulation. This protocol allowed us to titrate the responsivity of lc-LysM GEPII 1.0 to neuronal activity in a very controlled manner. We believe that this approach will be useful to characterize the performance of future novel mutants of lc-LysM GEPII 1.0 or of other K⁺ sensors and allow comparisons with respect to their capacity to resolve K⁺ dynamics in response to neuronal activity. Similar approaches have been used for the characterization of Ca²⁺ sensors of the GCaMP series, which involved comparing the performance of novel variants with respect to their response to action potentials evoked by field stimulation²⁰.

4.2.2 Limitations of the study

The major caveat of this study is that neuronal activity is usually accompanied by intracellular acidification¹¹⁹ which could also affect the signal of lc-LysM GEPII 1.0. Since the amplitude of the activity-mediated acidification usually correlates with the strength of the activity, an alternative explanation of the results could be that the observed decrease in the K⁺ levels during intense activity is a pH artifact. In fact, spreading depolarizations elicit a pronounced decrease in intracellular pH both in slices¹²³ and *in vivo*¹²⁴. In line with this, the optogenetic titration experiments of lc-LysM GEPII 1.0 warrant special consideration, as ChrimsonR is also permeable to protons and optogenetically induced acidification potentially adds to the activity mediated acidification¹²⁵. Indeed, an intense optogenetic stimulation protocol with an opsin with similar kinetics than ChrimsonR can acidify neurons by up to 0.54 pH units¹²⁶. However, the stimulation protocol used in the current study was over 65 times less intense. Therefore, the acidification evoked by proton permeability of ChrimsonR during optogenetic stimulation is negligible and the overall acidification is governed by the activity-mediated acidification.

Data on the pH sensitivity of Ic-LysM GEPII 1.0 is not available; however, it is derived from GEPII 1.0 by only 3 point mutations and therefore likely displays a comparable pH sensitivity. As GEPII 1.0 is largely insensitive to pH changes within the physiological range²¹, it is reasonable to assume that Ic-LysM GEPII 1.0 is also not heavily pH dependent. However, during more extreme acidifications, GEPII 1.0 does display a decrease in the FRET signal at saturating levels of K⁺. As Ic-LysM GEPII 1.0 is expected to be saturated or to be close to saturation in the neuronal cytosol, a similar pH dependence could potentially explain the observed decrease in the FRET signal *in vitro*. However, we observed an increase in the fluorescence lifetime of the donor of Ic-LysM GEPII 1.0 in response to peri-infarct depolarizations, which also corresponds to a decrease of the K⁺ levels. Fluorescence lifetime of GFP-based fluorescent proteins, including CFP, displays a pH sensitivity and acidification correlates with a decrease in the fluorescence lifetime^{127,128}. Therefore, if the intracellular acidification accompanying the PID elicits a pH-induced change of the fluorescence lifetime, a decrease rather than the observed increase would be expected during the *in vivo* experiments. While pH changes could also influence the lifetime via inducing conformational changes that affect FRET efficiency, the pH sensitivity of genetically encoded sensors is generally governed by the fluorescent proteins¹⁰⁷. Therefore, it is unlikely that activity-mediated acidification explains the observed results, and it is more likely that Ic-LysM GEPII 1.0 did indeed respond to the activity-induced K⁺ decrease. However, the possibility of a contribution of pH to the signal cannot be fully ruled out. Measurement of the pH dynamics induced by the different stimulation paradigms with a genetically encoded sensor for pH¹²⁹ would help to unravel the extent of the acidification. In addition, assessing the pH sensitivity of Ic-LysM GEPII 1.0, for example using Dead Cell Imaging, would help to further address this problem.

Another potential caveat of this study concerns the K⁺ measurements during optogenetic stimulation of neurons. ChrimsonR does not exhibit a strong ion selectivity and is not only permeable to Na⁺ and protons but also displays K⁺ permeability¹²⁵. Therefore, the observed decrease in the FRET ratio in response to optogenetic stimulation could be a result of a large K⁺ outflow through ChrimsonR rather than due to induction of neuronal activity. However, this scenario is unlikely as stimulation of ChrimsonR reliably evoked action potentials during Ca²⁺ imaging, which should amplify the evoked ion changes. In contrast, pure K⁺ efflux through ChrimsonR should lead to hyperpolarization and therefore neuronal inhibition. Indeed, the activation of novel K⁺-selective channelrhodopsins leads to efficient neuronal silencing through K⁺ efflux¹³⁰.

4.2.3 Comparison of Ic-LysM GEPII 1.0 with other K⁺ sensors

In study I, we characterized Ic-LysM GEPII 1.0 towards its capacity to resolve K⁺ dynamics during neuronal activity. Genetically encoded K⁺ sensors have a brief history and to date, only

few of these sensors have been published²¹⁻²⁴. Accordingly, this is the first detailed study assessing a genetically encoded K⁺ sensor in the context of neuronal activity. To achieve precise measurement of K⁺ dynamics with respect to neuronal activity, a genetically encoded K⁺ sensor should display a low affinity for K⁺ with a K_D close to the neuronal [K⁺]_i of around 140 mM⁸. Furthermore, as acidification accompanies neuronal activity, it should be pH insensitive within the physiologic range. Furthermore, high dynamic range and fast kinetics can help to resolve slight changes of the K⁺ levels during mild activity. We will compare lc-LysM GEPII 1.0 with other published sensors with respect to these criteria.

lc-LysM GEPII 1.0 is one of 4 affinity variants of GEPII 1.0 and displays the lowest affinity of all these variants with a K_D of 27.4 mM. GEPIIs were introduced by the Malli lab in 2017, making them the first genetically encoded K⁺ sensors ever published²¹. Since then, two other groups have developed genetically encoded K⁺ sensors. Shen and colleagues introduced three new sensors in 2019, employing the same binding protein (Kbp) used for GEPIIs²². They developed a cyan/yellow-FRET-based sensor named KIRIN1 and a red-shifted variant KIRIN1-GR, using a green/red FRET pair. In addition, they introduced the first single-fluorophore K⁺ sensor GINKO1 by inserting Kbp into a circular permuted eGFP. All three sensors display a remarkably high K⁺ affinity with their K_D ranging from 0.42 to 2.56 mM. As this affinity should lead to saturation of these sensors in the neuronal cytosol, it renders them inadequate for measuring neuronal K⁺ dynamics. As GINKO1 also responded to Na⁺ ions, the same group developed a variant called GINKO2 with no Na⁺ sensitivity²⁴. These modifications also led to a lower affinity of GINKO2 (K_D of 15.3 mM). However, due to their nature as single fluorophore sensors, GINKOs display a high pH sensitivity, which complicates the interpretation in experiments where pH changes occur.

Overall, the affinity of the discussed sensors, including lc-LysM GEPII 1.0, is too high for ideal measurement of neuronal intracellular K⁺ dynamics. A recently published family of genetically encoded K⁺ sensors named KRaIONs aimed to overcome this issue by using a modified Kbp as a binding domain to reduce the affinity of the resulting sensors. The resulting sensors KRaION1, KRaION1/D9N and KRaION2 display favorably low K⁺ affinities with K_Ds of 69, 138 and 96 mM, respectively²³. Interestingly, these sensors showed substantially higher affinities after expression in cells, highlighting the importance of the experiments performed in study I. Despite these inconsistencies, the affinity of KRaIONs is considerably better suited for measuring neuronal K⁺ dynamics than that of any other genetically encoded K⁺ sensor, including lc-LysM GEPII 1.0. However, KRaIONs are, like GINKOs, single-fluorophore sensors and are therefore vulnerable to pH changes. Indeed, KRaION1 displays a dramatic pH sensitivity with signal changes of about 300% between pH 6 and 8. While the pH sensitivity is not reported for the other two variants, they almost certainly display a similar pH sensitivity as

they differ from KRaION1 by only point mutation in the Kbp domain. Due to this extreme pH sensitivity, KRaIONs are not suitable for measuring activity mediated K^+ dynamics in neurons, as neuronal activity elicits cytosolic acidification.

In conclusion, there is currently no genetically encoded K^+ sensor perfectly suited for reliable detection of activity-mediated K^+ dynamics in neurons, as all existing sensors suffer from either inadequate affinity (GEPiIs, KIRINs), high pH sensitivity (KRaIONs) or both (GINKOs). Unless novel strategies address the pH sensitivity of single fluorophore sensors¹³¹, FRET sensors are the more promising class for resolving activity-mediated K^+ dynamics. Therefore, of the sensors available, Ic-LysM GEPiI 1.0 appears to be the K^+ sensor currently best suited for resolving activity-mediated K^+ dynamics in neurons, since it displays a rather high pH stability as well as the lowest K^+ affinity of all existing FRET-based K^+ sensors. However, the promising modifications made to Kbp for the development of KRaIONs represent an exciting possibility to further optimize Ic-LysM GEPiI 1.0 with respect to its affinity.

4.3 Study II: Assessing the pH sensitivity of genetically encoded sensors with Dead Cell Imaging

4.3.1 Detecting pH artifacts of genetically encoded sensors can be challenging

As previously discussed, genetically encoded sensors are vulnerable to pH changes due to their nature as proteins. Therefore, a potential pH change accompanying a certain stimulus can lead to an artifactual response. It is however not always straightforward to identify if a sensor response to such a stimulus is due to a pH artifact rather than an actual change of the analyte levels.

The original publication of a genetically encoded sensor usually reports its pH sensitivity. Therefore, in case of the observation of a pH change during an experiment, one can assess at least qualitatively if the observed response could be a pH artifact. However, the information on the pH sensitivity is lacking for some sensors¹³² or not reported for all sensor variants. For example, study one of this thesis used the K^+ sensor Ic-LysM GEPiI 1.0. The original publication only describes the pH sensitivity of the variant GEPiI 1.0, not of Ic-LysM GEPiI 1.0 or other variants²¹. This lack of information can make it difficult to interpret the results obtained with such a sensor if pH changed during the experiment. However, even if data on the pH sensitivity is available it can be challenging to decipher if an observed signal corresponds to a real change in analyte levels or a pH artifact, as analyte levels and pH might change independently from each other. The observed response might be also a combination of a pH artifact and real analyte changes. Due to this problem, measurement of neuronal K^+ with the sensor GINKO2 in response to neuronal activity yielded inconclusive results²⁴. In addition, pH

is also a potent second messenger and can elicit physiological responses and real changes in the analyte levels¹²². This adds another layer of complexity as simply changing the extracellular pH is not a suitable pH control since this would simply reproduce the pH mediated analyte change. We developed Dead Cell Imaging as an easy way to address the pH sensitivity of genetically encoded sensors. The following sections will discuss the key advantages and limitations of Dead Cell Imaging and compare it with other methods.

4.3.2 Advantages of Dead Cell Imaging

One key advantage of Dead Cell Imaging is that it addresses the pH sensitivity of a genetically encoded sensor independent from the dynamic physiological response of its analyte to pH changes. Since PFA fixation eliminates cellular function, changing the pH cannot lead to any biological response that involves alterations of the analyte levels. Therefore, as sensor fluorescence is preserved during PFA fixation and reacts to pH changes, all signal changes depend only on the pH sensitivity of the sensor rather than concomitant analyte changes.

Another advantage of Dead Cell Imaging is that it allows assessment of the pH sensitivity of a genetically encoded sensor with respect to its kinetics. This is especially interesting for FRET-based sensors as they contain two fluorescent proteins with different pH responses. As we show using the ATP sensor ATeam1.03⁵⁷, this can lead to complex pH responses. In a live cell imaging setting, ATeam1.03 responds to a GABA-induced acidification with an initial peak that is followed by a sustained decrease in the FRET ratio. The reason behind this biphasic pH response of ATeam1.03 is that both fluorescent proteins of this sensor exhibit a pH-induced decrease in their fluorescence intensity, however with different kinetics. Dead Cell Imaging reproduced this biphasic response, proving that both the initial increase and the subsequent decrease in the FRET signal are likely attributable to a pH artifact.

The data on the pH sensitivity of ATeam1.03 in the original publication suggests that acidification leads to a decrease in the FRET signal⁵⁷. However, this calibration was performed using purified sensor protein diluted in buffers of different pH values, which only provides data on the endpoint of the pH sensitivity and does not resolve the initial response. Therefore, the published data on pH sensitivity of ATeam1.03 does not explain the initial increase in response to GABA. This might lead to misinterpretation of this signal as a real GABA-induced ATP increase. Furthermore, a short GABA application would have only elicited an increase in the FRET ratio. This would not have raised suspicion of a pH artifact, as the signal does not change in the direction expected for pH-mediated effects. Since Dead Cell Imaging resolves the dynamic pH response of a sensor over time, it allows a more accurate description of complex pH effects on genetically encoded sensors, especially in response to short stimuli.

A final advantage of Dead Cell Imaging is that it is an easy and affordable method of assessing the pH sensitivity of a sensor. The main purpose of this method is to address the pH sensitivity of a sensor for usage in a live cell imaging experiment. Therefore, we assume that the infrastructure for sensor expression and an appropriate imaging setup are available. Given these circumstances, Dead Cell Imaging requires little more than PFA fixation of cells expressing the sensor and performing an imaging experiment with simple buffers of different pH. No time-consuming purification of the sensor protein or technically challenging multiplex-imaging with a pH sensor⁸⁷ is required for assessing the pH sensitivity of a genetically encoded sensor. This might especially help laboratories that want to apply genetically encoded sensors to answer specific questions, but do not have the existing infrastructure or resources to address this important problem.

4.3.3 Limitations of Dead Cell Imaging

Despite the previously described advantages of Dead Cell Imaging, there are also important limitations of this method to consider. Most importantly, the presented method involves fixation of the cells and therefore the sensor with PFA, which is a highly reactive chemical agent that can crosslink proteins as well as other macromolecules¹³³. Due to its high reactivity in combination with the vast number of potential targets within a cell, it is impossible to accurately predict to what extent a certain protein, in this case the genetically encoded sensor of interest, will be affected. It is however clear that the sensor protein examined with Dead Cell Imaging is not fully comparable to a native, non-fixed sensor. Therefore, careful interpretation of the results obtained with Dead Cell Imaging is important.

We found that the lactate sensor Laconic did not respond to lactate application after PFA fixation. This cannot be explained by lactate being unable to enter the PFA-fixed cells, since we permeabilized our PFA-fixed cells using a protocol that allows antibodies to penetrate¹³⁴, which are several orders of magnitudes bigger than lactate. Also, Triton X-100, the reagent used for permeabilization, has been used for extraction of native proteins and is unlikely to cause the loss of function of Laconic¹³⁵. This indicates that PFA fixation indeed impaired sensor function.

However, we could still observe the fluorescence of both individual FRET channels, which displayed pH sensitivity. Previous reports indicated that PFA fixation alters the fluorescence lifetime of eYFP¹³⁶. However, Joosen and colleagues showed that this effect is due to the mounting medium, while PFA fixation itself does not affect the fluorescence lifetime of GFP-derived fluorescent proteins¹³⁷. Since the fluorescence lifetime is an intrinsic property of a fluorophore and is highly sensitive to various factors, including fluorophore structure¹³⁸, we can safely assume that PFA fixation does not alter the fluorophore itself. This is likely because the

β -can structure of GFP-derived fluorescent proteins, consisting of 11 tightly packed β -sheets with no obvious clefts, shields the fluorophore from the environment^{39,139}. While the gaps are too small to allow diffusion of molecules such as formaldehyde towards the fluorophore, protons are small enough to penetrate to the fluorophore^{138,140}. PFA fixation does not significantly influence the tertiary structure of proteins¹⁴¹, therefore the protective β -barrel is preserved and continues to protect the chromophore in its fixed state. This could explain why fixed fluorescent proteins keep their fluorescence as well as their pH sensitivity largely intact.

Another limitation of Dead Cell Imaging arises from the fact that PFA fixation can impair binding of the molecule of interest and therefore the evoked conformation changes. Some genetically encoded sensors show different pH sensitivities depending on the concentration of the molecule of interest. For instance, the ATP sensor ATeam1.03 shows a decrease in the FRET signal during acidification in the presence of 8 mM ATP, while it shows an increase in the absence of ATP⁵⁷. Since PFA fixation can make sensors insensitive and the conformation of the fixed sensor (bound vs. unbound) is hard to predict or influence, Dead Cell Imaging cannot resolve differences of the pH sensitivity with respect to different sensor conformations.

4.3.4 Implications for the interpretation of results obtained with Dead Cell Imaging

As discussed above, PFA fixation cannot alter the fluorescence and pH sensitivity of GFP-derived fluorescent proteins, however, it can crosslink and therefore impair the function and possibly the pH sensitivity of the binding domain or linker regions of genetically encoded sensors. A signal of a genetically encoded sensor during Dead Cell Imaging therefore mainly reflects the intrinsic pH sensitivity of the fluorescent proteins of the sensor, and the pH sensitivity of fixed fluorescent proteins reflects that of unfixed fluorescent proteins. Accordingly, Dead Cell Imaging can confirm that an effect observed during live cell imaging is indeed a pH artifact rather than an actual change in the levels of the molecule of interest. While the pH sensitivity of a genetically encoded sensor is typically defined by the fluorophore¹⁰⁷, the possibility of the sensing domain dependent pH artifact cannot be fully ruled out. Therefore, the absence of a response during Dead Cell Imaging is not sufficient to prove that a response during live cell imaging reflects a real change of analyte levels. For example, PFA fixation might conceal the pH sensitivity of other parts of the sensor such as the binding domain or the flexible linkers.

We will apply the discussed implications to the results obtained in study II. We can safely assume that the responses to GABA observed during live cell imaging using Laconic and ATeam1.03 are pH artifacts of the respective sensors, since we observed the same dynamics during dead cell imaging. The live cell imaging signal of LiLac in response to GABA however

differed from the Dead Cell Imaging signal. In both settings we observed an immediate decrease, yet the signal recovered during live cell imaging and showed a transient increase which was absent during Dead Cell Imaging. We likely can attribute the decrease in the signal to a pH artifact. However, the absence of the delayed increase in the signal during Dead Cell Imaging does not prove that this delayed increase is a real signal. Potentially this signal could arise from a pH-sensitive conformational change in the binding domain of LiLac that has been crosslinked during PFA fixation and therefore cannot respond during Dead Cell Imaging. Since the LiLac signal is not ratiometric, the delayed increase during live cell imaging could also stem from neuronal shrinkage, leading to an apparent increase in the signal. Since PFA fixed cells do not show volume regulation, Dead Cell Imaging would be unable to account for such an effect. Therefore, the increase in the signal of LiLac might reflect a real change in the cytosolic lactate levels but could also be a pH artifact unrelated to the fluorophore of LiLac. Therefore, additional experiments are required to answer this question.

4.3.5 Comparison of Dead Cell Imaging with other methods to assess pH sensitivity of genetically encoded sensors

In study II, we introduced Dead Cell Imaging as a novel and cost-effective method to assess the pH sensitivity of a genetically encoded sensor. As discussed above, Dead Cell Imaging can confirm the presence of a pH artifact; however, it cannot prove the absence of pH interference. The following paragraphs will compare Dead Cell Imaging with the two main methods of assessing pH sensitivity.

The gold standard of assessing the pH sensitivity of a genetically encoded sensor involves purification of the sensor protein and diluting it in buffers of different pH. This procedure is usually performed by the laboratories developing a genetically encoded sensor and is part of the sensor characterization that often also involves measuring the temperature sensitivity, specificity, and kinetics of the respective sensor. This approach provides reliable data on the pH sensitivity as it uses unmodified sensor protein. In addition, these measurements utilize only buffers, therefore, this eliminates potential interference by pH-mediated analyte changes due to cellular adaptations. However, elimination of the cellular environment also has drawbacks as molecular crowding is known to contribute to protein stability^{142,143}, potentially leading to an overestimation of the pH sensitivity. In addition, purification of the sensor protein is a labor-intensive procedure. It often requires expression of the protein of interest with an affinity tag, which possibly has to be added first via cloning, and subsequent affinity chromatography¹⁴⁴. While the technology for that is well established, especially laboratories that do not develop biosensors but only apply them for their research might lack the experience or the equipment to perform these experiments.

Another method to address the problem of pH sensitivity of genetically encoded sensors is co-imaging of the sensor of interest with a genetically encoded pH sensor. This elegant technique allows following the pH dynamics in response to a certain stimulus during measurement of the sensor of interest⁸⁷. This allows a cell-specific correlation of the sensor readout with a potential pH change and therefore helps to detect artifacts. In addition, given a pH calibration was performed at the end of the experiment, it allows correction of pH artifacts and therefore extraction of the real signal⁸⁷. This approach enables a direct assessment of the pH-sensitivity of a sensor and considers the cellular environment. However, since this method requires multiplexing, it also presents technical challenges and might not be compatible with all imaging setups. Furthermore, this method is unable to account for scenarios where a pH change directly modulates the analyte levels and it would mistake these analyte changes with pH artifacts. Finally, it is not straightforward to resolve complex kinetics of a pH artifact of a FRET sensor with this approach. Correcting the biphasic signal of ATeam1.03 in response to GABA might result in an overestimation of the initial peak. This is because acidification does not exhibit the same biphasic behavior and would only be linked to the signal decrease of ATeam1.03.

While other powerful methods to characterize genetically encoded sensors with respect to their pH sensitivity exist, they are not discussed here as they are out of scope for general application and are more suitable for development and screening of sensor variants⁶¹.

Taken together, in comparison with these two approaches, Dead Cell Imaging is less accurate in describing the general pH sensitivity of a genetically encoded sensor due to the modifications of the sensor protein by PFA fixation. While the pH sensitivity of the fluorescent proteins, which generally accounts for the main pH sensitivity of the sensor, is preserved, potential pH sensitivity of the sensing domain can be lost. However, Dead Cell Imaging requires less additional work and investment than the other methods and outperforms both with respect to addressing the kinetics of a pH artifact. Therefore, we propose Dead Cell Imaging as a method for laboratories that perform live cell imaging and want to confirm the suspicion of a pH artifact without extensive investment of time and resources in establishing one of the other two methods previously discussed. Dead Cell Imaging does not aim to replace any of those methods but rather is a quick and easy approach that can help to increase the awareness of pH artifacts and lower the effort to perform first control experiments.

4.4 Experimental considerations for live cell imaging

This thesis discusses different properties of genetically encoded sensors, including potential shortcomings. The sensor field is rapidly evolving and new, improved sensors will likely address problems of older versions, leading to more reliable readouts. However, proper

selection of the imaging setup and modalities can help to overcome or minimize artifacts during live cell imaging with genetically encoded sensors. In general, the two main considerations concern optimization of the imaging setup to maximize the readout quality and environmental control to avoid artifacts.

4.4.1 Optimization of the live cell imaging microscope

Maximizing the imaging quality is important for any microscopic application; however, this is even more important when it comes to live cell imaging. Improving the imaging setup will improve the signal-to-noise ratio, which can help detecting smaller effects. More importantly, it reduces the exposure of the sample to light, thereby minimizing both phototoxicity and photobleaching. The following section discusses the key components of a microscope that affect the imaging quality and therefore the readout of a live cell imaging experiment.

Excitation and emission path of the microscope should be adjusted according to the fluorescent spectra of the individual sensors¹⁴⁵. Limiting the excitation wavelength to the peak of the excitation spectrum can decrease phototoxicity by avoiding exposure of the cells with unnecessary light unable to excite the fluorophore. The range of collected emission should be selected as wide as possible while maintaining specificity to the fluorophore and avoiding spectral overlaps.

The choice of the objective directly determines how much light is collected and greatly affects the imaging quality. This governs how much excitation light is required for obtaining reasonable signal-to-noise ratios. The main parameters concerning the objective are the magnification and the numerical aperture (NA). While higher magnifications allow resolving more detailed structures, the magnification correlates inversely with the brightness of the resulting image¹⁴⁶. In contrast, the NA correlates directly with image brightness. Therefore, an objective with the lowest magnification that still provides sufficient resolution and the highest possible NA should be chosen for maximal light collection¹⁴⁷.

Finally, efficient detection of the emitted fluorescence is key for acquiring an image with high signal-to-noise ratio. Standard epifluorescence microscopes usually employ either a CCD or a CMOS camera, which exist in a wide range of price and performance. Unlike for filter sets and objectives, the camera of an imaging setup is usually not exchanged in between experiments and therefore should be suitable for a wide range of applications. There is no one-fits-all solution and it is difficult to define the optimal camera for an application¹⁴⁵. However, two main properties affecting signal-to-noise ratios to consider when selecting the camera are quantum efficiency and the camera noise. A high quantum efficiency, which is a wavelength-dependent variable, helps to detect a higher fraction of the incoming photons, thereby making the camera more sensitive¹⁴⁸. Camera noise is a variable that depends on different noise types,

namely thermal noise, readout noise, Poisson noise, and fixed-pattern noise¹⁴⁹. Evidently, low camera noise improves imaging quality and thus the signal-to-noise ratio.

As a rule of thumb, settings for a fluorescent live cell imaging experiment should not be optimized to collect the highest quality images but rather to minimize light exposure of the sample while still obtaining a sufficient signal-to-noise ratio. As image resolution is usually secondary in most live cell imaging experiments using genetically encoded sensors, camera binning can be a helpful way of improving signal-to-noise ratios at the cost of image quality¹⁴⁸.

4.4.2 Environmental control

Proper control of the environment is crucial for maintaining cell health on the microscope throughout the imaging session and for avoiding artefacts. The main parameters to consider with respect to this are composition of the medium, maintaining stable extracellular pH and temperature, and avoiding stress factors such as phototoxicity or shear stress.

Given that the signal of most genetically encoded sensors is sensitive to fluctuations of pH and temperature, it is evident that these parameters need to be efficiently controlled. Stage-top incubators or full microscope enclosures allow efficient temperature control¹⁵⁰. However, most live cell imaging experiments using genetically encoded sensors rely on continuous perfusion of the cells to provide stimuli or drugs. Therefore, these approaches are not feasible as they limit access to the cells or result in constant exchange of the heated buffer with fresh, cold buffer. Heating the superfused buffer using inline solution heaters can help to overcome these limitations.

Buffering of the imaging solution maintain a stable, physiological pH throughout the experiment. A major buffer system responsible of maintaining cellular and whole-body pH is the $\text{CO}_2/\text{HCO}_3^-$ buffering system that relies on the equilibrium between the two components in aqueous solutions¹⁵¹. It is the most common buffer system in cell culture media and can also be applied to live cell imaging experiments. However, bicarbonate-buffered solutions outgas over time, leading to an alkalization of the media, thereby negating the buffering ability. To prevent this, bicarbonate-buffered solutions require constant gassing with 5% CO_2 to maintain pH stability and buffering capacity, which poses an additional technical challenge. An easier way of achieving stable physiological pH levels is using HEPES-buffered solutions, which do not require additional action such as gassing. However, bicarbonate is not only a key buffer of cellular pH, it also is involved in several important physiological processes such as ion transport, volume regulation and metabolic signaling¹⁵¹⁻¹⁵³. These processes are absent or not fully functional in the absence of bicarbonate. Therefore, the use of a CO_2 -dependent buffering system is important to obtain physiologically meaningful data and should be preferred over a HEPES-buffered system.

Regardless of the chosen buffering system, the medium also should recapitulate the native environment of the measured cell type to ensure physiological behavior. For neurons, the cell type measured in this thesis, this is of particular importance as their firing behavior is strongly dependent on extracellular ion concentrations¹⁵⁴. Therefore, a common imaging solution for neurons is artificial cerebrospinal fluid (aCSF)^{114,155}, which mimics ionic concentrations of CSF.

5 Future directions

This thesis focuses on live cell imaging with genetically encoded sensors and addresses potential pitfalls that can lead to misinterpretation. This thesis features two studies that examine different sensor-related limitations.

Study I provided a characterization of Ic-LysM GEPII 1.0 in the context of activity-mediated neuronal K^+ dynamics. Since the affinity of Ic-LysM GEPII 1.0 is too high to reliably detect K^+ dynamics in response to spontaneous or mild activity, future work should focus on improving Ic-LysM GEPII 1.0. The main objective towards that is lowering the affinity for K^+ , making the sensor more responsive to minor changes of the neuronal K^+ levels of around 140 mM. A promising approach could be modifying the binding domain of Ic-LysM GEPII 1.0 using the optimizations developed for KRaIONs as a template²³. In addition, utilization of improved, novel FRET pairs could help to increase the dynamic range, thereby increasing the signal-to-noise ratio and allowing better detection of small signals⁹². While Ic-LysM GEPII 1.0 displays a decent pH stability, further optimization with respect to that aspect would help to increase the robustness of the results obtained with this sensor.

Study II describes Dead Cell Imaging, a novel method that allows addressing the pH sensitivity of genetically encoded sensors in an easy and cost-effective manner. Future work might help to address the main caveat of this method, namely the modification of the sensor protein by PFA. As this leads to a loss of sensor function, it might also alter the pH sensitivity of the binding domain. This compromises the effectiveness of Dead Cell Imaging to reflect the pH sensitivity of genetically encoded sensors. Combination of Dead Cell Imaging with established methods of antigen retrieval might help to return the sensor protein in a more native state. This would help making data on pH sensitivity of a sensor obtained with Dead Cell Imaging more meaningful and comparable to that of the unfixed protein. Furthermore, a fixation protocol named SHIELD has been proposed to preserve protein function better than fixation by PFA¹⁵⁶. Future experiments can determine if this protocol improves Dead Cell Imaging and provides more reliable data on the pH sensitivity of genetically encoded sensors.

6 References

- 1 Squire, L. *et al.* *Fundamental neuroscience*. (Academic press, 2012).
- 2 Gerstner, W., Kistler, W. M., Naud, R. & Paninski, L. *Neuronal dynamics: From single neurons to networks and models of cognition*. (Cambridge University Press, 2014).
- 3 Dowling, J. E. *Neurons and networks: an introduction to behavioral neuroscience*. (Harvard University Press, 2001).
- 4 Südhof, T. C. Neurotransmitter release. *Pharmacology of Neurotransmitter Release*, 1-21 (2008).
- 5 Bean, B. P. The action potential in mammalian central neurons. *Nature Reviews Neuroscience* **8**, 451-465 (2007).
- 6 Barnett, M. W. & Larkman, P. M. The action potential. *Practical neurology* **7**, 192-197 (2007).
- 7 Sen, A. K. & Post, R. Stoichiometry and localization of adenosine triphosphate-dependent sodium and potassium transport in the erythrocyte. *Journal of Biological Chemistry* **239**, 345-352 (1964).
- 8 Attwell, D. & Laughlin, S. B. An energy budget for signaling in the grey matter of the brain. *Journal of Cerebral Blood Flow & Metabolism* **21**, 1133-1145 (2001).
- 9 Somjen, G. G. Ion regulation in the brain: implications for pathophysiology. *The Neuroscientist* **8**, 254-267 (2002).
- 10 Wright, S. H. Generation of resting membrane potential. *Advances in physiology education* **28**, 139-142 (2004).
- 11 Kocsis, J., Malenka, R. & Waxman, S. Effects of extracellular potassium concentration on the excitability of the parallel fibres of the rat cerebellum. *The Journal of Physiology* **334**, 225-244 (1983).
- 12 Meeks, J. P. & Mennerick, S. Selective effects of potassium elevations on glutamate signaling and action potential conduction in hippocampus. *Journal of Neuroscience* **24**, 197-206 (2004).
- 13 Bellot-Saez, A., Kékesi, O., Morley, J. W. & Buskila, Y. Astrocytic modulation of neuronal excitability through K⁺ spatial buffering. *Neuroscience & Biobehavioral Reviews* **77**, 87-97 (2017).
- 14 Kofuji, P. & Newman, E. Potassium buffering in the central nervous system. *Neuroscience* **129**, 1043-1054 (2004).
- 15 David, Y. *et al.* Astrocytic dysfunction in epileptogenesis: consequence of altered potassium and glutamate homeostasis? *Journal of Neuroscience* **29**, 10588-10599 (2009).
- 16 Capuani, C. *et al.* Defective glutamate and K⁺ clearance by cortical astrocytes in familial hemiplegic migraine type 2. *EMBO Molecular Medicine* **8**, 967-986 (2016).
- 17 Scanziani, M. & Häusser, M. Electrophysiology in the age of light. *Nature* **461**, 930-939 (2009).
- 18 Grienberger, C. & Konnerth, A. Imaging calcium in neurons. *Neuron* **73**, 862-885 (2012).
- 19 Looger, L. L. & Griesbeck, O. Genetically encoded neural activity indicators. *Current opinion in neurobiology* **22**, 18-23 (2012).
- 20 Zhang, Y. *et al.* Fast and sensitive GCaMP calcium indicators for imaging neural populations. *Nature* **615**, 884-891 (2023).
- 21 Bischof, H. *et al.* Novel genetically encoded fluorescent probes enable real-time detection of potassium in vitro and in vivo. *Nature Communications* **8**, 1422 (2017).
- 22 Shen, Y. *et al.* Genetically encoded fluorescent indicators for imaging intracellular potassium ion concentration. *Communications biology* **2**, 18 (2019).
- 23 Torres Cabán, C. C. *et al.* Tuning the sensitivity of genetically encoded fluorescent potassium indicators through structure-guided and genome mining strategies. *ACS sensors* **7**, 1336-1346 (2022).
- 24 Wu, S.-Y. *et al.* A sensitive and specific genetically-encoded potassium ion biosensor for in vivo applications across the tree of life. *PLoS biology* **20**, e3001772 (2022).

-
- 25 Hochreiter, B., Pardo Garcia, A. & Schmid, J. A. Fluorescent proteins as genetically encoded FRET biosensors in life sciences. *Sensors* **15**, 26281-26314 (2015).
- 26 Cormack, B. P., Valdivia, R. H. & Falkow, S. FACS-optimized mutants of the green fluorescent protein (GFP). *Gene* **173**, 33-38 (1996).
- 27 Lambert, T. J. FPbase: a community-editable fluorescent protein database. *Nature methods* **16**, 277-278 (2019).
- 28 Sauer, M., Hofkens, J. & Enderlein, J. *Handbook of fluorescence spectroscopy and imaging: from ensemble to single molecules*. (John Wiley & Sons, 2010).
- 29 Stokes, G. G. XXX. On the change of refrangibility of light. *Philosophical transactions of the Royal Society of London*, 463-562 (1852).
- 30 Valeur, B. & Berberan-Santos, M. N. *Molecular fluorescence: principles and applications*. (John Wiley & Sons, 2012).
- 31 Ai, H.-w., Henderson, J. N., Remington, S. J. & Campbell, R. E. Directed evolution of a monomeric, bright and photostable version of Clavularia cyan fluorescent protein: structural characterization and applications in fluorescence imaging. *Biochemical Journal* **400**, 531-540 (2006).
- 32 Nagai, T. *et al.* A variant of yellow fluorescent protein with fast and efficient maturation for cell-biological applications. *Nature biotechnology* **20**, 87-90 (2002).
- 33 Förster, T. Zwischenmolekulare energiewanderung und fluoreszenz. *Annalen der physik* **437**, 55-75 (1948).
- 34 Cardullo, R. A. & Parpura, V. Fluorescence resonance energy transfer microscopy: theory and instrumentation. *Methods in cell biology* **72**, 415-430 (2003).
- 35 Shimomura, O., Johnson, F. H. & Saiga, Y. Extraction, purification and properties of aequorin, a bioluminescent protein from the luminous hydromedusan, Aequorea. *Journal of cellular and comparative physiology* **59**, 223-239 (1962).
- 36 Morise, H., Shimomura, O., Johnson, F. H. & Winant, J. Intermolecular energy transfer in the bioluminescent system of Aequorea. *Biochemistry* **13**, 2656-2662 (1974).
- 37 Prasher, D. C., Eckenrode, V. K., Ward, W. W., Prendergast, F. G. & Cormier, M. J. Primary structure of the Aequorea victoria green-fluorescent protein. *Gene* **111**, 229-233 (1992).
- 38 Ormö, M. *et al.* Crystal structure of the Aequorea victoria green fluorescent protein. *Science* **273**, 1392-1395 (1996).
- 39 Yang, F., Moss, L. G. & Phillips Jr, G. N. The molecular structure of green fluorescent protein. *Nature biotechnology* **14**, 1246-1251 (1996).
- 40 Chalfie, M., Tu, Y., Euskirchen, G., Ward, W. W. & Prasher, D. C. Green fluorescent protein as a marker for gene expression. *Science* **263**, 802-805 (1994).
- 41 Heim, R., Prasher, D. C. & Tsien, R. Y. Wavelength mutations and posttranslational autoxidation of green fluorescent protein. *Proceedings of the National Academy of Sciences* **91**, 12501-12504 (1994).
- 42 Levashina, E. A., Ohresser, S., Lemaitre, B. & Imler, J.-L. Two distinct pathways can control expression of the gene encoding the Drosophila antimicrobial peptide metchnikowin. *Journal of molecular biology* **278**, 515-527 (1998).
- 43 Spergel, D. J., Krüth, U., Hanley, D. F., Sprengel, R. & Seeburg, P. H. GABA- and glutamate-activated channels in green fluorescent protein-tagged gonadotropin-releasing hormone neurons in transgenic mice. *Journal of Neuroscience* **19**, 2037-2050 (1999).
- 44 Reichel, C. *et al.* Enhanced green fluorescence by the expression of an Aequorea victoria green fluorescent protein mutant in mono- and dicotyledonous plant cells. *Proceedings of the National Academy of Sciences* **93**, 5888-5893 (1996).
- 45 Yang, T.-T., Cheng, L. & Kain, S. R. Optimized codon usage and chromophore mutations provide enhanced sensitivity with the green fluorescent protein. *Nucleic acids research* **24**, 4592-4593 (1996).
- 46 Wang, M., Da, Y. & Tian, Y. Fluorescent proteins and genetically encoded biosensors. *Chemical Society Reviews* (2023).

-
- 47 Chudakov, D. M., Matz, M. V., Lukyanov, S. & Lukyanov, K. A. Fluorescent proteins and their applications in imaging living cells and tissues. *Physiological reviews* **90**, 1103-1163 (2010).
- 48 Berlin, S. *et al.* Photoactivatable genetically encoded calcium indicators for targeted neuronal imaging. *Nature methods* **12**, 852-858 (2015).
- 49 Lee, S., Song, Y.-K. & Baker, B. J. Engineering photoactivatability in genetically encoded voltage and pH indicators. *Frontiers in Cellular Neuroscience* **13**, 482 (2019).
- 50 Fosque, B. F. *et al.* Labeling of active neural circuits in vivo with designed calcium integrators. *Science* **347**, 755-760 (2015).
- 51 Moeyaert, B. *et al.* Improved methods for marking active neuron populations. *Nature communications* **9**, 4440 (2018).
- 52 Sadoine, M. *et al.* Designs, applications, and limitations of genetically encoded fluorescent sensors to explore plant biology. *Plant Physiology* **187**, 485-503 (2021).
- 53 Zhang, Z., Cheng, X., Zhao, Y. & Yang, Y. Lighting up live-cell and in vivo central carbon metabolism with genetically encoded fluorescent sensors. *Annual Review of Analytical Chemistry* **13**, 293-314 (2020).
- 54 Day-Cooney, J., Dalangin, R., Zhong, H. & Mao, T. Genetically encoded fluorescent sensors for imaging neuronal dynamics in vivo. *Journal of neurochemistry* **164**, 284-308 (2023).
- 55 Maeshima, K. *et al.* A transient rise in free Mg²⁺ ions released from ATP-Mg hydrolysis contributes to mitotic chromosome condensation. *Current Biology* **28**, 444-451. e446 (2018).
- 56 Vinkenborg, J. L. *et al.* Genetically encoded FRET sensors to monitor intracellular Zn²⁺ homeostasis. *Nature methods* **6**, 737-740 (2009).
- 57 Imamura, H. *et al.* Visualization of ATP levels inside single living cells with fluorescence resonance energy transfer-based genetically encoded indicators. *Proceedings of the National Academy of Sciences* **106**, 15651-15656 (2009).
- 58 Klarenbeek, J., Goedhart, J., Van Batenburg, A., Groenewald, D. & Jalink, K. Fourth-generation epac-based FRET sensors for cAMP feature exceptional brightness, photostability and dynamic range: characterization of dedicated sensors for FLIM, for ratiometry and with high affinity. *PLoS one* **10**, e0122513 (2015).
- 59 Hung, Y. P., Albeck, J. G., Tantama, M. & Yellen, G. Imaging cytosolic NADH-NAD⁺ redox state with a genetically encoded fluorescent biosensor. *Cell metabolism* **14**, 545-554 (2011).
- 60 Bermejo, C., Haerizadeh, F., Takanaga, H., Chermak, D. & Frommer, W. B. Dynamic analysis of cytosolic glucose and ATP levels in yeast using optical sensors. *Biochemical Journal* **432**, 399-406 (2010).
- 61 Koveal, D. *et al.* A high-throughput multiparameter screen for accelerated development and optimization of soluble genetically encoded fluorescent biosensors. *Nature Communications* **13**, 2919 (2022).
- 62 San Martin, A. *et al.* Imaging mitochondrial flux in single cells with a FRET sensor for pyruvate. *PLoS one* **9**, e85780 (2014).
- 63 Helassa, N. *et al.* Ultrafast glutamate sensors resolve high-frequency release at Schaffer collateral synapses. *Proceedings of the National Academy of Sciences* **115**, 5594-5599 (2018).
- 64 Marvin, J. S. *et al.* A genetically encoded fluorescent sensor for in vivo imaging of GABA. *Nature methods* **16**, 763-770 (2019).
- 65 Patriarchi, T. *et al.* Ultrafast neuronal imaging of dopamine dynamics with designed genetically encoded sensors. *Science* **360**, eaat4422 (2018).
- 66 Ermakova, Y. *et al.* SypHer3s: a genetically encoded fluorescent ratiometric probe with enhanced brightness and an improved dynamic range. *Chemical Communications* **54**, 2898-2901 (2018).

-
- 67 Pak, V. V. *et al.* Ultrasensitive genetically encoded indicator for hydrogen peroxide identifies roles for the oxidant in cell migration and mitochondrial function. *Cell metabolism* **31**, 642-653. e646 (2020).
- 68 Vu, C. Q., Fukushima, S.-i., Wazawa, T. & Nagai, T. A highly-sensitive genetically encoded temperature indicator exploiting a temperature-responsive elastin-like polypeptide. *Scientific Reports* **11**, 16519 (2021).
- 69 Yang, H. H. *et al.* Subcellular imaging of voltage and calcium signals reveals neural processing in vivo. *Cell* **166**, 245-257 (2016).
- 70 Delarue, M. *et al.* mTORC1 controls phase separation and the biophysical properties of the cytoplasm by tuning crowding. *Cell* **174**, 338-349. e320 (2018).
- 71 Ovechkina, V. S., Zakian, S. M., Medvedev, S. P. & Valetdinova, K. R. Genetically encoded fluorescent biosensors for biomedical applications. *Biomedicines* **9**, 1528 (2021).
- 72 Patterson, G. H., Knobel, S. M., Sharif, W. D., Kain, S. R. & Piston, D. W. Use of the green fluorescent protein and its mutants in quantitative fluorescence microscopy. *Biophysical journal* **73**, 2782-2790 (1997).
- 73 Wachter, R. M. & Remington, S. J. Sensitivity of the yellow variant of green fluorescent protein to halides and nitrate. *Current Biology* **9**, R628-R629 (1999).
- 74 Miesenböck, G., De Angelis, D. A. & Rothman, J. E. Visualizing secretion and synaptic transmission with pH-sensitive green fluorescent proteins. *Nature* **394**, 192-195 (1998).
- 75 Galletta, L. J., Haggie, P. M. & Verkman, A. Green fluorescent protein-based halide indicators with improved chloride and iodide affinities. *FEBS letters* **499**, 220-224 (2001).
- 76 Tang, S. *et al.* Design and application of a class of sensors to monitor Ca²⁺ dynamics in high Ca²⁺ concentration cellular compartments. *Proceedings of the National Academy of Sciences* **108**, 16265-16270 (2011).
- 77 Hanson, G. T. *et al.* Investigating mitochondrial redox potential with redox-sensitive green fluorescent protein indicators. *Journal of Biological Chemistry* **279**, 13044-13053 (2004).
- 78 Kostyuk, A. I., Demidovich, A. D., Kotova, D. A., Belousov, V. V. & Bilan, D. S. Circularly permuted fluorescent protein-based indicators: history, principles, and classification. *International journal of molecular sciences* **20**, 4200 (2019).
- 79 Ataka, K. & Pieribone, V. A. A genetically targetable fluorescent probe of channel gating with rapid kinetics. *Biophysical journal* **82**, 509-516 (2002).
- 80 Siegel, M. S. & Isacoff, E. Y. A genetically encoded optical probe of membrane voltage. *Neuron* **19**, 735-741 (1997).
- 81 Baird, G. S., Zacharias, D. A. & Tsien, R. Y. Circular permutation and receptor insertion within green fluorescent proteins. *Proceedings of the National Academy of Sciences* **96**, 11241-11246 (1999).
- 82 Topell, S., Hennecke, J. & Glockshuber, R. Circularly permuted variants of the green fluorescent protein. *FEBS letters* **457**, 283-289 (1999).
- 83 Yu, Y. & Lutz, S. Circular permutation: a different way to engineer enzyme structure and function. *Trends in biotechnology* **29**, 18-25 (2011).
- 84 Kim, H., Ju, J., Lee, H. N., Chun, H. & Seong, J. Genetically encoded biosensors based on fluorescent proteins. *Sensors* **21**, 795 (2021).
- 85 Akerboom, J. *et al.* Crystal structures of the GCaMP calcium sensor reveal the mechanism of fluorescence signal change and aid rational design. *Journal of biological chemistry* **284**, 6455-6464 (2009).
- 86 Wang, Y., Shyy, J. Y.-J. & Chien, S. Fluorescence proteins, live-cell imaging, and mechanobiology: seeing is believing. *Annu. Rev. Biomed. Eng.* **10**, 1-38 (2008).
- 87 Berg, J., Hung, Y. P. & Yellen, G. A genetically encoded fluorescent reporter of ATP:ADP ratio. *Nature methods* **6**, 161-166 (2009).

-
- 88 Edwards, K. A. Periplasmic-binding protein-based biosensors and bioanalytical assay platforms: advances, considerations, and strategies for optimal utility. *Talanta Open* **3**, 100038 (2021).
- 89 Dwyer, M. A. & Hellinga, H. W. Periplasmic binding proteins: a versatile superfamily for protein engineering. *Current opinion in structural biology* **14**, 495-504 (2004).
- 90 Felder, C. B., Graul, R. C., Lee, A. Y., Merkle, H.-P. & Sadee, W. The Venus flytrap of periplasmic binding proteins: an ancient protein module present in multiple drug receptors. *AAps pharmsci* **1**, 7-26 (1999).
- 91 Moschou, E. A., Bachas, L. G., Daunert, S. & Deo, S. K. (ACS Publications, 2006).
- 92 Bajar, B. T., Wang, E. S., Zhang, S., Lin, M. Z. & Chu, J. A guide to fluorescent protein FRET pairs. *Sensors* **16**, 1488 (2016).
- 93 Elsliger, M.-A., Wachter, R. M., Hanson, G. T., Kallio, K. & Remington, S. J. Structural and spectral response of green fluorescent protein variants to changes in pH. *Biochemistry* **38**, 5296-5301 (1999).
- 94 Goedhart, J. *et al.* Structure-guided evolution of cyan fluorescent proteins towards a quantum yield of 93%. *Nature communications* **3**, 751 (2012).
- 95 Hockberger, P. E. *et al.* Activation of flavin-containing oxidases underlies light-induced production of H₂O₂ in mammalian cells. *Proceedings of the National Academy of Sciences* **96**, 6255-6260 (1999).
- 96 Lam, A. J. *et al.* Improving FRET dynamic range with bright green and red fluorescent proteins. *Nature methods* **9**, 1005-1012 (2012).
- 97 Deluca, M. Firefly luciferase. *Advances in enzymology and related areas of molecular biology* **44**, 37-68 (1976).
- 98 Wu, Y. & Jiang, T. Developments in FRET-and BRET-based biosensors. *Micromachines* **13**, 1789 (2022).
- 99 Nagai, T., Yamada, S., Tominaga, T., Ichikawa, M. & Miyawaki, A. Expanded dynamic range of fluorescent indicators for Ca²⁺ by circularly permuted yellow fluorescent proteins. *Proceedings of the National Academy of Sciences* **101**, 10554-10559 (2004).
- 100 Komatsu, N. *et al.* Development of an optimized backbone of FRET biosensors for kinases and GTPases. *Molecular biology of the cell* **22**, 4647-4656 (2011).
- 101 Lindenburg, L. & Merks, M. Engineering genetically encoded FRET sensors. *Sensors* **14**, 11691-11713 (2014).
- 102 Niino, Y., Hotta, K. & Oka, K. Simultaneous live cell imaging using dual FRET sensors with a single excitation light. *PloS one* **4**, e6036 (2009).
- 103 de Juan-Sanz, J. *et al.* Axonal endoplasmic reticulum Ca²⁺ content controls release probability in CNS nerve terminals. *Neuron* **93**, 867-881. e866 (2017).
- 104 Solovyova, N., Veselovsky, N., Toescu, E. & Verkhratsky, A. Ca²⁺ dynamics in the lumen of the endoplasmic reticulum in sensory neurons: direct visualization of Ca²⁺-induced Ca²⁺ release triggered by physiological Ca²⁺ entry. *The EMBO journal* **21**, 622-630 (2002).
- 105 Egelman, D. M. & Montague, P. R. Calcium dynamics in the extracellular space of mammalian neural tissue. *Biophysical journal* **76**, 1856-1867 (1999).
- 106 Gleichmann, M. & Mattson, M. P. Neuronal calcium homeostasis and dysregulation. *Antioxidants & redox signaling* **14**, 1261-1273 (2011).
- 107 Koveal, D. Functional principles of genetically encoded fluorescent biosensors for metabolism and their quantitative use. *Journal of Neurochemistry*, doi:10.1111/jnc.15878 (2023).
- 108 Lager, I., Looger, L. L., Hilpert, M., Lalonde, S. & Frommer, W. B. Conversion of a putative Agrobacterium sugar-binding protein into a FRET sensor with high selectivity for sucrose. *Journal of Biological Chemistry* **281**, 30875-30883 (2006).
- 109 Kikuta, S., Hou, B.-H., Sato, R., Frommer, W. B. & Kikawada, T. FRET sensor-based quantification of intracellular trehalose in mammalian cells. *Bioscience, biotechnology, and biochemistry* **80**, 162-165 (2016).

-
- 110 Nakano, M. *et al.* Genetically encoded ratiometric fluorescent thermometer with wide range and rapid response. *PLoS one* **12**, e0172344 (2017).
- 111 Zhang, C., Liu, M.-S. & Xing, X.-H. Temperature influence on fluorescence intensity and enzyme activity of the fusion protein of GFP and hyperthermophilic xylanase. *Applied microbiology and biotechnology* **84**, 511-517 (2009).
- 112 Kaur, H., Nguyen, K. & Kumar, P. Pressure and temperature dependence of fluorescence anisotropy of green fluorescent protein. *RSC advances* **12**, 8647-8655 (2022).
- 113 Leiderman, P., Huppert, D. & Agmon, N. Transition in the temperature-dependence of GFP fluorescence: from proton wires to proton exit. *Biophysical journal* **90**, 1009-1018 (2006).
- 114 Díaz-García, C. M. *et al.* Neuronal stimulation triggers neuronal glycolysis and not lactate uptake. *Cell metabolism* **26**, 361-374. e364 (2017).
- 115 Kalmbach, A. S. & Waters, J. Brain surface temperature under a craniotomy. *Journal of neurophysiology* **108**, 3138-3146 (2012).
- 116 Kneen, M., Farinas, J., Li, Y. & Verkman, A. Green fluorescent protein as a noninvasive intracellular pH indicator. *Biophysical journal* **74**, 1591-1599 (1998).
- 117 Liu, A. *et al.* pHmScarlet is a pH-sensitive red fluorescent protein to monitor exocytosis docking and fusion steps. *Nature Communications* **12**, 1413 (2021).
- 118 Casey, J. R., Grinstein, S. & Orłowski, J. Sensors and regulators of intracellular pH. *Nature reviews Molecular cell biology* **11**, 50-61 (2010).
- 119 Xiong, Z.-Q., Saggau, P. & Stringer, J. L. Activity-dependent intracellular acidification correlates with the duration of seizure activity. *Journal of Neuroscience* **20**, 1290-1296 (2000).
- 120 Kaila, K., Paalasmaa, P., Taira, T. & Voipio, J. pH transients due to monosynaptic activation of GABAA receptors in rat hippocampal slices. *Neuroreport* **3**, 105-108 (1992).
- 121 Tantama, M., Martínez-François, J. R., Mongeon, R. & Yellen, G. Imaging energy status in live cells with a fluorescent biosensor of the intracellular ATP-to-ADP ratio. *Nature communications* **4**, 2550 (2013).
- 122 Fang, Y. *et al.* Smad5 acts as an intracellular pH messenger and maintains bioenergetic homeostasis. *Cell Research* **27**, 1083-1099 (2017).
- 123 Zhou, N., Gordon, G. R., Feighan, D. & MacVicar, B. A. Transient swelling, acidification, and mitochondrial depolarization occurs in neurons but not astrocytes during spreading depression. *Cerebral cortex* **20**, 2614-2624 (2010).
- 124 Sun, X. *et al.* Simultaneous monitoring of intracellular pH changes and hemodynamic response during cortical spreading depression by fluorescence-corrected multimodal optical imaging. *Neuroimage* **57**, 873-884 (2011).
- 125 Klapoetke, N. C. *et al.* Independent optical excitation of distinct neural populations. *Nature methods* **11**, 338-346 (2014).
- 126 Hayward, R. F., Brooks III, F. P., Yang, S., Gao, S. & Cohen, A. E. Diminishing neuronal acidification by channelrhodopsins with low proton conduction. *Biophysical Journal* **122**, 540a (2023).
- 127 Betolngar, D.-B. *et al.* pH sensitivity of FRET reporters based on cyan and yellow fluorescent proteins. *Analytical and Bioanalytical Chemistry* **407**, 4183-4193 (2015).
- 128 Fredj, A. *et al.* The single T65S mutation generates brighter cyan fluorescent proteins with increased photostability and pH insensitivity. *PLoS One* **7**, e49149 (2012).
- 129 Tantama, M., Hung, Y. P. & Yellen, G. Imaging intracellular pH in live cells with a genetically encoded red fluorescent protein sensor. *Journal of the American Chemical Society* **133**, 10034-10037 (2011).
- 130 Govorunova, E. G. *et al.* Kalium channelrhodopsins are natural light-gated potassium channels that mediate optogenetic inhibition. *Nature neuroscience* **25**, 967-974 (2022).

-
- 131 van der Linden, F. H. *et al.* A turquoise fluorescence lifetime-based biosensor for
quantitative imaging of intracellular calcium. *Nature Communications* **12**, 7159
(2021).
- 132 Sadoine, M., Reger, M., Wong, K. M. & Frommer, W. B. Affinity series of genetically
encoded forster resonance energy-transfer sensors for sucrose. *ACS sensors* **6**,
1779-1784 (2021).
- 133 Hoffman, E. A., Frey, B. L., Smith, L. M. & Auble, D. T. Formaldehyde crosslinking: a
tool for the study of chromatin complexes. *Journal of Biological Chemistry* **290**,
26404-26411 (2015).
- 134 Ghrebi, S. S., Owen, G. R. & Brunette, D. M. Triton X-100 pretreatment of LR-white
thin sections improves immunofluorescence specificity and intensity. *Microscopy
Research and Technique* **70**, 555-562 (2007).
- 135 Makino, S., Reynolds, J. A. & Tanford, C. The binding of deoxycholate and Triton X-
100 to proteins. *Journal of Biological Chemistry* **248**, 4926-4932 (1973).
- 136 Ganguly, S., Clayton, A. H. & Chattopadhyay, A. Fixation alters fluorescence lifetime
and anisotropy of cells expressing EYFP-tagged serotonin1A receptor. *Biochemical
and biophysical research communications* **405**, 234-237 (2011).
- 137 Joosen, L., Hink, M., Gadella Jr, T. & Goedhart, J. Effect of fixation procedures on the
fluorescence lifetimes of Aequorea victoria derived fluorescent proteins. *Journal of
microscopy* **256**, 166-176 (2014).
- 138 Berezin, M. Y. & Achilefu, S. Fluorescence lifetime measurements and biological
imaging. *Chemical reviews* **110**, 2641-2684 (2010).
- 139 Zimmer, M. Green fluorescent protein (GFP): applications, structure, and related
photophysical behavior. *Chemical reviews* **102**, 759-782 (2002).
- 140 Heikal, A. A., Hess, S. T. & Webb, W. W. Multiphoton molecular spectroscopy and
excited-state dynamics of enhanced green fluorescent protein (EGFP): acid-base
specificity. *Chemical Physics* **274**, 37-55 (2001).
- 141 Toews, J., Rogalski, J. C. & Kast, J. Accessibility governs the relative reactivity of
basic residues in formaldehyde-induced protein modifications. *Analytica chimica acta*
676, 60-67 (2010).
- 142 Despa, F., Orgill, D. P. & Lee, R. C. Molecular crowding effects on protein stability.
Annals of the New York Academy of Sciences **1066**, 54-66 (2006).
- 143 Yuan, J. M. *et al.* The effects of macromolecular crowding on the mechanical stability
of protein molecules. *Protein Science* **17**, 2156-2166 (2008).
- 144 Wingfield, P. T. Overview of the purification of recombinant proteins. *Current
protocols in protein science* **80**, 6.1. 1-6.1. 35 (2015).
- 145 Ettinger, A. & Wittmann, T. Fluorescence live cell imaging. *Methods in cell biology*
123, 77-94 (2014).
- 146 Piston, D. W. Choosing objective lenses: the importance of numerical aperture and
magnification in digital optical microscopy. *The Biological Bulletin* **195**, 1-4 (1998).
- 147 Abramowitz, M., Spring, K. R., Keller, H. E. & Davidson, M. W. Basic principles of
microscope objectives. *BioTechniques* **33**, 772-781 (2002).
- 148 Salmon, W. C. & Waters, J. C. CCD cameras for fluorescence imaging of living cells.
Cold Spring Harbor Protocols **2011**, pdb. top113 (2011).
- 149 Lambert, T. J. & Waters, J. C. Assessing camera performance for quantitative
microscopy. *Methods in cell biology* **123**, 35-53 (2014).
- 150 Cole, R. Live-cell imaging: The cell's perspective. *Cell adhesion & migration* **8**, 452-
459 (2014).
- 151 Casey, J. R. Why bicarbonate? *Biochemistry and cell biology* **84**, 930-939 (2006).
- 152 Acin-Perez, R. *et al.* Cyclic AMP produced inside mitochondria regulates oxidative
phosphorylation. *Cell metabolism* **9**, 265-276 (2009).
- 153 Alka, K. & Casey, J. R. Bicarbonate transport in health and disease. *IUBMB life* **66**,
596-615 (2014).
- 154 Jefferys, J. Nonsynaptic modulation of neuronal activity in the brain: electric currents
and extracellular ions. *Physiological reviews* **75**, 689-723 (1995).

-
- 155 Baeza-Lehnert, F. *et al.* Non-canonical control of neuronal energy status by the Na⁺ pump. *Cell metabolism* **29**, 668-680. e664 (2019).
- 156 Park, Y.-G. *et al.* Protection of tissue physicochemical properties using polyfunctional crosslinkers. *Nature biotechnology* **37**, 73-83 (2019).

7 Acknowledgements

The PhD has been an intense stretch of years and while it was not always easy, I am very grateful for every bit of it. Not only have I enjoyed my time in the lab very much, but I am also convinced that I learned a lot, both scientifically and about myself. I am thankful to all the people that were involved in this journey in some way.

First of all, I would like to thank my supervisor Prof. Nikolaus Plesnila. You encouraged me to pursue my project while also giving me the flexibility to follow my own ideas. I always felt supported and really enjoyed my PhD in your lab. While I am also thankful for your scientific guidance and motivation, I especially appreciate the human aspect of your way of leading. You always showed that for you people are the priority and you were always willing to listen whenever there was a problem.

I also want to thank Farida Hellal for her mentoring and supervision. You were always incredibly helpful and provided me with invaluable input. Thank you for your constant support throughout my PhD. I always knew I could count on you, and you showed that you care.

A special thanks goes to Prof. Felipe Barros, who excited me about genetically encoded sensors and brain metabolism. The time I was able to spend in your lab before starting my PhD laid the groundwork for my project and taught me a lot, both scientifically and personally. Thank you also for your continued support throughout my PhD as a TAC member.

Furthermore, I want to thank my other TAC members, Prof. Bernd Sutor and PD Dr. Lars Kunz for their valuable input and the stimulating discussions during my TAC meetings.

I am very grateful to the Graduate School of Systemic Neurosciences for providing a unique framework for graduating and the possibility to interact with people from so many different fields. I especially thank Lena, Steffi and Katrin, who were always happy to help with any question regarding the GSN.

In addition, I would also like to express my gratitude to the members of the AG Plesnila. Hedwig, thank you for all your help with all the administrative work throughout the years, but even more for all the recipe suggestions, the heart-felt talks and for becoming a great friend. Thank you, Josh, for the always interesting conversations and good advice, both in the lab and outside of it over some beers. I also want to thank Becky for always letting me express my Bavarian need for some "grantIn". Thank you Uta for your help with my cells and in general for being the backbone of the lab. Severin, thank you for the fun times at the microscope and the never-ending stream of ideas. Finally, I also want to thank Gian Marco for always being a kind soul, a positive influence in the office next to me and a terrifying opponent at the kicker.

Furthermore, I also want to thank my all colleagues of the ISD, many of whom have become close friends over the years. I owe a special thanks to Jelena for the deep friendship we developed over the last years. Thank you for always being there whenever there is a need, for being honest, even if it is uncomfortable, simply, for being a true friend. I also want to thank Steffi for always having an open ear, for great music and even better evenings. Thank you Judit(h) for always entertaining conversations and wonderful vacations. Finally, thank you to Isabel for coffee breaks and all the evening sessions at the microscope.

I especially want to thank Vanessa, for being the most special person in my life and one of the strongest that I know. Thank you for all the constant support you provide, for your understanding and love, both in the good times and in more difficult ones. Thank you for balancing me out and for opening new perspectives.

Mein größter Dank gilt meiner Familie, speziell meinen Eltern und meiner Schwester Michaela. Danke für die bedingungslose Unterstützung, die ich seit jeher von euch bekommen habe. Ihr habt mich immer geduldig meinen Weg gehen lassen und wart da, wenn ich mich dabei verirrt habe. Ihr habt mich zu dem Menschen gemacht, der ich heute bin (und glücklicherweise mag ich diesen Menschen meistens) und mir immer Verantwortungsbewusstsein, Respekt, Neugier und vor allem Liebe vorgelebt.

8 Curriculum Vitae

Education

- Since 01/2018 **Institute for Stroke and Dementia Research, Munich**
Graduate School of Systemic Neuroscience
Ludwig-Maximilians-University,
Lab of Prof. Nikolaus Plesnila
PhD student
- 04/2014–10/2016 **Ludwig-Maximilians-University, Munich**
Master of Science in Biochemistry, grade: 1.3
- 10/2010–03/2014 **Ludwig-Maximilians-University, Munich**
Bachelor of Science in Chemistry and Biochemistry, grade: 1.3
- 2001–2010 **Gymnasium Grafing**
Abitur, grade: 1.8

Research experience

- 04-12/2017 **Centro de Estudios Cientificos, Valdivia, Chile**
Lab of Prof. Felipe Barros
Research intern
- 03-10/2016 **Institute for Stroke and Dementia Research, Munich**
Ludwig-Maximilians-University,
Lab of Prof. Nikolaus Plesnila
Master's thesis: Molecular alterations of GABAergic inhibition and glutamatergic excitation following cerebral ischemia
- 04–05/2015 **Ludwig-Maximilians-University, Munich**
Lab of Prof. Christian Ochsenfeld
Research intern
- 04–05/2015 **Ludwig-Maximilians-University, Gene Center, Munich**
Lab of Prof. Mario Halic
Research intern
- 10/2013-01/2014 **Max Planck Institute for Neurobiology, Munich**
Lab of Dr. Hiromu Tanimoto
Bachelor's thesis: The role of pickpocket1 expressing neurons in electric shock avoidance in Drosophila melanogaster

9 List of Publications

Accepted for Publication

Khalin, I., Heimbürger, D., Melnychuk, N., Collot, M., **Groschup, B.**, Hellal, F., ... & Klymchenko, A. S. (2020). Ultrabright fluorescent polymeric nanoparticles with a stealth pluronic shell for live tracking in the mouse brain. *ACS nano*, *14*(8), 9755-9770.

Auffenberg, E., Hedrich, U. B., Barbieri, R., Miely, D., **Groschup, B.**, Wuttke, T. V., ... & Freilinger, T. (2021). Hyperexcitable interneurons trigger cortical spreading depression in an Scn1a migraine model. *The Journal of clinical investigation*, *131*(21).

Burgstaller, S., Bischof, H., Rauter, T., Schmidt, T., Schindl, R., Patz, S., ..., **Groschup, B.**, ... & Malli, R. (2021). Immobilization of recombinant fluorescent biosensors permits imaging of extracellular ion signals. *Acs Sensors*, *6*(11), 3994-4000.

Khalin, I., Adarsh, N., Schifferer, M., Wehn, A., **Groschup, B.**, Misgeld, T., ... & Plesnila, N. (2022). Size-Selective transfer of lipid Nanoparticle-Based drug carriers across the blood brain barrier via vascular occlusions following traumatic brain injury. *Small*, *18*(18), 2200302.

Pham, T., Hussein, T., Calis, D., Bischof, H., Skrabak, D., Cruz Santos, M., ..., **Groschup, B.**, ... & Matt, L. (2023). BK channels sustain neuronal Ca²⁺ oscillations to support hippocampal long-term potentiation and memory formation. *Cellular and Molecular Life Sciences*, *80*(12), 369.

10 Affidavit

Eidesstattliche Versicherung/Affidavit

Hiermit versichere ich an Eides statt, dass ich die vorliegende Dissertation „Validation of genetically encoded sensors to measure intracellular potassium and metabolism in neurons„ selbstständig angefertigt habe, mich außer der angegebenen keiner weiteren Hilfsmittel bedient und alle Erkenntnisse, die aus dem Schrifttum ganz oder annähernd übernommen sind, als solche kenntlich gemacht und nach ihrer Herkunft unter Bezeichnung der Fundstelle einzeln nachgewiesen habe.

I hereby confirm that the dissertation „Validation of genetically encoded sensors to measure intracellular potassium and metabolism in neurons„ is the result of my own work and that I have only used sources or materials listed and specified in the dissertation.

München/Munich

04.12.2023

Bernhard Groschup

11 Declaration of Author Contributions

Study I: Probing Intracellular Potassium Dynamics in Neurons: *In vitro* and *In vivo* Assessment of a Genetically Encoded Sensor Dead Cell Imaging

Bernhard Groschup, Gian Marco Calandra, Constanze Raitmayr, Joshua Shrouder, Gemma Llovera, Asal Ghaffari Zaki, Sandra Burgstaller, Helmut Bischof, Emrah Eroglu, Arthur Liesz, Roland Malli, Severin Filser & Nikolaus Plesnila

B.G., S.B., H.B., R.M. and N.P. conceived the study and contributed to the study design. B.G., G.M.C., C.R., J.S., G.L., A.G.Z. and S.F. contributed to the acquisition and analysis of the data. B.G., E.E., A.L., R.M., S.F. and N.P. contributed to the interpretation of the data. B.G., S.F. and N.P. drafted the manuscript. All authors read and approved the final manuscript.

My contribution to this publication in detail: together with Severin Filser and Nikolaus Plesnila, I designed the study and the experiments. I performed neuronal cell culture, produced AAVs and performed all live cell imaging experiments *in vitro*, including optogenetic stimulations. Furthermore, I performed immunocytochemistry in neuronal cell cultures and contributed to the calibrations of purified sensor proteins. I interpreted the results and I drafted and revised the manuscript. Figures 1 and 2 as well as supplementary Figures 1, 2 and 4 comprise the data that I contributed to this study.

Study II: Assessing the pH sensitivity of genetically encoded sensors with Dead Cell Imaging

Bernhard Groschup, Constanze Raitmayr, Nikolaus Plesnila

B.G. and N.P. conceived the study and contributed to the study design. B.G. and C.R. contributed to the acquisition and analysis of the data. B.G. and N.P. contributed to the interpretation of the data. B.G. and N.P. drafted the manuscript. All authors read and approved the final manuscript.

My contribution to this publication in detail: together with Nikolaus Plesnila, I designed the study and the experiments. I performed all experiments, except for the pH measurements shown in Figure 1G, which were performed by Constanze Raitmayr. I interpreted the results and I drafted and revised the manuscript. All Figures, except Figure 1G, comprise the data that I contributed to this study.

München, den
Munich, 04.12.2023,

Bernhard Groschup

Prof. Nikolaus Plesnila
(Supervisor)